Roles of the nuclear RNA-binding proteins hnRNP M and ILF3 in Zika virus infection

by

Brett Charles Stephan Roughead

A thesis submitted in partial fulfillment of the requirements for the degree of

Master of Science

Department of Cell Biology
University of Alberta

ABSTRACT

Zika virus is a positive-sense RNA virus belonging to the *Flaviviridae* family of viruses, which include Dengue, Yellow Fever, Hepatitis C and West Nile viruses. Growing evidence suggests viral infection results in the subversion of numerous host cell factors to aid in viral replication. Despite the cytoplasmic replication cycle of ZIKV in infected cells, numerous host cell proteins implicated in the progression of the viral infection are host nuclear factors. We have focused on two nuclear factors, protein isoforms encoded by the interleukin enhancer-binding factor 3 (*ILF3*) gene, and the heterogeneous nuclear ribonucleoprotein M (hnRNP M). These proteins bind to RNA in host cells, and both of these proteins interact with ZIKV plus-strand viral RNA (+vRNA). Our goal has been to determine the possible roles of these proteins in ZIKV infection using a human tissue culture model system. NF90/NF110, encoded by the *ILF3* gene, are double-stranded RNA binding proteins implicated in transcription, translation, and host immune responses. Using immunofluorescence imaging, we show that NF90/NF110 relocalizes from the nucleus to the cytoplasm following infection. This redistribution of NF90/NF110 to the cytoplasm facilitates an association with ZIKV double-stranded RNA intermediates. In our examination of the depletion of NF90/NF110, we observed a resultant increase in ZIKV viral production suggesting these protein isoforms function to suppress viral infection.

hnRNP M also interacts with ZIKV +vRNA. However, during ZIKV infection we do not observe a detectable change in the nuclear localization of hnRNP M suggesting the bulk of hnRNP M appears to be physically separated from that of the ZIKV +vRNA. Thus, the observed physical interactions of hnRNP M with the ZIKV +vRNA may be

transient or occur between a subpopulation of hnRNP M and the viral RNA. Consistent with their association, depletion of hnRNP M from cells inhibits ZIKV production. This observation is possibly mediated through an increased responsiveness of the interferon- and dsRNA-induced protein kinase R (PKR) immune pathway. In support of this, we observed an increase in the levels of phosphorylated-PKR early in ZIKV infection in populations depleted of hnRNP M. These data suggest a pro-viral role of hnRNP M in the ZIKV life cycle.

For my loving family, and friends, and their unwavering support.

"Nothing in life is to be feared, it is only to be understood. Now is the time to understand more, so that we may fear less."

Marie Curie

In: "Our Precarious Habitat". Melvin A. Benarde, 1970

Acknowledgements

There are several people that have helped me throughout my journey as a grad student that I need to extend my thanks to. First and foremost, I am grateful to Dr. Richard Wozniak for providing me the opportunity to work in his research lab and be a part of his research team. Not only did Rick welcome me into his lab, he also worked with me to continue to play for the varsity basketball program at the University of Alberta which no doubt stole time away from my research endeavors but Rick allowed me the flexibility to excel at both. His passion for science and need for excellence constantly pushed me to learn and grow as a researcher and a student. I am truly grateful to have had the opportunity to learn from him and I will carry lessons learned with me for the rest of my life.

Moreover, I need to thank all the members of the Wozniak lab who I had the pleasure of working with. I extend my deepest thanks to Dr. Juliana Capitanio for training me and helping me learn the experiments and procedures and for the countless hours of troubleshooting. She remains one of the smartest people I have worked with. I would also like to thank Dr. Tadashi Makio and Dr. Chris Ptak for their help and support in the lab. They were a pleasure to work with and were always available to lend a hand. Lastly, I extend thanks to all of my fellow lab mates that I worked with, Natasha Saik, Karl Roesner, Dr. Diego Lapetina, and Nicole Love. It has been my absolute pleasure to work with them throughout my career as a graduate student.

The work that is presented in this thesis would not have been possible without the expertise of my committee and their labs. Dr. Lorne Tyrrell and Dr. Tom Hobman were always available to lend their knowledge in committee meetings and provided invaluable feedback. Lorne also provided unending encouragement and support in the pursuit of my future career in medicine and I extend my deepest thanks for that. Michael Joyce provided a very knowledgeable sounding board for the virology side of the project and provided guidance throughout my thesis and tenure in the lab. I also want to thank the rest of both Lorne's and Tom's labs who aided with protocols and reagents and friendly help.

Finally, the unwavering support of my family throughout this degree were essential to its completion. I am extremely grateful to have such amazing people in my corner and I would not have accomplished what I have without them. My parents offered nothing but support throughout my time in the lab and made me who I am today. My brothers' unending support and encouragement helped immeasurably along the way. I also need to acknowledge an extraordinary group of friends and teammates who were instrumental in my success in this journey and those ahead. There was, and will continue to be be, more than one beer shared alongside words of encouragement.

TABLE OF CONTENTS

LIST OF TABLES

LIST OF FIGURES

LIST OF ABBREVIATIONS

Abbreviation	*Definition*
CEA	carcinoembryonic antigen
CEACAM1	antigen-related cell adhesion molecule-1
CEAR	carcinoembryonic antigen receptor
cGAS	cyclic GMP-AMP synthase
CHIKV	Chikungunya virus
ChIRP-MS	comprehensive identification of RNA-binding proteins by mass spectrometry
CLAMP	cross-link-assisted mRNP purification
CMC	carboxymethyl cellulose
CRC	Colorectal cancer
CVB3	coxsackievirus B3
D2R	dopamine D2 receptor
DC-SIGN	C-type lectin receptor family receptors
DENV	dengue virus
DMEM	Dulbecco's modified essential media
DMSO	dimethylsulfoxide
DZF	zinc finger associated domain
E	envelope
EBOV	Ebola virus
eIF2a	eukaryotic protein synthesis initiation factor 2
EMT	epithelial-mesenchymal transition
ER	endoplasmic reticulum
ERAD	ER-associated degradation pathway
EtOH	ethanol
FBS	fetal bovine serum
FISH	fluorescence *in-situ* hybridization
HCV	hepatitis C virus
HEK	human embryonic kidney
hNPC	human neural progenitor cell
hnRNP	heterogeneous nuclear ribonucleoprotein
hnRNP M	heterogeneous nuclear ribonuclear protein M
HPV	human papillomavirus
HRP	horseradish peroxidase
IAV	influenza A virus
IF	immunofluorescence
IFIT3	interferon induced protein with tetratricopeptide repeats 3

IFITM	interferon-induced transmembrane protein
IFN	interferon
IFNA1	interferon alpha 1
IFNB1	interferon beta 1
IL6	interleukin 6
ILF3	interleukin enhancer binding factor 3
IPZ	importazole
IRE1β	inositol requiring 1-1
IRES	internal ribosome entry site
ISG	interferon-stimulated gene
Iver	ivermectin
JAK	Janus kinase
JEV	Japanese encephalitis virus
LMB	leptomycin B
LPS	lipopolysaccharide
MDA5	melanoma differentiation-associated protein 5
MEF	mouse embryonic fibroblast
MEM	minimal essential media
miRNA	micro RNA
MKP-1	mitogen-activated protein kinase 1
MOI	multiplicity of infection
mRNP	messenger ribonucleoprotein
mTOR	mammalian target of rapamycin
MX1	interferon-induced GTP-binding protein MX1
NF	nuclear factor
NF90	nuclear factor 90
NF110	nuclear factor 110
NFAT	nuclear factor of activated T cells
NFKB1	nuclear factor kappa B subunit 1
NLS	nuclear localization sequence
NP	nucleoprotein
NS	nonstructural
NTF	nucleocytoplasmic transport factor
OAS1	2'-5'-oligoadenylate synthetase 1
PAMP	pathogen associated molecular pattern
PBS	phosphate buffered saline
PCR	polymerase chain reaction
PKR	protein kinase R
Poly I:C	polyinosinic-polycytidylic acid

PRR	pattern recognition receptor
PV	poliovirus
RBD	RNA-binding domain
RdRP	RNA-dependent RNA polymerase
RIG-I	retinoic acid inducible gene I
RIP	RNA immunoprecipitation
RLR	RIG-I like receptor
RRM	RNA recognition motif
SeV	Sendai virus
sfRNA	subgenomic flavivirus RNA
SFV	Semliki Forest virus
SG	stress granule
shRNA	short hairpin RNA
SINV	Sindbis virus
SMA	spinal muscular atrophy
STAT	signal transducer and activator of transcription
STING	stimulator of interferon genes
TBEV	tick-borne encephalitis virus
TIM	T-cell immunoglobulin mucin
TLR	toll-like receptor
TNF	tumor necrosis factor alpha
uPA	urokinase-type plasminogen activator
UPR	unfolded protein response
UTR	untranslated region
VEGF	vascular endothelial growth factor
VSV	vesicular stomatitis virus
WNV	West Nile virus
ZIKV	Zika virus

1 INTRODUCTION

1.1 Zika Virus

Viruses are conceptually very simple biological particles, consisting of a genetic payload (DNA or RNA) and a protein shell. Some viruses are enveloped and have an external phospholipid envelope as well, making them less hardy in the greater environment. The genetic payload within viruses is varied between single- and double-stranded RNA and DNA [1], and this differentiation is one of the first ways viruses are classified. It is suspected that viruses have evolved along with cellular organisms since their initial emergence, and it is likely that the origin of living cells and viruses are both interdependent [2]. However, not all viruses affect organisms equally. For example, most viruses that affect prokaryotes are double-stranded (ds) DNA viruses. Conversely, the majority of viruses that infect eukaryotic organisms are RNA viruses [1]. RNA viruses also have the greatest impact on human health and manifest as infectious communicable diseases. These disease causing RNA viruses include (but are not limited to) Ebola virus, SARS-COV-1, SARS-COV-2, hepatitis C virus, polio virus, measles virus, and West Nile virus [1], [3], [4]. The positive-sense (+) RNA viruses replicate using the simplest strategy as their genetic + RNA payload serves as both the viral genome and mRNA, and following entrance into host cells can directly start translation and replication [5]. One family of +RNA viruses that causes many notorious infectious diseases is the *Flaviviridae* family of viruses. While the family contains approximately 70 viruses, some notable members include hepatitis C virus (HCV), Japanese encephalitis virus (JEV), West Nile virus (WNV), tick-borne encephalitis virus (TBEV), dengue virus (DENV), and Zika virus (ZIKV) [6].

Following sporadic human infections for 50 years, ZIKV emerged in the Pacific and Americas and culminated in outbreaks in French Polynesia (2013/2014) and Brazil shortly after resulting in ZIKV sparking health concerns and garnishing research interest [7]. ZIKV was originally characterized following the isolation of the virus from a rhesus monkey in the Zika forest in Uganda in 1947 [8]. ZIKV, like other *Flaviviruses,* is an arthropod-borne virus (sometimes referred to as an arbovirus) that is transmitted to humans and primates by the mosquito vectors *Aedes aegypti* and *Aedes albopictus* [9]. With the continuing advance of climate change, there are concerns that there will be a continuous geographic expansion in the habitable biomes of the mosquito vectors and the virus [10]. While vector transmission is common among *Flaviviruses*, ZIKV has been also shown to be sexually transmitted in humans, vertically transmitted from mother to child, and transferred by saliva and urine [9], [11]–[13]. While infection with ZIKV is generally asymptomatic, or results only in a mild self-limited illness, ZIKV has been implicated in Zika virus disease (symptoms including flu like symptoms, malaise, or rash), and there is now consensus that ZIKV is a causative agent in Guillain-Barre syndrome and microcephaly in infected newborns [10]. There is no vaccine available to prevent infection with ZIKV, however there are currently three vaccine candidates with US FDA fast track status [14]. It is likely that most vaccine development will be halted as a search for a SARS-COV-2 vaccine is undertaken.

1.1.1 ZIKV structure and replication

Zika virus is a +RNA virus with a genome approximately 10.8 kilobases in length. The ZIKV vRNA translated regions are flanked on the 5’ and 3’ ends by structured

UTRs, and the 5’ end is capped by a virally encoded enzyme with N6-adenosine methylation (m6A) to aid in genome stability [15]. This genome is translated into a single polyprotein that contains three structural and 7 non-structural proteins. The three structural proteins are the capsid protein (C), membrane protein (M) generated from the precursor premembrane protein (prM), and the envelope protein (E) [16]. The 7 non-structural proteins are NS1, NS2A, NS2B, NS3, NS4A, NS4B, and NS5. The putative roles of the protein and position in the polyprotein are shown in Figure 1.1. One of the most important viral proteins, and hallmarks of RNA viruses, is the RNA-dependent RNA polymerase (RdRP) domain contained in the NS5 protein. The ZIKV NS5 protein contains the RdRP domain, the C-terminal end, and also contains an N-terminal methyltransferase domain [17]. This protein plays three essential roles in the ZIKV lifecycle: interferon suppression, and ZIKV genome replication and capping [18]. The virion is a 50 nm enveloped particle that contains a linear positive sense genomic vRNA strand and multiple capsid (C) proteins. The outer layer of the virion, derived from host cell lipid bilayer is formed by 180 stochiometric pairs of M and E [19]. This gives the virion exceptional stability and allows it to survive in the stringent conditions presented by semen, saliva, and urine [11]–[13].

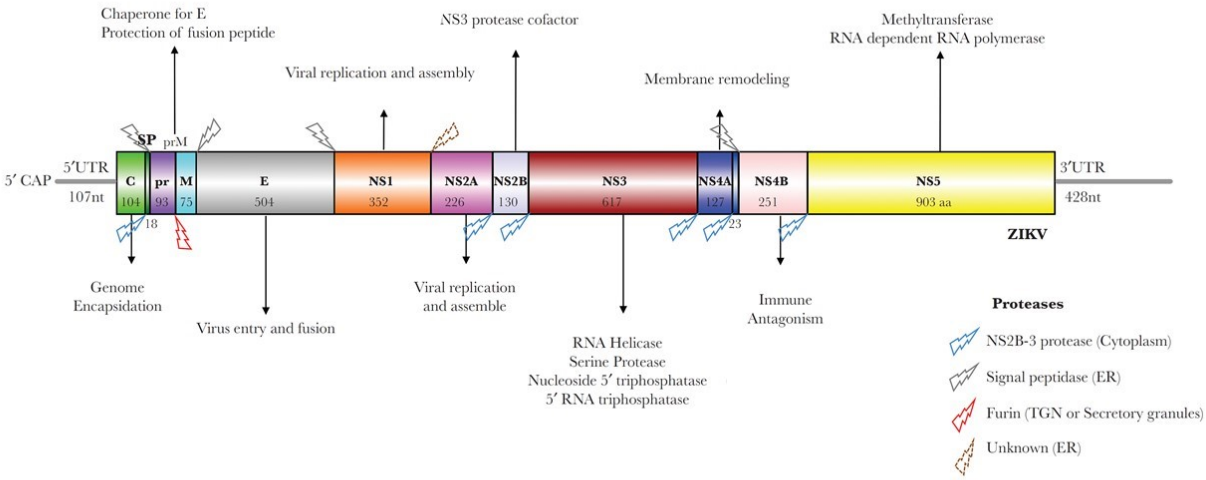

Figure 1.1 ZIKV polyprotein schematic.

The 3 structural proteins (C, prM/M, and E) and 7 nonstructural proteins (NS1, NS2A, NS2B, NS3, NS4A, NS4B, and NS5) are shown with their number of amino acid residues indicated. Cleavage sites and proposed proteases are shown by the color-coded lightning bolts. Grey lines on each end of the polyprotein represent the 3′ and 5′ untranslated regions (UTRs) and their nucleotide lengths are indicated. Information given is true for flaviviruses in general, but many aspects need to be verified for ZIKV. Adapted and reproduced with permission from (Sirohi and Kuhn, 2017) Journal of Infectious Diseases, original publication DOI:10.1093/infdis/jix515.

ZIKV entry into cells is facilitated by receptor and CLATHRIN-mediated endocytosis through interaction of the viral envelope protein (E) with host cell receptors. A number of receptors have been reported to facilitate viral entry into host cells: C-type lectin receptor family receptors (DC-SIGN); T-cell immunoglobulin mucin (TIM); and the TAM (TYRO3, AXL, and MER) family of receptors that recognize lipids in the viral membrane [20][21]–[24]. It appears that ZIKV entry into host cells is variable depending upon the level of virion maturation as well as the lineage of cell being infected. Studies of human clinical tissue samples and tissue culture, along with primate and mouse models, suggest that ZIKV is pantropic with preferred cell types for infection [25]. For example, studies have isolated high levels of ZIKV from brains of infants with microcephaly, placentas of pregnant women [26], and mature human neurons with a preference for human neural progenitor cells (hNPCs), suggesting a possible mechanism for microcephaly [27]. Following endocytosis, ZIKV also requires acidification of the endosome prior to the fusion of the viral membrane to the host cell membrane and the consequent release of genomic vRNA and capsid proteins into the cytoplasm of cells [28]. Once inside the host cell, ZIKV hijacks cellular pathways and subverts host proteins to assist in replication and assembly.

Viral RNA replication occurs in virus-induced intracellular ultrastructures known as replication complexes or factories [29]. The factories are formed using microtubules and intermediate filaments that surround the replication factory [29]. These also form in a number of *Flaviviridae* viruses including DENV, WNV, and HCV [29]–[31]. The roles of these replication factories have been suggested to: help hide viral components, especially the immunogenic dsRNA intermediates; to increase local concentrations of components required for replication and virion formation; and to

spatially coordinate portions of the replication cycle [32]. In infected cells, the genome of ZIKV is replicated via a negative-strand RNA intermediate. In these complexes, the capsid protein binds to the viral genome, which is enveloped by a lipid bilayer subverted from host cell membranes. This membrane is embedded with prM/M and E proteins that form an icosahedral matrix to protect the virion, and mediate entry into cells [33]. The virions mature through the host secretory pathway [34] and undergo post translational modification including the cleavage of prM by furin proteases to produce the mature M protein [35]. The mature and 'mosaic' partially mature infectious virions are released from infected cells [36].

The ZIKV genomic RNA contains 5' and 3' highly structured UTRs that are approximately 107 and 428 nucleotides in length (see Figure 1.2). As part of the ZIKV infection, the methytransferase domain of the ZIKV NS5 protein caps the 5' end of the viral genome as an initiation signal for translation and to protect the genome from degradation [37]. There is also evidence presented by Lichinchi et al. that suggests that further methylation of the ZIKV genome by host methyltransferases occurs and affects viral replication [38]. The 5' and 3' UTRs of the ZIKV genome have numerous roles. Viral UTRs are highly structured areas of the genome consisting of stem loops of viral RNA. For example, the 5' UTR is required for effective recruitment of the RdRP, and is also required for effective 5' capping of the genome [39]. The 3' UTR is an important interaction site for several host RNA-binding proteins with roles ranging from stress granule inhibition, replication, and have been implicated the pathogenesis of microcephaly [39]. Importantly, the 5' and 3' UTR structure stalls host exoribonucleases and results in the formation of subgenomic flavivirus RNA (sfRNA). Not only does this stalling of exoribonucleases result in decreased activity

of the nucleases, the resulting sfRNA act as important antagonists of the innate immune response [40], [41]. This observation is seen across the *Flavivirus* genus and provides more roles for vRNA than simply acting as genomic material and mRNA transcripts involved in the viral lifecycle.

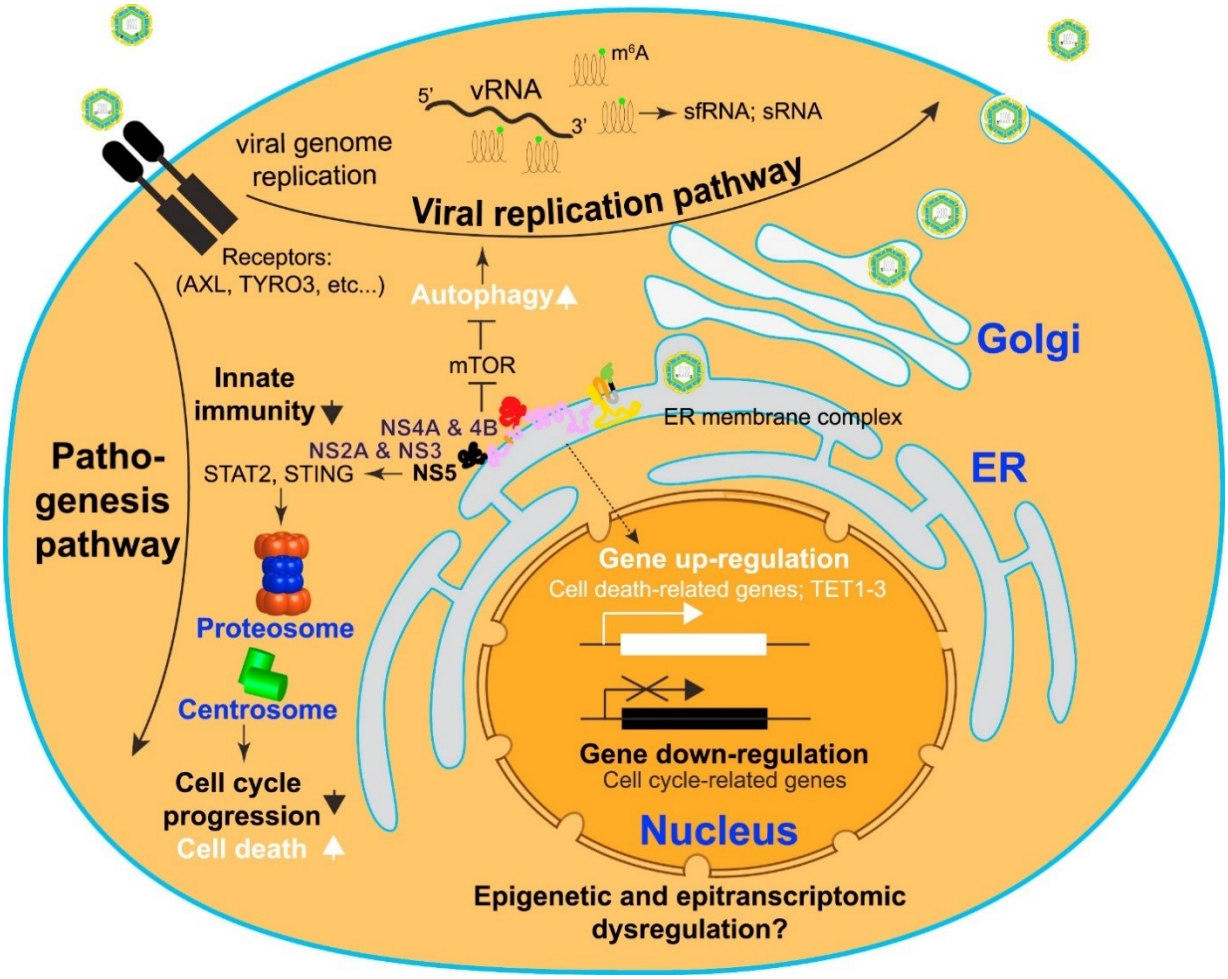

Figure 1.2: The life cycle of the Zika virus.

ZIKV virions enter the host cell through receptor-mediated endocytosis and the acidification of the endosomes facilitate viral membrane fusion with host membrane and virion content release into the cytoplasm. Genomic vRNA is then translated into a polyprotein by host machinery. Viral proteins affect host pathways by antagonizing the host immune response by degrading STAT2/STING or inducing numerous host cell pathways. Infection with ZIKV also results in the up- and down-regulation of many host genes to aid in replication. Viral proteins also modulate host pathways that result in the inhibition of neurogenesis and promotion of cell death. Reproduced with permission from (Ming et al. 2016) Cell Press, original publication DOI:10.1016/j.stem.2016.11.014.

1.1.2 Molecular mechanisms associated with ZIKV infection

As a positive sense single-stranded RNA virus, ZIKV results in the activation of the toll-like receptor TLR3, which senses dsRNA as it is generated throughout the replicative cycle of ZIKV [42]. The activation of TLR3 results in the activation of a downstream signaling pathway which involves numerous regulatory factors. The final step of the activation of this pathway results in the induction of type I and II IFNs, cytokines and interferon stimulated genes (ISGs) [42]. It has been demonstrated that the depletion of the dsRNA sensitive TLR3 in human skin fibroblasts results in a robust increase in the production of ZIKV RNA without any change in the type I IFN mRNA levels [43]. This TLR3 response pathway has been proposed to be a possible mechanism of microcephaly as it has been suggested that hyperactivation of the innate immune response from TLR3 activation results in impaired neurogenesis and an upregulation of apoptosis [44].

Both arms of the apoptosis pathway have also been suggested to be modulated during ZIKV infection. ZIKV infection was shown to result in a robust activation of the apoptosis effector protein, caspase-3 observed by immunofluorescence imaging. This was shown to be a mostly paracrine effect in nearby uninfected neurons mediated by the release of cytotoxic factors from infected cells [45]. This was described as another possible mechanism for ZIKV associated microcephaly in neonates. Ghouzzi et al. demonstrated that following infection of hNPCs with ZIKV, the tumor suppressor protein p53 was activated and subsequently resulted in increased apoptosis [46]. They also demonstrated that inhibition of p53 using drugs, or phosphorylation of p53, resulted in decreased apoptosis in hNPCs. Limonta et al. suggest that human fetal

astrocytes infected with ZIKV resist apoptosis and may act as reservoirs for ZIKV in the developing fetal brain [47].

Infection with ZIKV also results in the activation of autophagy as evidenced by the formation of autophagosomes in ZIKV infected skin fibroblasts [43]. Autophagy is a pathway that results in the lysosomal degradation of selected substrates, and plays mostly pro-viral roles in the viral lifecycle [48]. In ZIKV infections, it is suggested that the induction of autophagy is related to ER stress initiated by the viral proteins NS4A and NS4B that facilitate the induction of replication complexes [32]. NS4A/B are also implicated in the inhibition of the mTOR pathway (Figure 1.2) which also results in the induction of autophagy in host cells [49]. The pro-viral role of autophagy during ZIKV infection is supported by the observation that treating cells with rapamycin increases ZIKV replication, while inhibiting autophagy results in modest decreases in ZIKV replication [50]. Recent research by Lennemann and Coyne suggests that ZIKV NS2B/3 cleave the ER-autophagy specific receptor FAM134B [51]. This cleavage is suggested to result in ER expansion that provides an increase in membrane surfaces for invaginations that are a part of ZIKV viral replication. This observation is consistent with the observation that a depletion of interferon induced protein with tetratricopeptide repeats 3 (IFIT3) results in increased ER expansion and vacuolization and a concomitant increase in the replication of ZIKV in this condition [52].

The massive ER remodelling (described above) in ZIKV infection triggers the unfolded protein response (UPR) pathway. Infection with ZIKV results in ultrastructural changes of the host cytoskeleton and ER [29], and also results in the induction of

massive vacuolization (also derived from the ER) and later cell death [52]. These massive changes to the host ER, and excess translation of viral proteins, likely lead to ER stress and the induction of the UPR. The UPR consists of three proteins that sense either unfolded or misfolded proteins within the lumen of the ER (PERK, ATF6, and IRE1β). It functions to preserve ER homeostasis by inhibiting protein synthesis and the transcriptional induction of genes that code for protein chaperones as well as genes in the ER-associated degradation pathway (ERAD) [53]. Failing this function, the UPR ultimately leads to the apoptotic death of the cell. There is evidence that ZIKV infection activates all three of the arms of the UPR, but the result of this activation is dependent upon the cell type [54]. Inhibition of two arms alters the ZIKV infection: pharmacological inhibition of the PERK arm of the UPR in a mouse model restored neurogenesis but did not affect overall viral replication [55]; pharmacologic inhibition of IRE1β resulted in a decrease in ZIKV replication in mouse models as well as the prevention of microcephaly [55]; the role of the final arm of the UPR, ATF6, remains understudied in the context of ZIKV with only an increase in ATF6 expression observed in a mouse model [56]. While the mechanism of ZIKV induced modulation of the UPR is still unclear, the current consensus on the UPR and ZIKV is that it plays an important role in the pathogenesis of the ZIKV infection [57], and on microcephaly in particular.

1.1.3 ZIKV and the host immune response

Infection of organisms with pathogens has been occurring since the origin of single cell organisms, and it is likely that they have been co-evolving since [2]. As such, as viruses infect organisms, organisms fight back via immune responses, and this

results in an evolutionary 'arms race' between infectious agents and their hosts. ZIKV is no exception to this rule and the resultant interaction between viral infection and host immune responses following ZIKV infection is very complex and very interesting area of study.

One of the first defense systems against viral infections imposed by human host cells is mounted by the innate immune system. This system consists of pattern-recognition receptors (PRRs) that sense conserved features of 'non-self' pathogens [58]. The activation of these PRRs activate the transcription of type I IFNs. Secreted IFNs then activate cells in an autocrine and paracrine manner, resulting in the induction of an antiviral state in the infected cell as well as neighbouring cells. This antiviral state results in a signaling cascade and the eventual induction of IFN stimulated genes (ISGs) [59]. While replication of ZIKV has been shown to be inhibited by type I IFNs in cells [43], ZIKV has evolved to include several strategies to antagonize both signaling pathways using the non-structural proteins encoded by the ZIKV genome (see Figure 1.3).

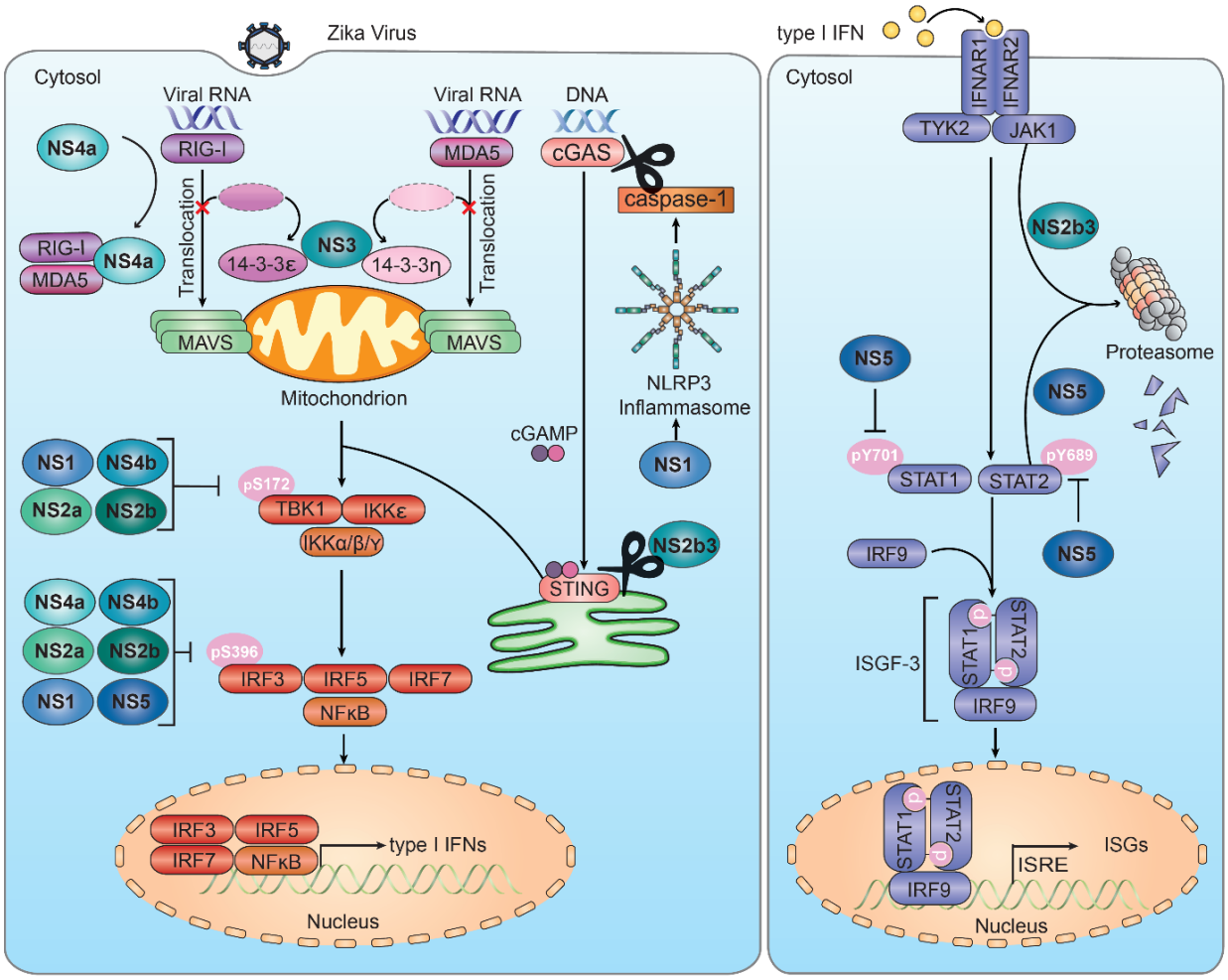

Figure 1.3: Inhibition of innate immune signaling pathways in viral replication.

Numerous ZIKV proteins are involved in inhibiting signal transduction following viral infection, that would normally lead to a robust induction of type I IFNs (left panel) and ISGs (right panel). Every ZIKV non-structural protein has been implicated in the antagonism of an aspect of the viral surveillance/type I IFN induction pathway, and the ISG activation pathway. TLR3/7 are also implicated in sensing ZIKV infection but are not included in this figure. Reused with access granted through MDPI Open Access Policy (Serman and Gack, 2019), original publication DOI: 10.3390/v11100970.

ZIKV infection results in the inhibition of IFN production by evading two major signaling modalities; the RIG-I like receptor-MAVS (RLR-MAVS) signaling and the cyclic GMP-AMP synthase – stimulator of interferon genes (cGAS-STING) axis. The RLRs include the retinoic acid-inducible gene I (RIG-I) and the melanoma differentiation-associated protein 5 (MDA5) that function as PRRs capable of detecting viral genomes in the cytoplasm. ZIKV NS4A has been shown to block this signalling pathway at the RLR level by blocking the RLR association with MAVS preventing downstream activation of the cascade [60]. The cGAS-STING axis was shown to be disrupted by either cleavage of STING by the viral protease complex NS2B/3 [61] or by the inflammasome mediated cleavage of cGAS following activation by NS1 [62]. The last step prior to activation of type I IFN production is TANK binding kinase 1 (TBK1) and interferon regulatory factor 3 (IRF3), proteins which ZIKV NS proteins were shown to inhibit. TBK1 was shown to be inhibited by viral NS1, NS2A, NS2B, and NS4B, while IRF3 was found to be antagonised by the ZIKV proteins NS2A, NS2B, NS4A, and NS4B [63], [64]. Most of the research that has shown that ZIKV NS proteins antagonize the host IFN production have been done outside of an active infection and so this remains an important area of study. There is also very little knowledge surrounding the effects of type II and III IFNs on ZIKV infection [65].

The other arm of immune signaling that ZIKV targets is the interferon-alpha/beta receptor (IFNAR) signalling pathway that is activated by type I IFNs and results in the induction of ISGs (See Figure 1.3 – right panel). Following the production and secretion of IFN from infected cells, IFN α/β binds to IFNAR1/2 and initiates the Janus kinase – signal transducer and activator of transcription (JAK-STAT) pathway and culminates with the induction of ISGs [66]. These ISGs are transcribed and translated

into immune effector proteins that directly or indirectly counter viral infections and so, in turn, ZIKV has established mechanisms of antagonizing the JAK-STAT pathway. Specifically, ZIKV has been shown to antagonize the pathway by: inhibiting the phosphorylation of STAT1 and STAT2; degrading JAK1; and degrading STAT2 [64], [67]. This inhibition of the induction of ISGs allows for a more robust ZIKV infection and replication in infected cells.

Along with the perturbation of host cellular pathways and immune responses described above, ZIKV has also been demonstrated to interfere with the production of stress granules (SGs). SGs act anti-virally as they stall host translational machinery components to inhibit viral replication. Hou et al. have demonstrated that ZIKV infection results in the inhibition of stress granule formation triggered by cellular stressors including ER stress and dsRNA [68]. The group also suggests that ZIKV subverts host SG components to promote viral replication as well. Together, these data regarding ZIKV and the immune system suggest that the battle between ZIKV and the host immune response are complex and there is much that remains to be understood.

Evidence suggests that infection with ZIKV results in the perturbation of numerous host cellular pathways and the subversion of multiple host proteins and functions to support viral replication. In this thesis, we will focus on both the effect of ZIKV infection on, and explore possible roles of, two host proteins: the heterogeneous nuclear ribonucleoprotein M (hnRNP M) and isoforms encoded by the interleukin enhancer binding factor 3 (*ILF3*) gene, NF90 and NF110.

1.2 hnRNP M – heterogeneous nuclear ribonucleoprotein M

1.2.1 Structure

The heterogeneous nuclear ribonucleoprotein M (hnRNP M) is an RNA binding protein that belongs to a family of more than twenty nuclear RNA-binding proteins that associate with heterogeneous nuclear RNA (hnRNPs). This family of proteins contributes to many aspects of nuclear metabolism such as mRNA stabilization during cellular transport, alternative splicing, and transcriptional and translational regulation [69].

The hnRNP family of proteins contain multiple functional domains connected by linker regions. The RNA recognition motifs (RRMs) are the most common domain, present in all family members, and they contact RNA through the RNP-1 and RNP-2 consensus sequences. These sequences bind RNA through hydrophobic interactions between two bases and four protein side chains (aromatic). This allows the RRM to bind single-stranded nucleic acids of variable length (including ssDNA) in a non-sequence specific manner [70]. While the RRMs themselves allow for the general binding of single-stranded nucleic acids, the linker regions, N- and C- terminals and the external RRM strands can allow for enhanced binding affinity for types or sequences of nucleic acids giving the RRM specificity [71].

hnRNP M is characterized by three RRMs, a glycine/methionine-rich region and a methionine/arginine-rich repeat motif (Figure 1.4) [72], [73]. There are four variants of hnRNP M (M1-4) that range in size from 68 to 72 kDa that represent spliced isoforms or posttranslational modifications [74], [75]. hnRNP M is also present in a

variety of other species including *Chironomus* and *Drosophila* and fulfills similar roles in those organisms as well [76].

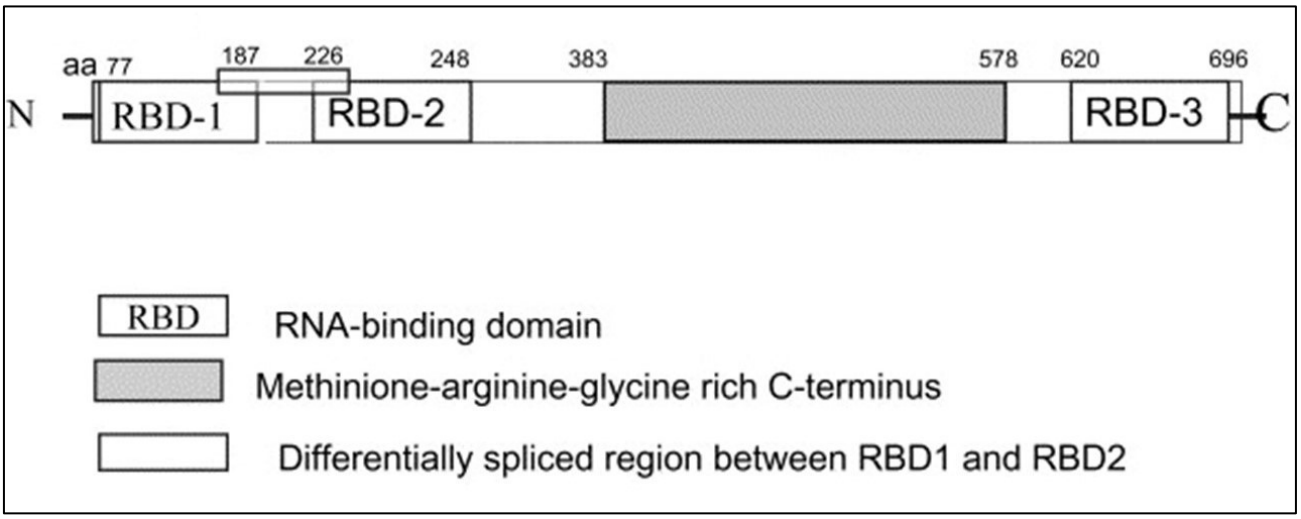

Figure 1.4: Schematic of the hnRNP M protein.

A schematic of the hnRNP M protein and its three RRMs as well as the Met-Arg-Gly rich domain. The numbers correspond to the amino acids. The differentially spliced region depicts the difference between the shorter hnRNP M1-2 and the longer hnRNP M3-4 isoforms. Adapted and reproduced with permission from (Bajenova et al, 2003) Experimental Cell Research, original publication DOI:10.1016/S0014-4827(03)00373-2.

1.2.2 Function and Pathology

hnRNP M is a protein with many diverse functions in cells with varying roles, expressions and even localizations that change in a cell type dependent manner. In most, if not all cells, hnRNP M is localized to the nucleus but in Kupffer cells (liver macrophages), some differentiated macrophages, and some cancer cells and cell lines (HT-29), it acts only as a cell surface protein and a receptor for carcinoembryonic antigen (CEA) [77]. In this role, investigators refer to hnRNP M protein as the CEA receptor (CEAR) and suggest that it may play a role in the anti-apoptotic and pro-metastatic properties of CEA in colon cancer cells [78]. There is abundant evidence that hnRNP M plays a role in the spliceosome complex and as a splicing regulatory protein and shows association with pre-mRNA complexes [73], [79]–[81]. Moreover, overproduction of hnRNP M has the ability to promote alternative splicing by inducing exon skipping and exon inclusion [81]. Given that hnRNP M is a primarily nuclear protein, there is also evidence that it is an RNA-binding protein that undergoes nucleocytoplasmic shuttling during pre-mRNA splicing and its return to the nucleus is facilitated by a nuclear localization sequence (NLS) and its interaction with Karyopherin β2 [82]. Chen et al. have shown that hnRNP M associates with the mammalian target of rapamycin (mTOR) via the protein Rictor and plays a role in the regulation of muscle differentiation [83]. This role was showing using a depletion of hnRNP M or Rictor that resulted in reduced myoblast differentiation, and that a reintroduction of hnRNP M to these cells rescued the phenotype. Another group has shown that hnRNP M plays a role in myoblast

differentiation by controlling promoter-dependent translation evidenced by both knockdown and overexpression of hnRNP M [84].

Given its extensive role in splicing, RNA metabolism, and transcription and translation, it is expected that hnRNP M would play a role in cancers. It has recently been identified as a novel biomarker for colorectal carcinoma [85] as its upregulation of both gene expression and protein levels were shown to be correlated with proliferation, invasion and metastasis of colorectal cancer. The group also showed that the depletion of hnRNP M in the CRC cell line LS174T resulted in a decrease in cell division and colony formation. Xu et al. has shown that hnRNP M promotes breast cancer metastasis by increasing the level of alternative splicing of certain genes that occurs during epithelial-mesenchymal transition (EMT). To examine this hypothesis, they depleted hnRNP M and observed that this depletion prevented EMT and inhibited breast cancer metastasis in mice. It was shown that this can be overridden by expressing the downstream alternative splice isoform of CD44 'rescuing' the EMT and metastasis phenotype of the breast tumors. Xu et al. also suggest that increases in hnRNP M are associated with more aggressive breast cancers and it also correlates with increased CD44s in patient specimens [86]. In contrast, hnRNP M is implicated in the genetic disease spinal muscular atrophy (SMA). hnRNP M is shown to play a role in exon 7 inclusion of survival motor neuron 1 and 2 (SMN1/2) gene expression and that the depletion of hnRNP M in this system results in exon 7 SMN1 and SMN2 gene skipping. Because of this, hnRNP M is considered as a possible therapeutic for SMA [87]. Lastly, hnRNP M is implicated in splicing changes in the carcinoembryonic antigen-related cell adhesion molecule-1 (CEACAM1) [88] and the dopamine D2

receptor (D2R) that play roles in carcinogenesis, and neurological and carcinogenic pathologies respectively.

1.2.3 Role in Infection

Not only does hnRNP M play a role in the splicing of genes involved in cancer and genetic diseases, there is also a body of evidence that it plays a part in different infections and the host immune response to them. In support of hnRNP M's role as a splicing factor, West et al. showed that the phosphorylation of hnRNP M at specific residues as a result of pathogen sensing resulted in the loss of Interleukin 6 (IL6) splicing repression and the expression of the full and biologically active spliced IL6 gene [89]. These data showed that in macrophages there are two activation states of hnRNP M based upon phosphorylation of hnRNP M's residues that resulted in differential expression of immune genes when infected with *Salmonella*. Moreover, loss of hnRNP M in these macrophages enhanced their ability to control both bacterial and viral infection and enhanced the macrophage immune response to infection mimetic treatments. Similarly, a group showed that dengue virus (DENV) infection could be decreased by depleting hnRNP M. This resulted in a decrease of both infectious titers produced as well as a decrease in DENV viral RNA levels in the cells although they did not provide any possible reasons for this effect [90]. Other data suggest that hnRNP M is a substrate of both poliovirus (PV) and coxsackievirus B3 (CVB3) as the protein gets cleaved during infection. hnRNP M fragments are shown to relocalize to the cytoplasm of infected cells and data are presented that suggest hnRNP M promotes both PV and CVB3 infection. When hnRNP M is depleted, poliovirus infection is delayed and inhibited to some degree and hnRNP M depletion results in a

decrease in extracellular virus and intracellular viral genomic RNA [91]. Whether this is a result of the increased responsiveness of the immune response genes in the context of hnRNP M depletion, or due to a direct role of hnRNP M in the lifecycle of the virus, was not explored. A study that examined the role of hnRNP M in Sendai virus infection (recently renamed murine respirovirus) showed that overexpression of hnRNP M resulted in a dampened immune response to infection while the depletion of hnRNP M resulted in a much stronger immune response and lowered viral replication [92]. This group suggests that hnRNP M may act as a decoy by impairing the RLRs ability to sense the viral PAMPs and provide a control mechanism for the host to prevent too strong an immune response.

In contrast to the above evidence however, research suggests that hnRNP M can act as a type of PRR that senses listeriolysin O and restricts the growth of *Listeria monocytogenes* in host cells. It was also reported that the knockdown of hnRNP M in these cells inhibited the listeriolysin O induced activation of the immune genes IFN-α, IFN-β and AP-1 and resulted in increased growth of the bacteria in the depleted cells [93]. In another instance where hnRNP M plays an anti-pathogen role, investigators examined the alphaviruses: Semliki Forest virus (SFV); Chikungunya virus (CHIKV); and Sindbis virus (SINV). These data from these viruses suggest that not only does hnRNP M bind to SINV RNA [94], but that depletion of hnRNP M results in enhanced replication of SFV, CHIKV and SINV [95]. hnRNP M was also shown to be redistributed to the cytoplasm of cells infected with SFV and depletion of hnRNP M directly lowered titers and viral genomic production in wild type SFV. The data for CHIKV and SINV both utilized luciferase replicons that lacked the structural proteins to examine the effect of hnRNP M depletion on them and so the effect of hnRNP M

depletion in these cells remains to be elucidated with full length/wild type viral infections.

The evidence presented above indicates that hnRNP M is involved in numerous host processes such as splicing, RNA metabolism, transcription and translation, cancers, and infections. However, despite this body of knowledge surrounding hnRNP M the is little evidence supporting its role in viral infections and no evidence suggesting a possible role in ZIKV infection. In this thesis, we will further discuss a possible role for the hnRNP M protein in the lifecycle of a ZIKV infection.

1.3 NF90/NF110

1.3.1 Structure

The interleukin enhancer binding factor 3 (*ILF3*) gene encodes up to 6 different splice variants as shown in Figure 1.5. All isoforms contain two copies of conserved double-stranded RNA binding domains (dsRBD1/2). There are various names for the isoforms of the *ILF3* gene. Consistent with previous descriptions, I will refer to two common protein isoforms, a 110kDa species as NF110 and a 90kDa species as NF90 (Table 1-1).

NF90	NF110
NF90b	NFAR-2
DRBP76	Ilf3
MPP4	NF110b
NFAR-1	TCP110
NFAT-90	
TCP80	

Table 1-1: Nomenclature used for the NF90 and NF110 isoforms encoded by the *ILF3* gene.

Alternate names used in literature. DRBP (double-stranded RNA-binding protein), MPP4 (M-phase phosphoprotein 4), NFAR (nuclear factor associated with double-stranded RNA), NFAT (nuclear factor of activated T cells), TCP (translation control protein). Names used in papers generally reflect the context in which the protein was discovered.

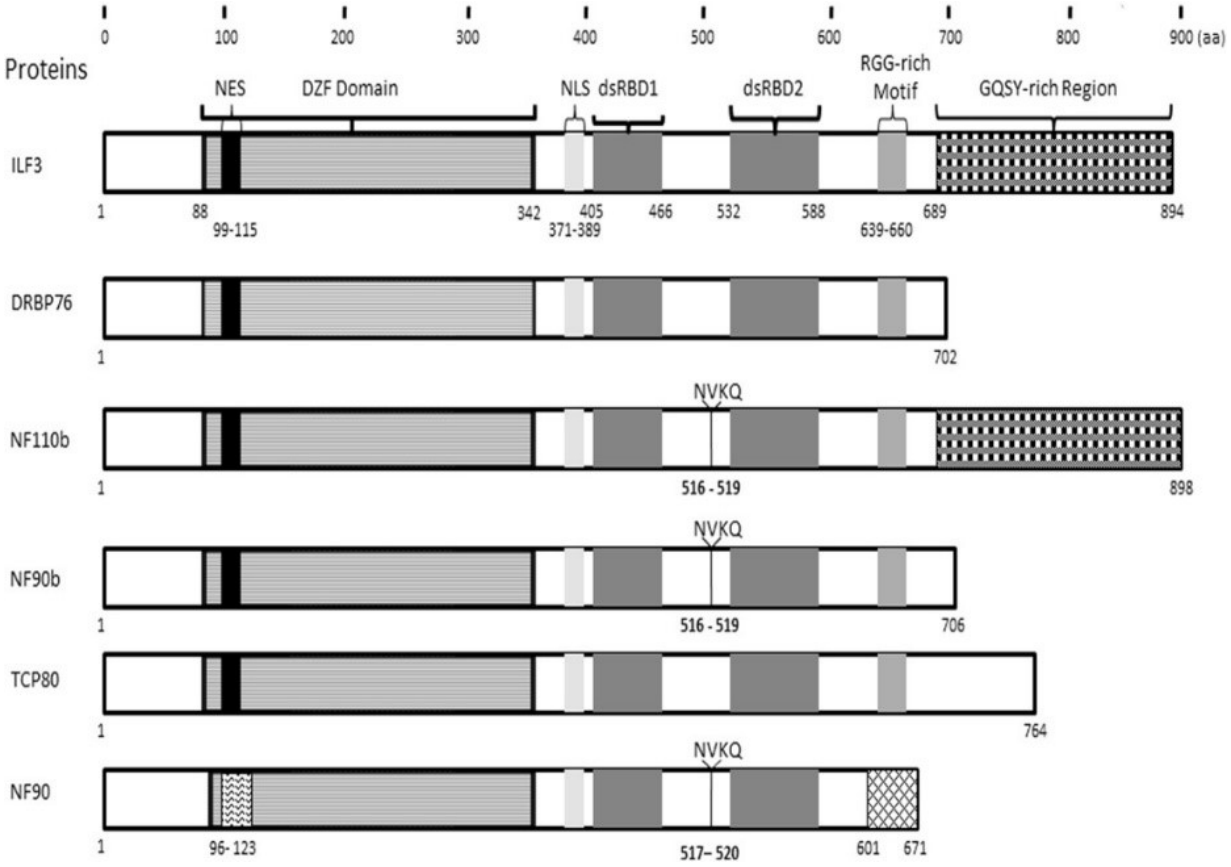

Figure 1.5: Schematic of the protein isoforms encoded by the *ILF3* gene.

Schematic representing the *ILF3* isoforms. Shown are the nuclear export signal (NES), the dsRNA binding motif and zinc finger associated domain (DZF Domain), the nuclear localization sequence (NLS), double stranded RNA binding domains (dsRBD1/2), the Arg/Gly-rich motif (RGG-rich Motif), and the Gly-Gln-Ser-Tyr-rich region (GQSY-rich Region). Adapted and reproduced with permission from (Patiño et al, 2014) Biochimie, original publication DOI:10.1016/j.biochi.2014.10.022/.

NF110 and its isoforms arise thanks to the presence of two frameshift; two splicing; and three alternate polyadenylation signals. Arguably the most important event is the two splicing events that transcripts can undergo. The first alternative splicing event that leads to the inclusion of the NVKQ tetrapeptide between the two dsRBDs, and the second alternative splicing event that leads to transcripts with a different 3' UTR [96]. One of the most divergent proteins from the list is the NF90 protein (see Figure 1.3) that arises from two splicing and two frameshift events that exclude the NES and another event that excludes the RGG-rich motif but maintains the NVKQ tetra-peptide [96]. The role of the NVKQ peptide is currently unknown

The RGG motif in the C-terminal region and the GQSY-rich region are both capable of binding nucleic acid but absent from NF90 (Figure 1.3). The DZF domain allows for the formation of a heterodimer with NF45 that helps to stabilize the proteins as a depletion of NF45 results in a drastic decrease in the levels of NF90 and NF110 [97]. The NLS and NES that exists in nearly all the isoforms results in the nuclear and cytoplasmic localization seen in *ILF3* and its isoforms. These nucleocytoplasmic transport signals also allow the *ILF3* isoforms to access the nuclear compartment for their role in gene expression, transcription, transcript stability and mRNA export. In concert, the NES allows the proteins access to the cytoplasm to participate in translation and participate in both immune and dsRNA responses. Each isoform contains two dsRBDs that bind readily to PKR [98], host cell dsRNAs [99] and viral dsRNAs [100], [101].

1.3.2 Function and Pathology

Isoforms encoded by the *ILF3* gene are nearly ubiquitous throughout human tissues, with little variability in expression levels and very high protein expression in all tissue types tested except for eye and blood specimens [102], [103].

Transcription was one of the first roles that NF110 was discovered to play. NF110 was found to be in the nuclear factor of activated T cells (NFAT) complex bound to the IL-2 promotor in T cells. Its presence was shown to allow for the transcription of IL-2 [104] which resulted in the name interleukin enhancer binding factor 3. Both NF90 and NF110 interact with protein kinase R (PKR) as they act as both a substrate to and a regulator of PKR [105] and help to facilitate the expression of double-stranded RNA response genes with a role in immunity. Given the predominantly nuclear expression of NF110, it is unsurprising that there is ample evidence that the protein can help to both positively and negatively regulate transcription in the cell. Its ability to either up- or down-regulate expression of genes is dependent upon the promotor [99]. The depletion of NF90 suppresses cell growth via the inhibition of DNA synthesis and interferes with mitotic control in HeLa cells resulting in giant multinucleated cells [97].

NF110 also plays a role in both the control of mRNA translation and mRNA turnover within cells as it is translocated to the cytoplasm of cells. Evidence suggests that NF90 prefers to associate with AU-rich areas in the 3’ UTRs of mRNAs and represses the translation of these transcripts [106]. A gene ontology search of the list that was found by RIP-chip showed a strong enrichment in M-phase dependent proteins and matches with other literature evidence of cell cycle involvement [107]. Interestingly,

NF90 appears to be able to both limit and enhance translation of certain transcripts as well as enhance the stability of some mRNAs [108]. Pfeifer et al. reported that NF90 and NF110 are involved in the regulation of the nuclear export of mRNA and in retaining transcripts in the nuclei of cells. They also suggest a role in stability as the two proteins remain associated with ribonucleoprotein complexes that are exported from the nuclei. A depletion of NF110 transcripts results in an increase of global translation and an increased susceptibility to infection with vesicular stomatitis virus (VSV) [109]. Some other transcripts that it appears to enhance the stability of include IL-2 in T cell activation [110], vascular endothelial growth factor (VEGF) in response to hypoxia [111], mitogen-activated protein kinase 1 (MKP-1) in oxidative stress [20], and three myogenic regulatory mRNAs in mice [107]. Exactly how NF110 functions to either suppress or enhance translation and how it achieves specificity remains to be elucidated.

Previous studies have reported that NF110 plays a role in microRNA biogenesis. MicroRNAs (miRNAs) are small RNAs that are approximately 22 nucleotides in length and help to regulate gene-expression post-transcriptionally. miRNAs have been implicated in allergies, cancer (as both pro- and anti-oncogenic factors), diseases and are being studied for possible therapeutics [112]–[114]. NF90 complexes with Drosha to form the microprocessor complex [115] and the NF90/NF45 complex acts as a negative regulator of a number of miRNAs by blocking the processing of pre-miRNAs (precursors to miRNAs) [116], [117]. Interestingly, there are other miRNAs that the NF90 complex elevates the expression of while still decreasing their pri-miRNA (precursor to pre-mRNAs) levels [118]. Given the numerous roles for miRNAs in infection, allergy, cancer and other diseases, alongside with the role that NF90 and

NF110 are playing in their biogenesis it is entirely expected that NF110 should be found playing a role in all of the aforementioned afflictions.

Given that NF110 has roles in transcription, translation, and miRNA biogenesis, it is not surprising that NF110 has been implicated in several different cancers. Notably, NF90 has been reported to be overexpressed in breast cancer, ovarian cancer, liver cancer, non-small cell lung carcinoma, nasopharyngeal carcinoma, gastric carcinoma, cervical, colorectal, bladder, and ovarian cancer [116], [119]–[127] (among many others). NF110 has been implicated in tumorigenic functions with changes to miRNA, long non-coding RNAs, oncogene expression changes, immune pathway changes, and angiogenesis with the cancers mentioned. With respect to breast cancer, evidence suggests that NF110 depletion led to a significant decrease in the level of migration, invasion, cell growth, and *in vivo* breast tumor development. Interestingly, elevated nuclear, but not cytoplasmic, NF110 (assayed using immuno-histochemistry) correlated with high grades of human breast cancer specimens and urokinase-type plasminogen activator (uPA) expression [119]. Lastly, NF110 depletion also resulted in decreased cell activity in gastric tumor cell lines [123].

1.3.3 Role of *ILF3* encoded proteins in infection

From the initial characterization of NF110 as a transcriptional regulator of IL-2, the knowledge surrounding NF110 and its role in the immune response have expanded greatly. For example, following the autophosphorylation of PKR upon sensing dsRNA, a by-product of infection, phosphorylated PKR then in turn phosphorylates other proteins. The most well-known target is the α subunit of the eukaryotic protein synthesis initiation factor 2 (eIF2α). This results in the formation of stress granules

(SGs) and the arrest of global protein translation in response to viral infection [128]. Another protein that PKR phosphorylates is NF110. It targets all of the isoforms by phosphorylating NF110 at T188 and T315 which then result in the shutdown of translation [129]. It was then shown that NF110 interacts with PKR and plays a role in the formation of SGs [124]. Interestingly, the depletion of NF90/NF110 did not influence the levels of phosphorylated eIF2α. Because NF110 is required as a key regulator in the biogenesis of circRNAs, and is enrolled in the antiviral response, there is a corresponding decrease in the production of circRNAs during infection in cells depleted of NF90/NF110 [130]. Recent research suggests that NF110 assists in the translation of IFNB1 and ISGs during the antiviral host translational blockade. In this study, the authors show that depletion of NF110 does not result in lower gene expression of IFNB1, but it did result in decreased translation of IFNB1 and a subgroup of other ISGs implicating NF110 as a factor allowing the translation of ISGs despite the host translation blockade [131].

Not only does NF110 play an important role in the translation of host ISGs, it also directly affects the viral lifecycle by interacting with the viral genome. NF110 has the ability to bind host RNAs and DNAs [99], and thus it is thought that NF110 and NF90 have the ability to bind to viral nucleic acids [100], [101]. Consistent with this idea, NF90 interacts with the 3’ UTRs of DENV genomic RNA and acts as a positive regulator of DENV infection. Moreover, DENV infection facilitates the redistribution of NF90/NF110 to the cytoplasm of infected cells [100]. Similarly to DENV, HCV requires NF90 for efficient replication and also results in the redistribution of NF90 to the replication complexes of HCV infected cells [132]. Still other data examining HCV suggest that NF110 and NF90 are recruited to facilitate the 5’ to 3’ genome

circularization and interaction. The authors also postulate that the recruitment of NF110 to the replication factories may also weaken the host antiviral defense [101]. NF110 also interacts with bovine viral diarrhea virus (BVDV) genomic material and participates in the circularization of the viral RNA genome to aid in replication [133]. Lastly, NF110 interacts with the 3’ UTR of the tick-borne encephalitis virus (TBEV) and the loss of the 3’ stem loop structures resulted in decreased interaction of NF90/NF110 with the TBEV RNA [134]. The authors did not explore the possible role that NF90/NF110 binding to the TBEV genome might have.

NF110 and its isoforms not only interact with viral genomes, but they also interact with viral proteins to play roles in viral infections. The influenza A virus (IAV) nucleoprotein (NP) interacted with NF90 in a non-RNA dependent manner, and the depletion of NF90 resulted in a massive increase of IAV replication suggesting an antiviral role in IAV infection [135]. Similarly, NF90 binds to HIV Rev and interferes with the ability of Rev to facilitate RNA export. Not only is this inhibition accomplished by binding to Rev-response elements (RRE-RNA), NF90 also binds to HIV Rev itself via a protein-protein interaction [136]. In human papillomavirus (HPV) infections, NF90, in concert with NF45, aided the expression of the viral E6 protein that targets host p53 for degradation. Depletion of the NF90/NF45 complex resulted in decreased E6 expression, increased p53 production and an increase in the downstream p21 protein attenuating viral production and promoting cell death [137]. In the human rhinovirus serotype 2 (HRV2), this same NF90/NF45 complex was found to inhibit viral translation initiation at the HRV2 IRES [138]. NF90 also interacts with the Ebola virus (EBOV) protein VP35 and suppresses the function of the viral polymerase attenuating the infection [139].

The evidence above suggests that isoforms encoded by the *ILF3* gene have numerous roles in the lifecycle of the host cell from transcription and translation, to miRNA biogenesis and cancer. The isoforms are also implicated in numerous infections and cancers. Despite this growing body of knowledge, there is no evidence suggesting a role of NF90/NF110 in the lifecycle of ZIKV infection. In this thesis, we will further discuss a possible role for NF90/NF110 in the lifecycle of a ZIKV infection.

2 MATERIALS AND METHODS

2.1 Cell Culture

2.1.1 Immortalized cell lines

Human cell lines including HEK293T (ATCC), A549 (ATCC), and African Green Monkey Vero E6 cells (ATCC) were maintained in Dulbecco's modified Eagles medium (DMEM) (Thermo Fisher Scientific Cat No. 11965-092). Media was supplemented with 10% fetal bovine serum (FBS) (Thermo Fisher Scientific Cat No. 12483-020) and 1% penicillin-streptomycin solution (Thermo Fisher Scientific Cat No. 15070-063). All adherent cell lines were kept at 25% to 90% confluence and cultured to a passage of 12 max. All cell lines were maintained at 5% CO_2 and 37°C. Trypsin-EDTA 0.05% solution (Thermo Fisher Scientific Cat No. 25300-062) was utilized to detach adherent cell lines for sub-culturing as required. Preservation of cell lines was done by freezing in Recovery Cell Culture Freezing Medium (Thermo Fisher Scientific Cat No. 12648-010) at -80°C.

2.1.2 Cell viability assays

Precise determination of cell cytotoxicity following ZIKV infection (Figure 1) was performed using the Cell Cytotoxicity Assay Kit (Abcam, Cat No. ab112119). Cells were seeded in 96 well black wall flat bottom plates (10^4 cells/well) and infected with ZIKV as described in 1.3.2. Assay solution was added to cells (1/5 volume of growth media) and incubated for 1 hour at 37°C. Mitochondrial dehydrogenase activity was measured based on the reduction of oxidized non-fluorescent blue resazurin to red fluorescent resorufin following the acceptance of an electron from the mitochondrial respiratory chain in live cells. Produced resorufin is directly proportional to the number of living cells. Fluorescence readings were recorded using a CLARIOstar microplate reader (BMG Labtech).

Determination of cell viability of shRNA treated cells (Figure 13F) was performed using the CellTitre-Glo Luminescent Cell Viability Assay (Promega, Cat No. G7670). Following lentiviral transduction for 72h as described in 1.3.2, cells were seeded into

96 well white wall flat bottom plates (10^4 cells/well) to begin measurement at 72h post transduction. Assay solution was prepared as per manufacturers guidelines and added to growth media in equivalent volumes. This assay is based on the quantitation of the ATP present as an indicator of metabolically active cells. Cellular ATP facilitates the reaction of luciferin to the luminescent oxyluciferin. The amount of ATP is directly proportional to the number of cells present in the culture. Mixtures were allowed to equilibrate at room temperature for 10 minutes prior to measurement. Luminescence was measured using a SYNERGY plate reader.

2.2 Viral infections

2.2.1 Zika virus production

Vero cells were seeded at a density of 10^5 cells/mL in T175 flasks for 16 hours prior to infection in DMEM with 10% FBS and HEPES was added to supplement buffering abilities. Cells were infected (MOI of 1) of serially passaged ZIKV (generously provided by Dr. Tom Hobman, University of Alberta). Supernatants containing ZIKV were collected 24h, 48h and 72h post infection. Supernatants were then centrifuged at 500g for 10 minutes to clear cell debris. Supernatants were then aliquoted and stored at -80°C.

2.2.2 Quantification of plaque forming units

ZIKV titers were determined by infecting Vero cells with serial 10-fold dilutions. Vero cells were seeded in 24 well plates at $2x10^5$ cells per well. Six serial dilutions were used, and each dilution was done in technical duplicate. Cells were infected for 1 hour and then media was replaced with 1mL 1.5% carboxymethylcellulose (CMC) in minimal essential media. Cells were plaqued for 4 days at 37°C and 5% CO_2. Cells were then fixed by adding 1mL of 10% formaldehyde solution to the plaqueing media for 30 minutes at room temperature. Following fixation, media was removed and wash multiple times with water then excess water was removed by tapping on paper

towel. Staining solution was then added (10% ethanol, 0.1% crystal violet in water) and incubated for 15 minutes. Stain was removed and wells were washed with water and dried. Plaques were then counted for each viral sample and plaque forming units per mL were calculated.

2.2.3 Infection of mammalian cells with ZIKV

A549 cells were seeded at a density of $2x10^5$ cells/mL in chosen plates. Cells were then infected with previously titered ZIKV at an MOI of 3 and incubated at 37°C in 5% CO_2 for 1 hour. Following incubation, innocula was replaced with DMEM (10% FBS and 1% PenStrep). Cells were then collected as per each experiment at times indicated.

2.3 Lentivirus production and shRNA mediated host protein depletion

2.3.1 Lentivirus production in HEK293t cells

Lentivirus pseudo-particles were produced in HEK293t cells in 6 well plates, or T75 flasks to scale, as previously described [31]. Cells were transfected with the necessary plasmids for lentiviral production using Lipofectamine 3000 (Thermo Fisher Scientific, Cat No. L3000008). Plasmids used for lentiviral production were the previously described [140]: HIV gag-pol (11.4 µg), vesicular stomatitis virus glycoprotein (4.5 µg), and the pLKO.1 pure shRNA as indicated (15µg, Sigma-Aldrich Mission shRNA), see table 2-1. Samples labeled control shRNA contain an shRNA sequence targeted to a non-mammalian transcript for control. Cells were transfected according to the manufacturers protocol. Supernatants were collected at 24h and 54h post transduction. Supernatants were cleared by centrifugation at 500g for 5 minutes. The lentiviral pseudo-particles were then concentrated using Lenti-X Concentrator (Clontech, Cat No. 631231), reconstituted in DMEM, aliquoted and flash frozen in liquid nitrogen prior to storage at -80°C. Viral titers were determined by

transducing A549 cells were serially diluted lentiviral pseudo-particles and then selecting for transduced cells with 2 µg/mL puromycin dihydrochloride (Thermo Fisher Scientific, Cat No. A1113803) for 7 days. Colonies of surviving cells in each well were counted and the colony forming units were then calculated.

2.3.2 Transduction with lentiviral pseudo-particles

A549 cells were seeded 16h before transduction with lentiviral pseudo-particles for a 50-80% confluence at time of transduction. Cells were then transduced with an MOI of 2 in DMEM media with 10% FBS and 8 µg/mL of hexadimethrine bromide (AKA Polybrene, Sigma-Aldrich, Cat No. H9268). Transduced cells were incubated for 24 hours at 37°C in 5% CO_2 for 24 hours at which point the media was replaced with fresh DMEM with 10% FBS, 1% PenStrep and 2 µg/mL. Cells were subcultured as necessary and seeded for infection or downstream use 72h post transduction.

Target mRNA	Clone ID
NF90/NF110	TRCN0000014581
hnRNP M	TRCN000001245
Control	SHC002
All clones purchased from Sigma-Aldrich	

Table 2-1: Lentiviral shRNA clones.

2.4 Nucleocytoplasmic transport inhibitor treatment

A549 cells were seeded 16 hours prior to beginning experiment. Depending on the experiment, infection with ZIKV was carried out prior to treatment with nucleocytoplasmic transport inhibitors. For treatments, nucleocytoplasmic transport inhibitors were diluted into DMEM media containing 10% FBS and 1% PenStrep and added to cells for 6 hours. Three nucleocytoplasmic transport inhibitors were used:

Leptomycin B (LMB, Sigma-Aldrich, Cat No. L2913), Importazole (IPZ, Sigma-Aldrich, Cat No. SML0341), and Ivermectin (Iver, Sigma-Aldrich, Cat No. 18898). LMB was reconstituted in ethanol to a stock concentration of 18.5 µM. IPZ and Iver were reconstituted in DMSO to a stock concentration of 40 mM and 50 mM, respectively. Final working concentrations for drug treatments was 18.5 nM LMB, 40 µM IPZ, and 10 µM Iver.

2.5 SDS-PAGE and western blot

Whole cell lysates were collected from samples following infection or treatments as indicated, in 2x Sample buffer and promptly boiled at 90°C. Proteins were then resolved by SDS-PAGE and transferred to nitrocellulose membranes (0.2 µM, Bio-Rad, Cat No. 9004-70-0). Membranes were blocked in 5% skim milk in PBSt (PBS containing 0.1% Tween 20) and incubated with primary antibodies overnight at 4°C. Following 3 washes with PBSt, secondary antibodies conjugated to HRP were used to visualize primary antibody binding. Blots were visualized using Amersham ECL Western Blotting Detection System (GE Healthcare Life Sciences, Cat No. CA95038-570L) and detected on a GE ImageQuant LAS4000 imager.

2.6 Immunofluorescence microscopy

A549 cells were grown on round coverslips (Fisherbrand, Miroscope Cover Glass, Cat No. 12-545-81, 12CIR.-1.5) in 24 well plates and treated or infected as indicated. Following the end of the experiment, cell supernatants were removed, and cells were washed twice with PBS and then fixed for 10 minutes at room temperature with PBS containing 3.65% formaldehyde (Sigma-Aldrich, Cat No. F8775). Cells were then permeabilized for 2 minutes at room temperature with PBS containing 0.4% Triton X-100 (Thermo Fisher Scientific, Cat No. BP151-500). Cells were then washed with PBS then blocked in 2.5% skim milk in PBSt for at least 1 hour at 4°C. Cells were

probed with indicated primary antibodies in 2.5% skim milk in PBSt overnight at 4 ° C. Cells were then washed 3 times with PBSt prior to incubation with secondary antibodies conjugated to fluors at 4 ° C for 4 hours, then washed with PBSt 3 times. Cells were post fixed for 10 minutes in 3.65% formaldehyde in PBS then washed twice with PBS. Cell nuclei were mounted with DAPI Fluoromount G (Thermo Fisher Scientific, Cat No. 00-4959-52). Epifluorescence images were acquired with an Applied Precision Deltavision Elite microscope, 60x/1.40 NA Oil UIS2 BFP1 objective lens and analyzed using Image J [141].

Analysis and quantification of cytoplasmic/nuclear ratios (Figure 12B) was done with ImageJ scripts and R scripts respectively. Original scripts were written by Juliana S. Capitanio and modified here for these quantifications (see Appendix A).

2.7 Antibodies

Commercial antibodies used include anti-α-tubulin (Sigma-Aldrich, Cat No. T6074), lamin B (abcam, Cat No. ab16048), dsRNA (Scicons, Cat No. J2), pan-*Flaviviral* envelope glycoproteins (Millipore, Cat No. MAB10214), anti-Ilf3 (abcam, Cat No. ab92355), anti-Ilf3 (abcam, Cat No. ab133354), anti-PKR (abcam, Cat No. ab32506), anti-PKR (phosphor T446) (abcam, Cat No. ab32036), anti-hnRNP M M1-M4 (abcam, Cat No. ab177957), anti GAPDH (abcam, Cat No. ab128915), and goat anti-ZIKV NS5 sera (generously provided by Dr. Thomas Hobman, University of Alberta). Secondary antibodies include goat anti-rabbit IgG-HRP (Bio-Rad Cat No. 170-6515), goat anti-mouse IgG-HPR (Bio-Rad Car No. 170-6516), donkey anti-goat IgG-HRP (Santa Cruz Biotechnology, Cat No. sc2020) for western blotting. Alexa Fluor 488 donkey anti-rabbit (Thermo Fisher Scientific, Cat No. A21206), Alexa Fluor 488 donkey anti-mouse (Thermo Fisher Scientific, Cat No. A21202), Alexa Fluor 594 donkey anti-mouse (Thermo Fisher Scientific, Cat No. A21203), Alexa Fluor 594 goat anti-rabbit (Thermo Fisher Scientific, Cat No. A11012), Alexa Fluor 647 goat anti-mouse (Thermo Fisher Scientific, Cat no. A21237), Alexa 647 goat anti-rabbit (Thermo Fisher Scientific, Cat No. A21246), Alexa Fluor 555 donkey anti-goat (Thermo Fisher

Scientific, Cat No. A21432), and Alexa Fluor 647 donkey anti-goat (Thermo Fisher Scientific, Cat No. A21447), were used for indirect immunofluorescence microscopy.

2.8 Single molecule RNA fluorescent *in situ* hybridization

To visualized single RNA molecules in infected cells, we used a fluorescence *in situ* hybridization (FISH) protocol. This assay works by increasing the signal to noise ratio obtained when 45-50 probes of 20 nucleotides, each labelled with an individual fluor, are hybridized to a single RNA molecule. Because several probes exist for each target sequence, the probability of on target binding is increased. The rate of false positives is decreased as tens of probes in a single sequence are needed to generate a detectable fluorescent signal. We designed 7 sets of probes (see table 2-2/2-3) targeting the ZIKV genomes. Two probe sets were designed to hybridize with the positive strand of the ZIKV vRNA (GenBank Accession KF993678.1). Probe set 1 is labelled as 5’ vRNA Probe in our figures and hybridizes to nucleotides 1500-3500 of the ZIKV +vRNA. Probe set 2 is labelled as 3’ vRNA Probe in our figures and hybridizes to nucleotides 6500-8500 of the ZIKV +vRNA. Probe set 1 is labelled with Quasar 570 fluors and probe set 2 is labelled with Quasar 670 fluors.

Table 2-2: 5′ ZIKV vRNA FISH probe-set.

FISH probes labelled with Quasar 570 fluors hybridizing to ZIKV (KF993678.1) positive strand RNA between nucleotides 1515 to 3483.

Probe Sequence
ctagaaccacgacagtttgc
agtttatccattttcaggcg
ggtacacagggagtatgaca
ccgggatcttagtgaatgtg
ctgagctggaaccttgcaag
cagtgattacagggttagcg
gcatcatcttagagttctca
cccaaatggtggatcaagtt
ccgactcctatgacaatgta
ctctcacagtggcttcaaat
caagactgccattctcttgg
caactgatccaaagtcccag
cttgcccaatgagttgagag
atgatttgaaagctgctcca
tgtgagaaccaggacattcc
agatccattctttgtattca
taaggccaagcacataaggg
cagagacggctgtggataag
ggcttcaacgtcgttataga
caatctacgaggggagtcag
cttgaaacagaggagatccc
cttctactgatctccacatg
tcttccaggattgcgttgag
aacgaccgtcagttgaactc
atggggtttttacagatcc
gaagtacgattttccccaag
tatttgtctttgctgctctg
tgtcaccatccacgacaaag
ttccatgctctatgtttgag
ccatgatcctccacaagaaa
acactagtgtgaaatacccc
tagcctagatcactgtgtac
tcgttcttctcactctcaat
gttttcatctcgatcaggtg
cacaatgtgtgggactttgg
cactttcttctattccatct
ccagctaaagacttgggtat
ctggtgttgtgatggctgag
tttcatttgggtcctgtaac
accgaatttcaagctcttca
tggttgatctcagagatggt
gaacgacagtgggggcattg
cataccaacagccatcttta
atgtgatcagttgatcctgc
cactccaagggagaagtgat
tgcaccatgagcagaatcac
ctgccattgatgtgcttatg
ctcattgaaaatcctcccag

Table 2-3: 3’ ZIKV vRNA FISH probe-set.

FISH probes labelled with Quasar 670 fluors hybridizing to ZIKV (KF993678.1) positive strand RNA between nucleotides 6542 to 8483.

Probe Sequence
aattctggctggctcaattt
ttctctggctcaggtatgag
gttgtcctgaggagatcttt
gtaatcaagcccagaagacc
caaccatccgagttcattgg
ttagatggcttaggtcactc
caggtcaatgtccattgaga
gtcaaagcagcgtagatagc
gacggctggggtaatgaaag
gtatgaagtggtcactgcat
tcgccattaaggagtagttg
tttgcccataccaaacaaca
caaagtcccatgcgtagaat
gtagcaacctatcattagca
tagggtcaggggtgttaatt
cacgagcaaaatgatggcca
cgacagggttcttcatgatg
tcaatgtcagtcaccactat
ttgggggtcaattgtcattg
acggctactgctatgagtag
gaagttgcagctgtgatcag
tccagtacttgttcggagag
acacagtgaagtggctgtag
attagagaagctccagccaa
cagcgtttcttgttactgtg
tgtaggagtagaactccagg
tgccacatccaagatcaatg
cttgaactttgcggatggtg
ccttttgtgtatcctttcac
ccactcttaagacggactat
tcagccgccatatgaaagac
cctatatcacacagcaacgt
tccacttcaggactagatga
accatggagaggactctgag
ggtctttttttcaagccaatc
gggcacaacacttttataca
tttccatcatagtgctggtg
atctcatgtgtagagttgcg
cgtggtggacacacttttta
attcacatcctcctcatatt
cttcatgttgggagcttcag
tctcaatgcggttaccaatg
gtcaaagaaccacgtttccg
atgtcctatatgggtggttc
ctcatagcttccatggtaag
tattagagaggacgctgacc
ttttgacaggagcctgacaa
tcatggctattcctgtgact

2.8.1 FISH sample preparation

All steps indicated were done under strict RNAse free procedures and using RNAse free materials and solutions. Following depletions and infections with ZIKV as indicated, cells on round coverslips (Fisherbrand, Miroscope Cover Glass, Cat No. 12-545-81, 12CIR.-1.5) were fixed with 3.65% formaldehyde (Sigma-Aldrich, Cat No. F8775) in PBS for 10 minutes. Cells were then washed twice with PBS and permeabilized with 70% ethanol in water for one hour at 4 ° C. Cells were then incubated in wash buffer containing 10% formamide (Sigma-Aldrich, Cat No. 221198) in a 2X saline sodium citrate buffer (SSC, Sigma-Aldrich, Cat No. S6639) for 5 minutes at room temperature. Indicated probes were hybridized in a humidified chamber at 37 ° C for 16 hours in hybridization buffer (Probe sets 1 and 2 in table 2-2/2-3) (Buffer contained 125 nM probes, 100 mg/mL dextran sulfate (Millipore, Cat No. S4030) and 10% formamide in 2X SSC). Primary antibodies were added in with the hybridization buffer and probes at double the concentration used in immunofluorescence experiments. After hybridization, cells were washed twice with wash buffer for 30 minutes at 37 ° C. Cells were then incubated at 37 ° C for 30 minutes with secondary antibodies conjugated with Alexa Fluor 488. Cells were again washed twice with wash buffer. Cells were then post fixed with 3.65% formaldehyde in PBS for 10 minutes at room temperature and then washed twice with PBS. Slips were mounted on slides using DAPI Fluoromount G. Samples were then imaged using an Applied Precision Deltavision Elite microscope, 60x/1.40 NA Oil UIS2 BFP1 objective lens and analyzed using Image J [141].

2.9 Total cellular RNA purification and reverse transcription

Following indicated depletions and/or infections, cells were collected using TriZOL Reagent (Thermo Fisher Scientific, Cat No. 15596026) as per the manufacturer's recommendations. 1 µg of RNA was then treated with DNAse I (Thermo Fisher Scientific, Cat No. 18068015) and reversed transcribed into cDNA with random primers (Thermo Fisher Scientific, Cat No. 48190011) by the Superscript II reverse

transcriptase (Thermo Fisher Scientific, Cat No. 18064014) as per the manufacturer's specifications.

2.10 Quantitative polymerase chain reactions

Following isolation and reverse transcription of total cellular RNA, cDNA was analyzed with real-time PCR reaction performed with SYBR green super mix (Quantabio, Cat No. 95056-500). Primers specific to each transcript were used to assess for transcript levels in samples (see Table 2-4). Changes in the levels of each specific mRNA are shown as fold-changes, between control or depleted cells. Results were analyzed using the comparative Ct method. Quantitative PCR reactions were performed in an Mx3000P QPCR system (Agilent Technologies 401403) using PerfeCTa SYBR Green Supermix (Quantabio, Cat No. 95056-500). Primers were designed using Primer-BLAST [142]. Primers directed against the interferon stimulated genes (IFNA1, IFNB1, MX1, OAS1, PKR, NFKB1, and TNF) were generously provided by Dr. Lorne Tyrrell (University of Alberta). qPCR results were analyzed with Microsoft Excel (Microsoft, Office 2016).

Table 2-4: Primers list.

Gene	Primer	Sequence
HPRT	Forward	CCTGGCGTCGTGATTAGTG
HPRT	Reverse	ACACCCTTTCCAAATCCTCAG
TUBULIN	Forward	GGAACCCACAGTCATTGATGAA
TUBULIN	Reverse	GCCCTCGGGCATAGTTATTG
ACTIN	Forward	CTGTGGCATCCACGAAACTA
ACTIN	Reverse	AGCACTGTGTTGGCGTACAG
GAPDH	Forward	GCACCGTCAAGGCTGAGAAC
GAPDH	Reverse	TGGTGAAGACGCCAGTGGA
ZIKA	Forward	CCTTGGATTCTTGAACGAGGA
ZIKA	Reverse	AGAGCTTCATTCTCCAGATCAA
IFNA1	Forward	AACTCCCCTGATGAATGC
IFNA1	Reverse	CTGCTCTGACAACCTCCC
IFNB1	Forward	CAATTTTCAGTGTCAGAAGCTCC
IFNB1	Reverse	AAAGTTCATCCTGTCCTTGAGG
MX1	Forward	ACCTGATGGCCTATCACCAG
MX1	Reverse	TTCAGGAGCCAGCTGTAGGT
OAS1	Forward	TCGGACGGTCTTGGAATTAG
OAS1	Reverse	AGGAGGTCTCACCAGCAGAA
PKR	Forward	TTAGTGACCAGCACACTCGC
PKR	Reverse	ATGCCAAACCTCTTGTCCAC
NFKB1	Forward	GGGAAAGTTATTGAAACCACAGAG
NFKB1	Reverse	GTTAGAGTGACCTCACCATTCC
TNF	Forward	CTCACCCACACCATCAGC
TNF	Reverse	GAAGACCCCTCCCAGATAGA

3 RESULTS

3.1 Replication of ZIKV in the human A549 cell line.

For our analysis of ZIKV production, we have used the lung epithelial carcinoma cell line A549 as a host for viral infection. Previous reports describing the use of this cell lines have reported that cells infected with an MOI of 3 show > 60% viability at time points up to 48h post infection followed by a progressive decrease in viable cells to ~10 % by 120h post infection [47]. We observed > 80% viability up to 48h post ZIKV infection (Figure 3.1). Thus, in general, our experiments were performed with a 48h window.

For most of our experiments, we assessed the levels of infection in individual cells and the cell populations using antibodies directed against double stranded (ds) RNA, ZIKV envelope (E) protein, or the non-structural 5 (NS5) protein. As shown in Figure 3.2, immunofluorescence analysis revealed the presences of these viral antigens at 12 and 24h post infection. Using the dsRNA antibody, the viral genome was detected in the cytoplasm of infected cells and signal levels generally increased as the time of infections increased from 12 to 24h. This signal was above the background seen in the uninfected control cells, which arises from endogenous host cell dsRNA substrates. Another method utilized to directly examine the ZIKV genomic RNA was fluorescence in situ hybridization (FISH). To detect the presence of the ZIKV genome, we utilized two probe sets, each labeled with a distinct fluorophore, that hybridize to ORF regions positioned near the 5’ and 3’ ends of the viral genome (between nucleotides 1,500-3,500 and 6,500-8,500 of the 10,141 nucleotide viral genome). We utilized both probe sets and colocalized signals to increase the confidence of assigning the localization of the ZIKV genome. In Figure 3.3, we show that at 24h

post infection, the viral RNA strongly localizes to distinct regions of the cytoplasm, which likely represent virus replication factories in the cytoplasm of infected cells.

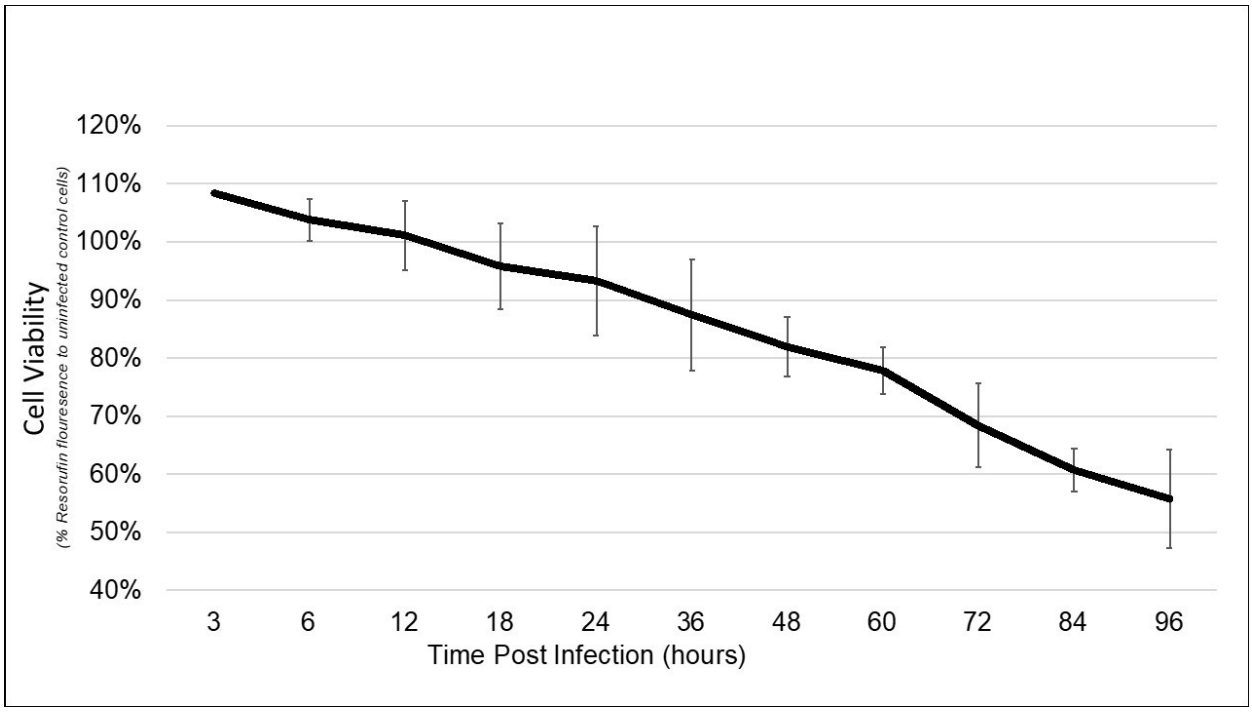

Figure 3.1: ZIKV infection results in reduced viability in A549 cells.

A549 cells were infected with ZIKV. Viability was evaluated by mitochondrial dehydrogenases activity at time points from 3h to 96h post infection. Values shown for cell viability are a percentage of the viability of uninfected A549 cells. Error bars represent triplicate biological replicates. These data were produced in collaboration with Dr. Juliana Capitanio.

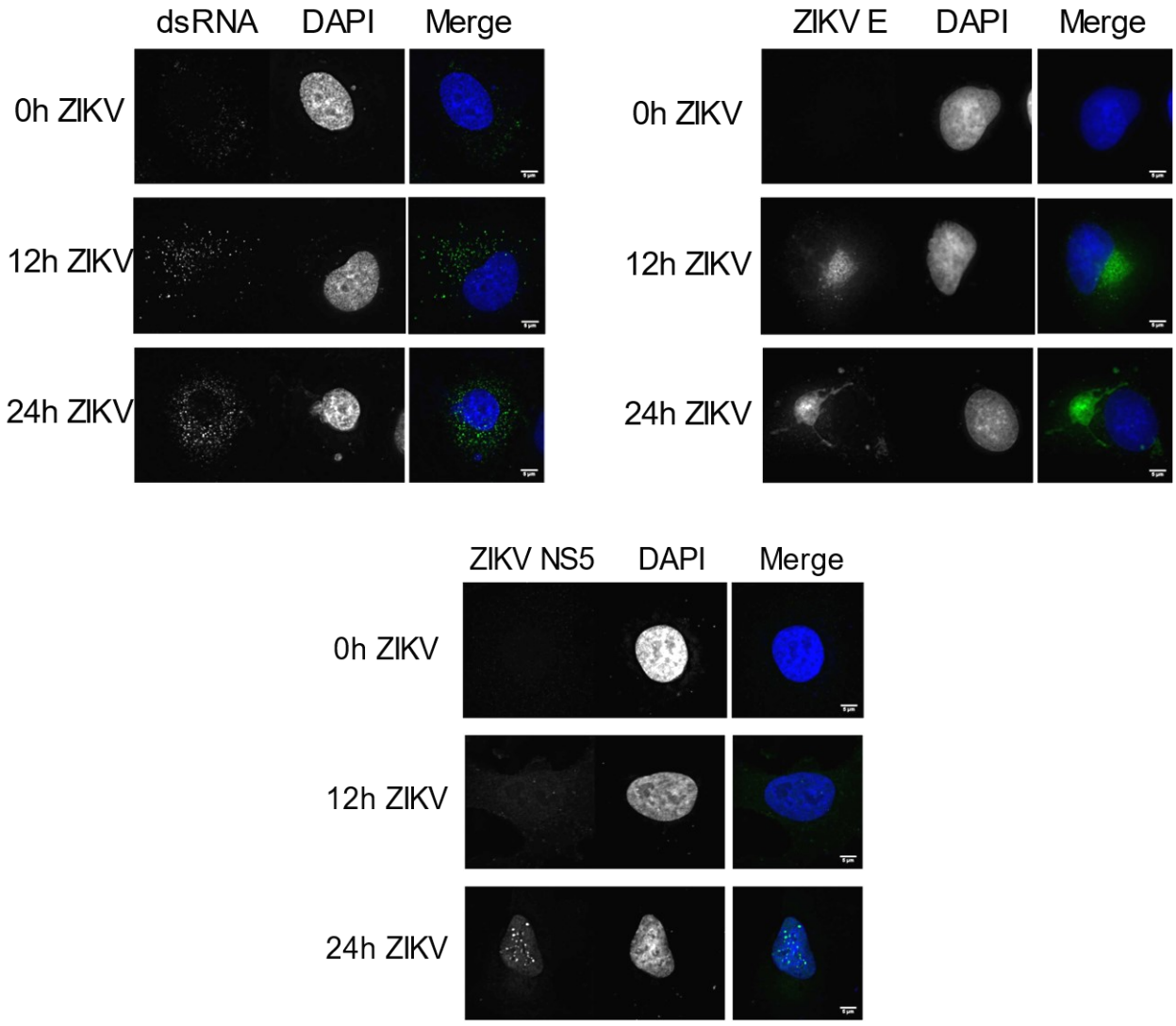

Figure 3.2: Characterization of ZIKV infection in A549 cells.

A549 cells were infected with ZIKV. ZIKV antigen localizations were examined by indirect immunofluorescence using antibodies directed against dsRNA, E protein, and NS5 at 0, 12, and 24h post infection. The position of the nucleus was determined using the DNA stain DAPI (blue). Merged images show the immunofluorescence signal pseudo colored in green. Representative images were acquired with an epiflourescent microscope and then deconvolved. Scale bars, 5 µm.

To visualize viral proteins in infected cells, we utilized immunofluorescence (IF) analysis. In Figure 3.2, we show ZIKV E protein presence in the cytoplasm of infected cells. This signal is distributed throughout the cell at 12h post infection, however by 24h the viral E protein becomes concentrated within what are likely viral factories in the cytoplasm. ZIKV NS5 has a different distribution in infected cells. NS5 functions as an RNA-dependent RNA polymerase in the synthesis of the viral genome. NS5 proteins also possess methyltransferase activity, which is used in RNA capping of the viral genome [17]. At 12h post infection, NS5 signal is broadly distributed throughout the cell. By 24h post infection, NS5 shows a predominantly nuclear localization. There are bright puncta of NS5 protein in the nucleus, some of which outline the nucleoli visualized in the denser perinucleolar heterochromatin in the DAPI channel in infected cells. It has been suggested that these may be sites of splicing [143]. There is also NS5 signal in the cytoplasm that localizes to the same area as the vRNA signal (Figure 3.3). The strong nuclear localization of NS5 is detected throughout the *Flavivirus* genus, however, the function of this nuclear pool of NS5 is currently unknown [144].

Evidence in the literature also suggests that there are striking cytoskeletal rearrangements in ZIKV infection [29]. We utilized immunofluorescence to assess the presence of tubulin exclusion zones in A549 cells infected with ZIKV. The data in Figure 3.4 show that tubulin exclusion and cytoskeletal rearrangements are present in virally infected A549 cells. These rearrangements of microtubules and intermediate filaments have been described to surround the viral replication factories that form in invaginations towards the ER lumen. More importantly, Cortese et al. showed that these rearrangements were necessary for efficient ZIKV replication using drugs that target the cytoskeleton [29].

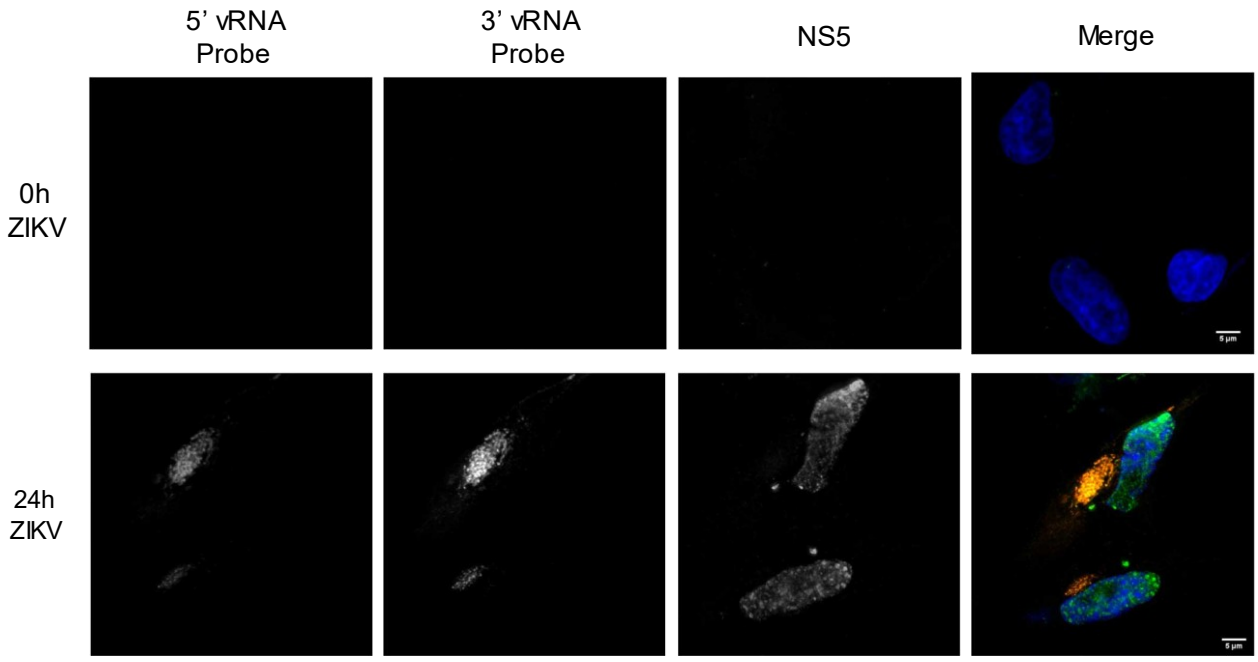

Figure 3.3: Characterization of vRNA localization in infected A549 cells.

A549 cells were infected for 24h or mock infected. Fluorescence in situ hybridization (FISH) was used to examine the localization of ZIKV +vRNA. smFISH probes that hybridize to the 3' (nucleotides 1,500-3,500) and 5' (nucleotides 6,500-8,500) ends of the ZIKV ORF were hybridized to ZIKV plus strand RNA. The position of the nucleus was determined using the DNA stain DAPI (blue). The localization of ZIKV NS5 was determined by indirect immunofluorescence using an antibody targeted against NS5. Merged images show NS5 pseudo coloured green, 3' probes pseudo coloured yellow, and 5' probes pseudo coloured red. Representative images were acquired with an epiflourescent microscope and then deconvoluted. Scale bars, 5 μm.

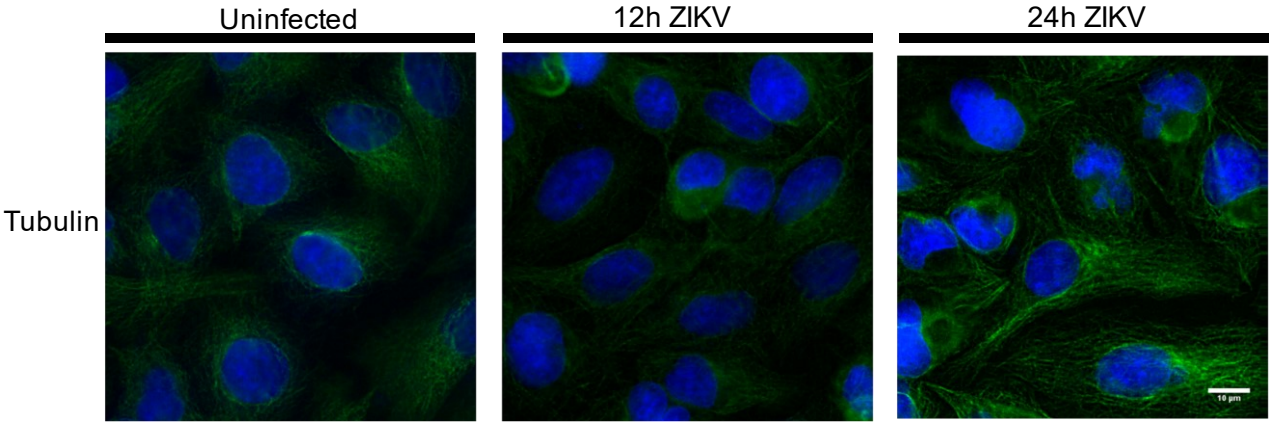

Figure 3.4: Characterization of cytoskeletal rearrangements in ZIKV infection in A549 cells.

A549 cells were infected with ZIKV for 12 or 24h. Tubulin exclusion from viral replication factories was examined by indirect immunofluorescence using an antibody directed against tubulin. The position of nuclei was determined using the DNA stain DAPI (blue). Representative images were acquired with an epifluorescence microscope and deconvolution microscope. Scale bars, 10 µm.

3.2 ZIKV genome interacts with the nuclear proteins NF90/NF110 and hnRNP M

The virus genome must utilize numerous cellular pathways to facilitate replication of its genome and the formation of virions. Our goal has been to define host cell factors that facilitate these processes, and in particular, to examine the role of host nuclear proteins in the ZIKV production. As described in the Introduction section, the life cycle of the ZIKV, like other member of the *Flaviviridae* family of viruses, is thought to occur in the cytoplasm where the viral genome is translated and replicated, and virions are assembled within a virally-induced membrane compartment associated with the ER [29]. Curiously, however, genomic RNA of various *Flaviviridae* viruses, including, for example, hepatitis C virus (HCV), have been shown to interact with proteins that reside in the nucleus [101], [132]. Recent work by our collaborators has also detected interactions between the ZIKV genome and various nuclear proteins [145]. Using comprehensive identification of RNA-binding proteins by mass spectrometry (ChIRP-MS), they identified peptides derived from numerous host cell proteins in association with ZIKV RNA. Within this list, we identified two nuclear proteins, one encoded by the *ILF3* gene and the other by the hnRNP M gene, which were among the most highly represented by peptides hits identified using the ChIRP-MS assay (Table 3-1). *ILF3*-encoded isoforms and hnRNP M were selected for further analysis based on the previous observations showing that *ILF3*-encoded isoforms, including NF90 and NF110, play an important regulatory role, both positive and negative, in production of other viruses [100], [132], [133], [135], [136] and, by contrast, the complete lack of information on the role hnRNP M.

Rank	Protein ID	UniProtID	Log2 (ZIKV/Control)
38	hnRNP M	P52272	3.20
66	ILF3	Q12906	2.67

Table 3-1: Peptide hits corresponding to the *ILF3* gene and hnRNP M show association with ZIKV genomic RNA.

Data from collaborators', Flynn and Carette, ChIRP-MS experiment [145]. Huh7.5.1 cells were infected with ZIKV and then crosslinked and solubilized. Biotinylated antisense oligonucleotides were used to pull down target ZIKV vRNA along with associated proteins/complexes. Eluted proteins were subjected to LC-MS/MS. The rank of enrichment, protein ID, UniProtID, and fold change (Log2) are shown.

As an initial step in the analysis of the functional role of the *ILF3*-encoded isoforms and hnRNP M binding to the ZIKV genome, we examined whether ZIKV infection alter the cellular distribution of NF110 or hnRNP M (Figure 3.5 and 3.7). For these experiments, A549 cells were infected with ZIKV and cells were examined by IF analysis every 12 hours over a 48h time course using antibodies directed against NF110 and hnRNP M. Infected cells were identified by IF analysis using anti-E protein antibodies. As shown in Figure 3.5, the nuclear distribution of hnRNP M in infected cells (identified by viral E protein accumulation) was unaltered throughout the infection time course and appeared similar to uninfected cells. Conversely, the cellular distribution of NF110 was altered throughout the time course of infection starting at 12h post infection. As shown in Figure 3.6, much of the NF110 remained nuclear, but we also observed a visible increase in the cytoplasmic pool of NF110, with the bulk of the NF110 cytoplasmic signal in the areas containing ZIKV E protein. Utilizing a separate antibody that binds both the NF90 and NF110 isoforms *ILF3*-encoded isoforms, we observed a similar overall distribution pattern including an increase in the cytoplasm signal in ZIKV infected cells (Figure 3.7A). In addition, these antibodies appear to bind additional antigen in the nucleolus, likely due to it recognition of NF90. However, it remains to be further investigated whether the cytoplasmic signal arises solely from the NF110 or from combination of the NF90 and NF110. Cumulatively, these data suggest that, in infected cells, there is an accumulation of NF110 within, or in the vicinity of, the cytoplasmic viral replication factories, while the nuclear distribution of hnRNP M does not change during ZIKV infection.

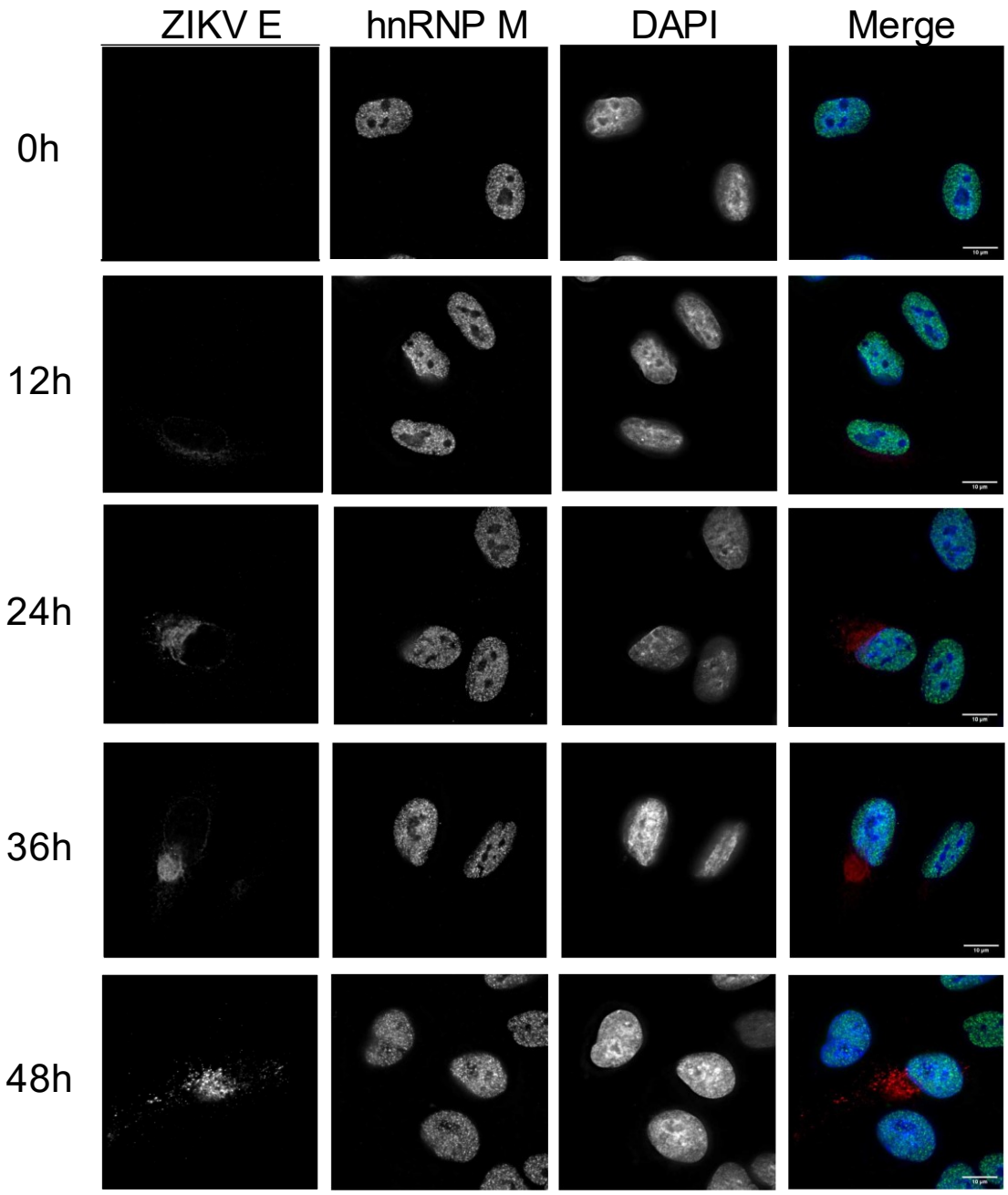

Figure 3.5: hnRNP M distribution is not altered with ZIKV infection.

A549 cells were infected with ZIKV. The localization of hnRNP M and ZIKV E were studied using indirect immunofluorescence with antibodies targeted towards hnRNP M and the ZIKV E protein. Time-points of infection ranging from mock to 48h of infection were examined. The position of the nuclei was determined using the DNA stain DAPI (blue). Merged images show hnRNP M pseudo coloured in green, and ZIKV E protein pseudocoloured in red. Representative images were captured using epiflourescent microscopy and deconvoluted. Scale bars, 10 μm.

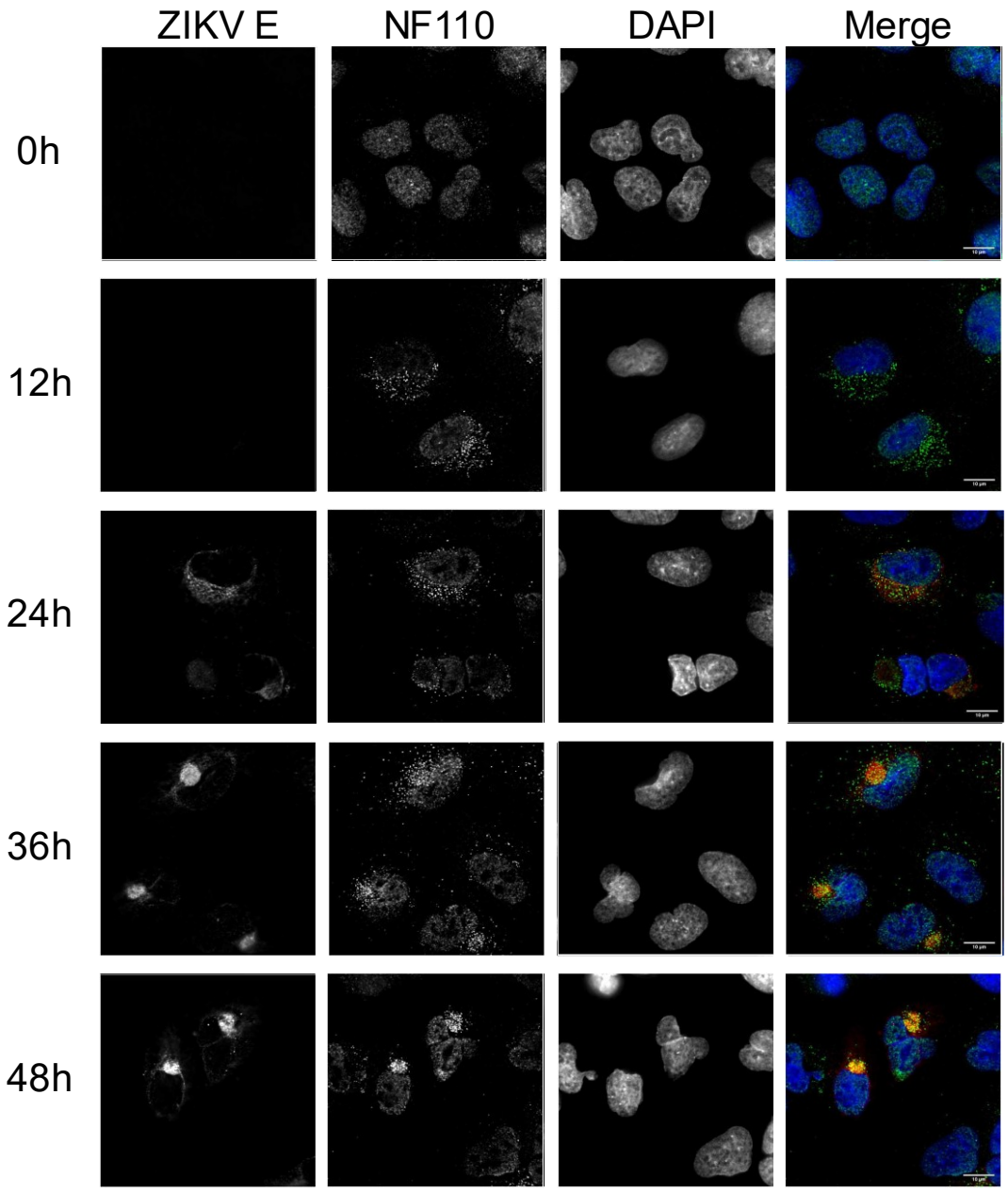

Figure 3.6: ZIKV infection results in redistribution of NF110 to the cytoplasm of infected cells.

A549 cells were infected with ZIKV. Host NF110 and ZIKV E protein antigen locations were determined using indirect immunofluorescence with antibodies directed against NF110 and ZIKV E protein. Time points ranging from 0 to 48h post infection were analyzed. The position of nuclei was determined using the DNA stain DAPI. Merged images show ZIKV E protein pseudo coloured red, and NF110 pseudo coloured green. Representative images were captured using epiflourescent microscopy and deconvolved. Scale bars, 10 μm.

3.3 NF110 associates with the ZIKV genome in infected cells

The redistribution of NF110 during ZIKV infection (Figure 3.6), as well as data showing that peptide hits corresponding to *ILF3* isoforms interacts with the ZIKV genome [145], prompted us to further examine the distribution of NF90 and NF110 in infected cells relative to ZIKV genomic RNA. For these experiments, we used antibodies directed against NF110 alone or both NF90 and NF110 and compared their cellular localization pattern to that produced by dsRNA-directed antibodies (Figure 3.7A).

Both the NF110 specific and the NF90/NF110 antibodies detected numerous cytoplasmic foci that overlapped with the dsRNA signal in the cytoplasm of infected cells at 12h post infection (Figure 3.7B). In addition to the overlapping signals produced by the anti NF90/NF110 and dsRNA antibody signals, non-overlapping cytoplasmic foci were visible with both antibodies (see inlayed images). These data are consistent with observations showing that NF110, and possibly NF90, are associated with ZIKV genomic RNA. When taken together, these data lead us to conclude that ZIKV RNA binds to NF110 and induces its redistribution to the cytoplasm of infected cells.

Figure 3.7: NF110 colocalizes with cytoplasmic viral dsRNA markers.

A549 cells were infected with ZIKV and the colocalization of NF90/NF110 and dsRNA was assayed using indirect immunofluorescence. Antibodies directed against dsRNA, NF110, and NF90/NF110 were used. **(A)** Cells were infected for 24h and then subjected to secondary immunofluorescence and probed with antibodies directed against NF110 and NF90/NF110 as indicated. An antibody directed against dsRNA was also used. Merged images show the host NF110 or NF90/NF110 pseudo coloured in green, and dsRNA pseudo coloured in red. The position of the nuclei was determined using the DNA stain DAPI. **(B)** Cells were either mock infected or infected for 12h as indicated. Samples were subjected to indirect immunofluorescence using antibodies directed against NF110 and dsRNA. Merged images show host NF110 pseudo coloured in green, and dsRNA pseudo coloured in red. Nuclei positions were determined using the DNA stain DAPI. Representative images were captured using epifluorescence microscopy and deconvolution. Scale bars, 10 μm.

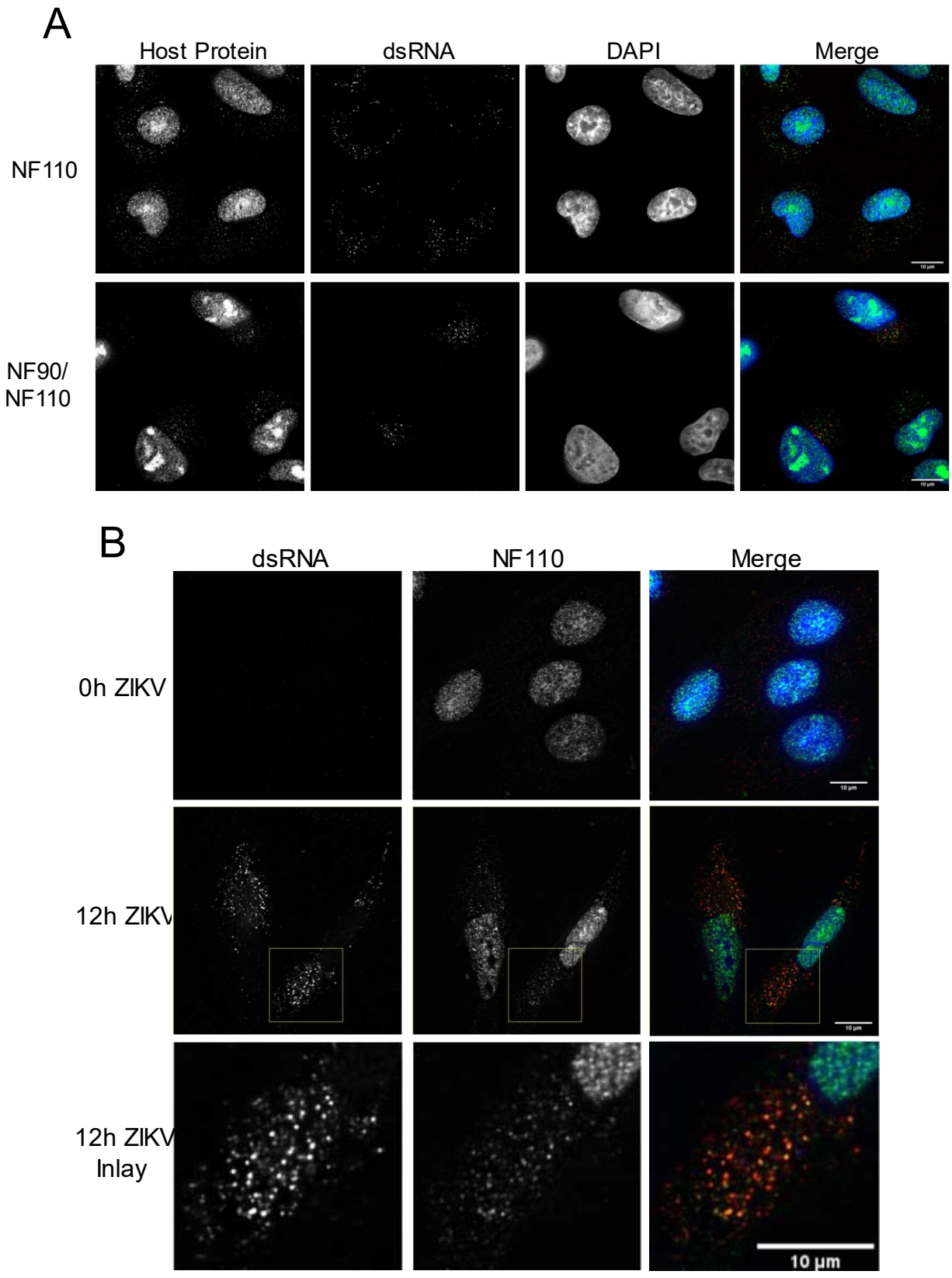
A
Host Protein
dsRNA
DAPI
Merge
NF110
NF90/
NF110
B
dsRNA
NF110
Merge
0h ZIKV
12h ZIKV
12h ZIKV
Inlay
10 µm

3.4 Poly I:C and IFN treatments alter hnRNP M and NF90/NF110

To better understand what might be causing the redistribution of NF110 seen following infection with ZIKV, we examined two pathways that are triggered by ZIKV infection outside of the context of an active ZIKV infection and its pleotropic effects. First, we transfected the viral dsRNA mimetic polyinosinic-polycytidylic acid (Poly I:C) into A549 cells to induce the immune response (IFN production and ISG expression) and RNA surveillance pathways triggered by ZIKV. Next, we treated cells with 100 international units per milliliter IFNα to assess the effect of IFN stimulation on the distribution of NF110.

We first assessed the changes in the distribution of NF90/NF110 and hnRNP M in A549 cells following a six-hour treatment with Poly I:C with indirect immunofluorescence (Figure 3.8). Captured images showed us that the dsRNA immunofluorescence signal increased in the Poly I:C treated cells and formed cytoplasmic puncta suggesting that the transfection with Poly I:C was successful. Following treatment with Poly I:C, NF110 was redistributed to the cytoplasm and showed a robust colocalization with the dsRNA puncta. This redistribution of NF110 to the cytoplasm of Poly I:C treated cells is similar to the redistribution seen in ZIKV infection (Figure 3.6 and 3.7). Using an antibody directed against NF90 and NF110, we observed a similar redistribution to the cytoplasm of transfected cells with colocalization of NF90/NF110 signal to dsRNA puncta in the cytoplasm. The NF90/NF110 antibody also appeared to show an exclusion of NF90/NF110 signal from the nucleoli in Poly I:C treated cells that is not observed in the mock treated cells.

This loss nucleolar and subsequent loss of nucleolar signal observed with the antibody directed against NF90/NF110 suggests that it may be NF90 that is enriched in the nucleolus as it is not observed using antibodies directed solely against NF110. Conversely, hnRNP M did not show any relocalization to the cytoplasm of Poly I:C treated cells although there may be an enrichment in the perinucleolar regions in the Poly I:C condition (Figure 3.8). Recent research suggests that treatment with Poly I:C results in the cytoplasmic redistribution of hnRNP M in HeLa cells [92] but we were unable to observe this phenotype in A549 cells. These results suggest that the transfection of Poly I:C into A549 cells is sufficient to induce redistribution of NF90 and NF110, but not hnRNP M.

Figure 3.8: Poly I:C treatment induces cytoplasmic relocalization of NF110.

A549 cells were mock treated or treated with Poly I:C for 6h. The distribution of host nuclear factors was analyzed using indirect immunofluorescence using antibodies directed against host hnRNP M, NF110, or NF90/NF110 as indicated. Poly I:C distribution was determined using an antibody directed against dsRNA. The position of nuclei was determined using the DNA stain DAPI. Merged images show Poly I:C dsRNA pseudo coloured in red. Host factors hnRNP M, NF110, and NF90/NF110 were pseudo coloured green. Representative images were captured using epiflourescent microscopy and deconvolved. Scale bars, 10 μm.

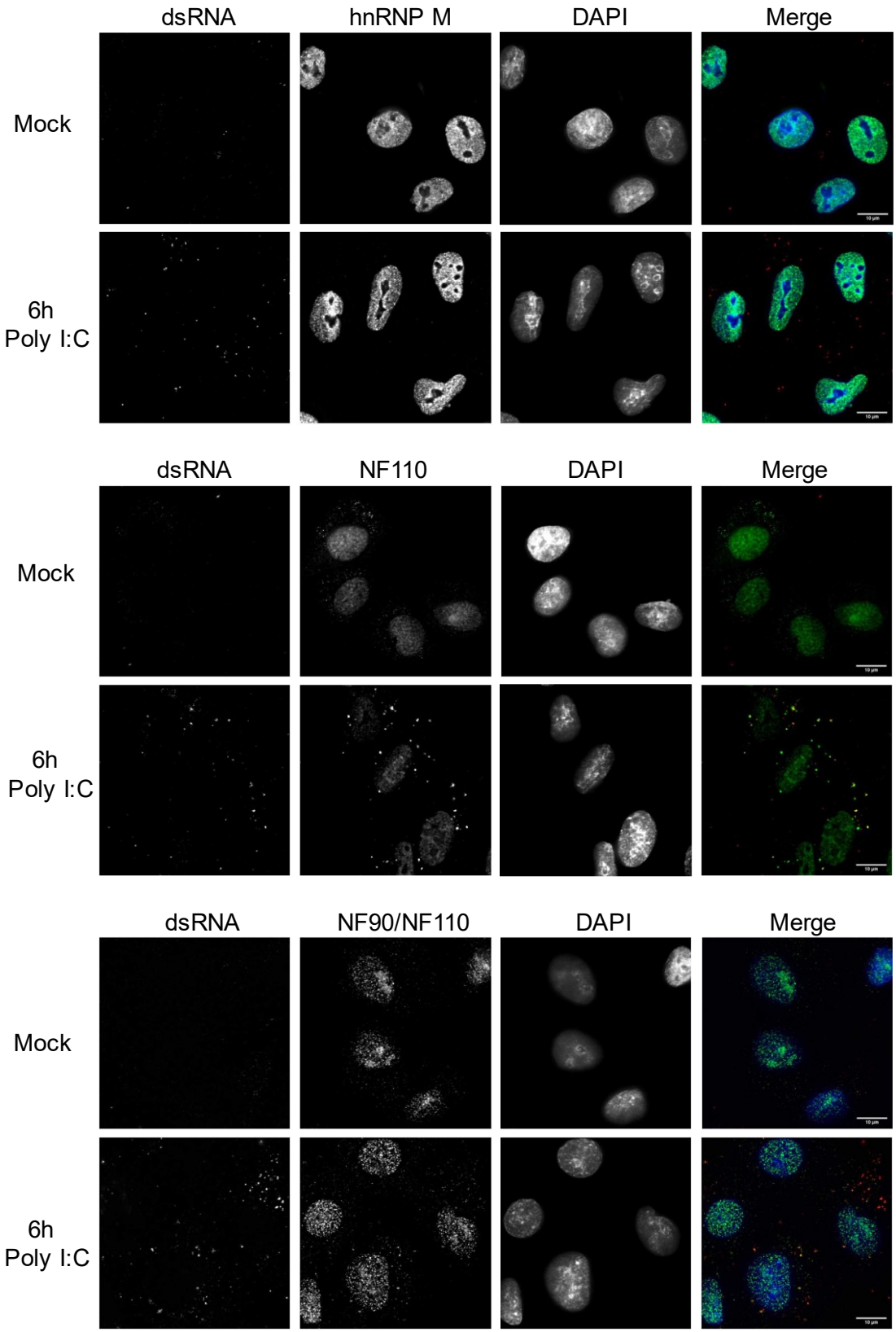
dsRNA
hnRNP M
DAPI
Merge
Mock
6h
Poly I:C
dsRNA
NF110
DAPI
Merge
Mock
6h
Poly I:C
dsRNA
NF90/NF110
DAPI
Merge
Mock
6h
Poly I:C

We next assessed the effect of isolated immune activation of the JAK-STAT pathway (as discussed in Section 1.1.3) on the localization of NF110 by treating A549 cells with 100 international units of IFNα per milliliter of media for 6h. We assessed the effect of IFNα treatment on cells to isolate the effects of immune induction in cells without the widespread pleiotropic effects that infection with wild type ZIKV induces. Following IFN treatment, we examined the localization of NF110, hnRNP M, and PKR by indirect immunofluorescence (Figure 3.9). The inclusion of PKR in this experiment was to act as a positive control following IFN treatment as previous evidence suggests that PKR is a well-documented interferon-stimulated gene (ISG) [146]. Upon IFN treatment, NF110 did not display any notable differences in signal distribution. The antibody directed at NF90/NF110 did show an increased fluorescent signal in the cytoplasm of cells compared to the mock condition following treatment with IFN. This observation suggests that NF90 levels may be selectively increased following IFN treatment in A549 cells. When we examined the effect of IFN treatment on the distribution of hnRNP M, we observed that the hnRNP M fluorescent signal appeared decreased compared to the mock treated cells. While we did not examine the effects of IFN on the levels of hnRNP M protein by western blot, this observation is supported by published RNA-seq data [147]. These data from human primary epithelial cells show a downregulation of hnRNP M expression of 2-fold following IFN treatment. Finally, we observed that fluorescence levels produced using antibodies directed at PKR increased greatly following treatment with IFN. Goulet et al. showed that there was a 3.5-fold induction of PKR following a 6h treatment with IFN, consistent with the increased intensity of PKR signal we observed in the INF treated cells. These data suggest that hnRNP M protein levels may be reduced as a result of the induction of

an antiviral state following treatment with type I IFN. Conversely, these data suggest that NF90 and PKR protein levels in A549 cells increase in response to type I IFN treatment.

Figure 3.9: IFNα treatment alters hnRNP M and NF110 in A549 cells.

A549 cells were either treated 100 IU/mL IFNα for 6 hours or mock treated with PBS. Host protein distributions were examined by indirect immunofluorescence using antibodies directed against hnRNP M, NF110, NF90/NF110, or PKR. The position of nuclei was examined using the DNA stain DAPI. Merged images show host proteins pseudo coloured in green and nuclei pseudo coloured in blue. Representative images were captured using epiflourescent microscopy and deconvolved. Scale bars, 10 μm.

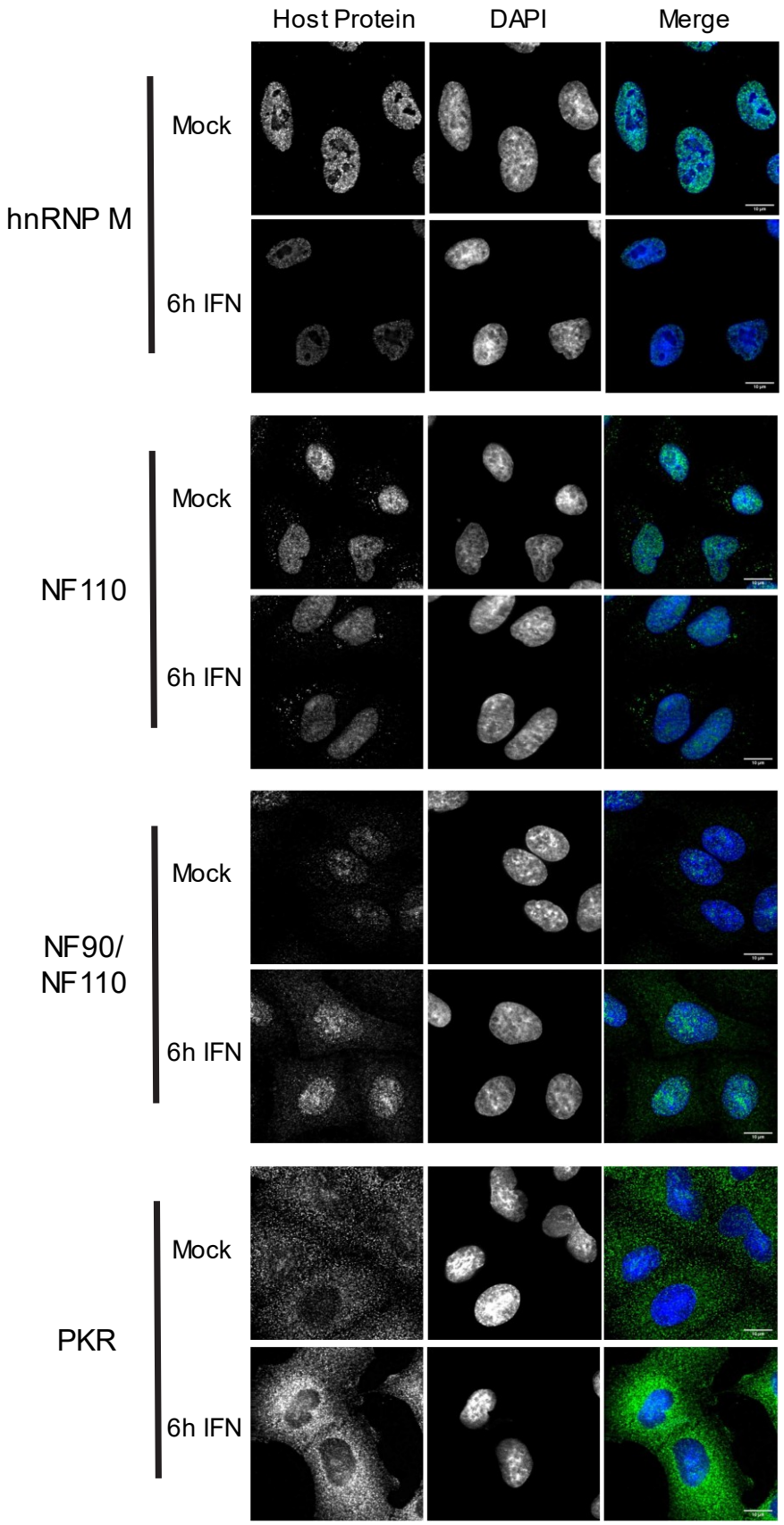
Host Protein
DAPI
Merge
hnRNP M
Mock
6h IFN
NF110
Mock
6h IFN
NF90/
NF110
Mock
6h IFN
PKR
Mock
6h IFN

3.5 Inhibition of nuclear import alters NF110 distribution in ZIKV infected A549 cells

Data suggest that hnRNP M interacts with ZIKV RNA (Table 3-1), however, we were unable to observe any colocalization of hnRNP M with ZIKV induced dsRNA nor were we able to observe a redistribution of hnRNP M in infected cells (Figure 3.5). To assess if nucleocytoplasmic shuttling of hnRNP M provides an opportunity for hnRNP M to associate with viral RNA, but not accumulate in the cytoplasm of infected cells, we performed indirect immunofluorescence to observe the localization of hnRNP M and NF110 following perturbation of host nucleocytoplasmic transport using small molecule inhibitors (Figure 3.10 and 3.11). To block nucleocytoplasmic transport, we used Leptomycin B (LMB) to block Xpo1-mediated nuclear export, and Importazole (IPZ) and Ivermectin (Iver) to block karyopherin α/β- and β-mediated nuclear import, respectively. To ensure any changes in localization due to the drug vehicles could be accounted for, we also tested ethanol (vehicle used for LMB) and DMSO (vehicle used for IPZ and Iver) as indicated.

We first assessed the effects of the nucleocytoplasmic inhibitors on the localization of hnRNP M and NF110 in uninfected cells (Figure 3.10). Following 6h of treatment with the transport inhibitors, we subjected the samples to indirect immunofluorescence. We did not observe any changes between the drug treatments and their vehicles for either hnRNP M or NF110.

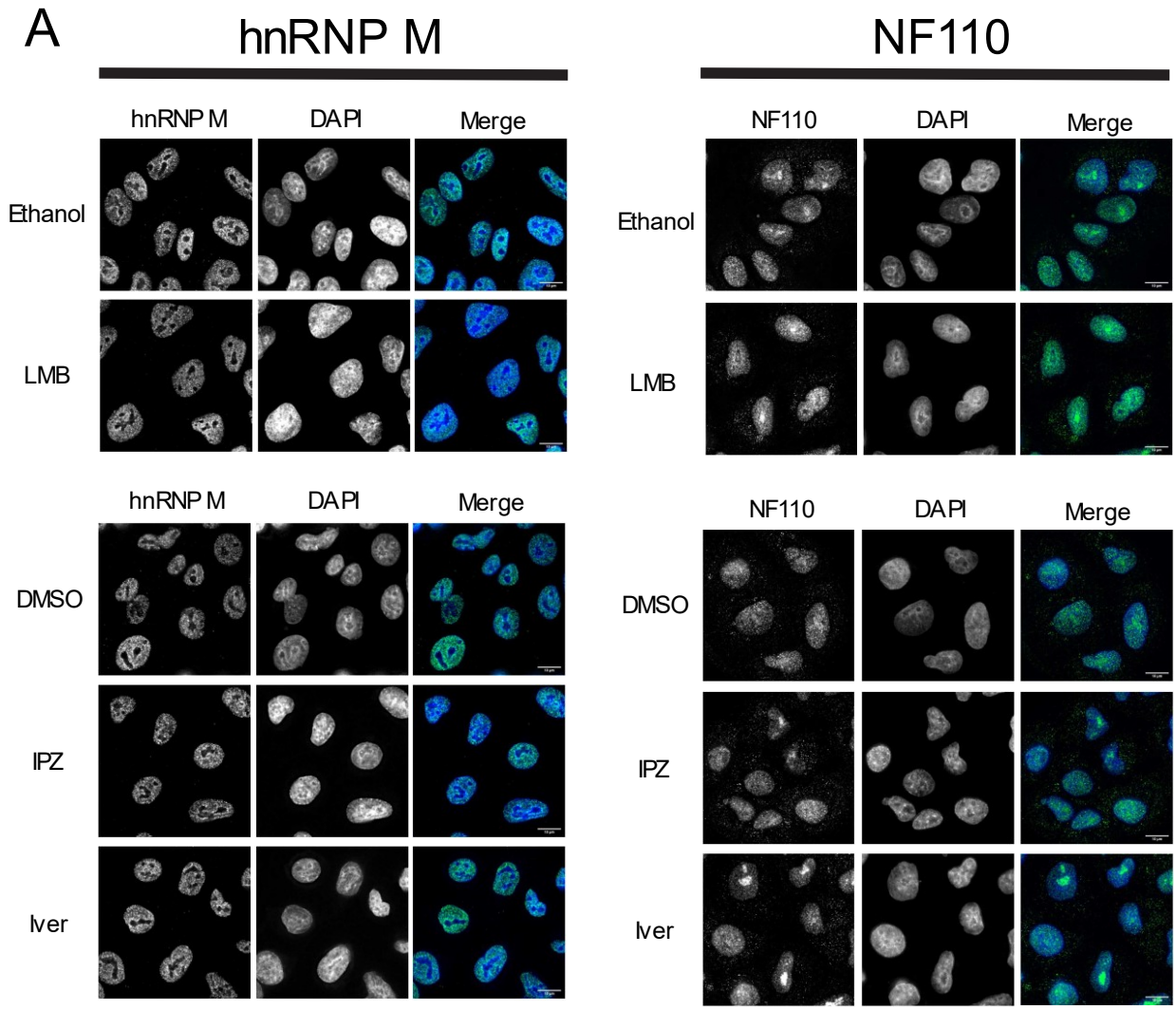

Figure 3.10: Inhibition of nucleocytoplasmic transport does not alter the distribution of hnRNP M or NF110 in uninfected cells.

A549 cells were treated with indicated nucleocytoplasmic transport (NTF) inhibitors for 6h. Drug treatments are indicated to the left side of the panel sets. Ethanol is the vehicle control for Leptomycin B (LMB) which targets Xpo1 mediated export. DMSO is the vehicle control for Importazole (IPZ) and Ivermectin (Iver) which target karyopherin α/β and karyopherin β transport, respectively. Indirect immunofluorescence using antibodies directed against hnRNP M and NF110 was used to examine the distribution of host nuclear factors. Merged images show hnRNP M or NF110 pseudo coloured in green as indicated. The position of nuclei was determined using the DNA stain DAPI. Representative images were captured using epiflourescent microscopy and deconvolved. Scale bars, 10μm.

To test if nucleocytoplasmic shuttling of hnRNP M was induced by infection of A549 cells with ZIKV, we infected cells for 18h and then treated the cells with nucleocytoplasmic transport inhibitors for 6h. These samples were then subjected to indirect immunofluorescence analysis to observe changes in distribution (Figure 3.11). Antibodies directed against ZIKV E protein were used to assess the viral infection in cells. As with nucleocytoplasmic transport (NTF) inhibitor treatment on uninfected cells, treatment with NTF inhibitors following 18h of ZIKV infection did not result in any alteration of hnRNP M distribution in ZIKV infected cells (Figure 3.11A). Similarly, inhibition of nuclear export with LMB did not affect the localization of NF110 in ZIKV infected cells. However, treatment with the NTF inhibitors, IPZ and Iver, resulted in a decreased cytoplasmic NF110 signal as compared to the DMSO vehicle control condition (Figure 3.11A). To determine if this change in distribution was significant, we quantified the change in distribution by calculating a cytoplasmic:nuclear fluorescence ratio in infected cells for each drug treatment (Figure 3.11B). We used an extended depth of field algorithm to create 2D images from images stacks captured using epifluorescence microscopy. We then created measured the mean fluorescence intensity in both the cytoplasm and nuclei of infected cells and obtained a cytoplasmic to nuclear ratio of NF110 fluorescence intensities. This was done for each drug and vehicle treatment and the results are shown in Figure 3.11B. This quantification revealed a decreased NF110 cytoplasmic:nuclear fluorescence ratio in infected cells treated with IPZ and Iver compared to the DMSO vehicle control (Figure 3.11B). This observation is contrary to what we would expect with the inhibition of nuclear import. The

inhibition of nuclear import should result in an increase of cytoplasmic intensity for a given protein, however we see the opposite with NF110. One possible explanation for this is that a cofactor required for the redistribution of NF110 to the cytoplasm of cells infected with ZIKV is prevented access to the nucleus of infected cells by the import inhibitors IPZ and Iver. Conversely, because inhibition of nuclear import with Iver results in an attenuated ZIKV infection [148] (and evidenced by decreased ZIKV E protein intensity compared to the DMSO vehicle controls in Figure 3.11A), it may be that the decreased level of ZIKV infection does not induce the same redistribution of NF110 in cells treated with Ivermectin or IPZ compared to DMSO treated cells.

Figure 3.11: Nucleocytoplasmic import inhibitors alter NF110 localization in ZIKV infected cells.

A549 cells were infected with ZIKV for 18h then subjected to a 6h nucleocytoplasmic transport inhibitor treatment. The distribution of hnRNP M or NF110 was assayed with indirect immunofluorescence using antibodies directed against hnRNP M or NF110. **(A)** Drug treatments are indicated to the left side of the panel sets. Ethanol is the vehicle control for Leptomycin B (LMB) which targets Xpo1 mediated export. DMSO is the vehicle control for Importazole (IPZ) and Ivermectin (Iver) which target karyopherin α/β and karyopherin β transport, respectively. Images showing hnRNP M and NF110 are indicated at the top of the panels. The position of nuclei was determined using the DNA stain DAPI (blue). Merged images show ZIKV E protein pseudo coloured in red, and host hnRNP M or NF110 pseudo coloured in green. Representative images were acquired using epiflourescent microscopy and deconvolved. Scale bars, 10μm. **(B)** Acquired images were analyzed using an extended depth of field algorithm and the cytoplasmic to nuclear fluorescence ratios in infected cells was calculated for NF110 in the presence of nucleocytoplasmic transport inhibitors. Results from 2 biological replicates were analyzed with ANOVA followed by Tukey HSD tests for p-values between the drug and the vehicle controls. Significance is indicated as *** < 0.0005.

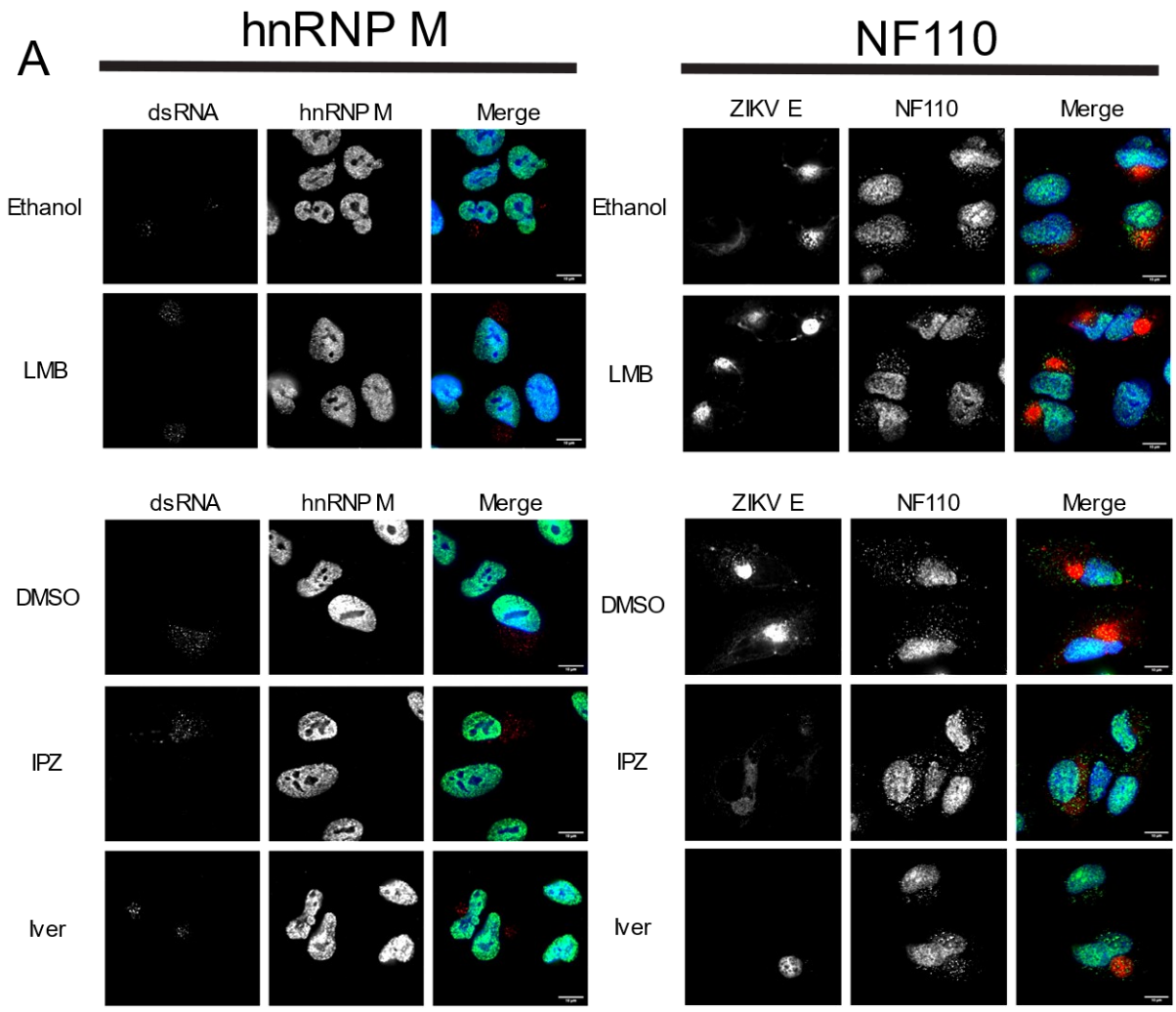
A
hnRNP M
NF110
dsRNA
hnRNP M
Merge
ZIKV E
NF110
Merge
Ethanol
LMB
DMSO
IPZ
Iver

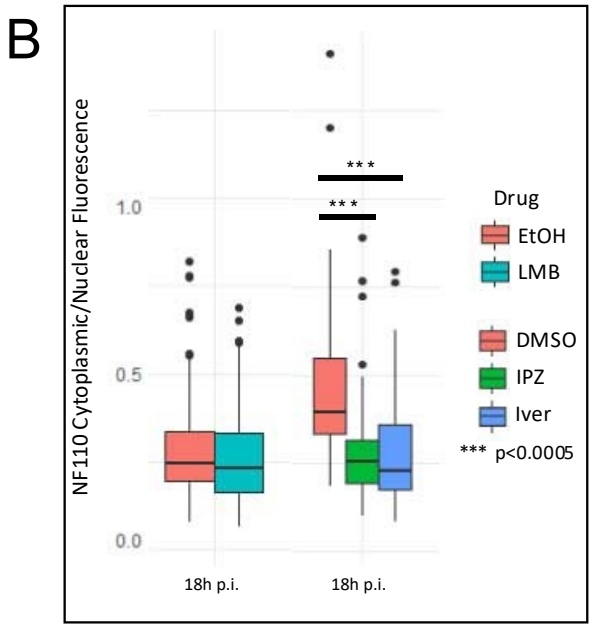
B
NF110 Cytoplasmic/Nuclear Fluorescence
1.0
0.5
0.0
***
***
18h p.i.
18h p.i.
Drug
EtOH
LMB
DMSO
IPZ
Iver
*** p<0.0005

3.6 Depletion of NF110 or hnRNP M alters the viral lifecycle

Evidence suggests that isoforms encoded by the *ILF3* gene and hnRNP M interact with ZIKV +vRNA (Table 3-1), and that NF90/NF110, but not hnRNP M, redistribute following ZIKV infection (Figure 3.5-6), but these data do not suggest a possible role of these proteins in the ZIKV lifecycle. To investigate whether NF110 or hnRNP M were required for efficient ZIKV replication, we depleted host cells of either NF110 or hnRNP M, and we examined the effects of depletion of these host nuclear factors on different aspects of the ZIKV lifecycle. To deplete the host proteins, we used a lentiviral pseudovirus vector system to deliver shRNA expression constructs targeting the mRNA transcripts for either NF110 or hnRNP M. As a negative control, we used a non-mammalian scrambled control shRNA in the same backbone and lentiviral pseudovirus vector as the shRNA targeting NF90/NF110 and hnRNP M. As shown by western blot analysis of whole cell lysates from lentivirus transduced cells (Figure 3.12A), we achieved depletion of hnRNP M and both the NF90 and NF110 isoforms. To ensure that the depletion of NF90/NF110 and hnRNP M was not affecting the growth or viability of the cells within the time constraints of our experiments, we used an ATP-based luciferase assay (Figure 3.12F). When we analyzed data from these experiments, we observed that the depletion of hnRNP M did not result in a decrease in the growth or viability of the cells compared to the control. NF90/NF110 however had a 20% reduction in cell viability by 108h post transduction. While this is a significant decrease in viability, previous research suggests that this is due to a decrease in the rate of cell growth rather than a decrease in cell viability [97]. These data suggest that we were able to obtain a knockdown of both NF90/NF110 and

hnRNP M, and that the depletion of those nuclear factors did not significantly affect the viability of A549 cells.

Figure 3.12: Depletion of NF90/NF110 or hnRNP M influences the ZIKV lifecycle.

A549 cells were transduced in media (supplemented with polybrene) with lentiviruses containing shRNAs targeting *ILF3* (NF90/NF110), hnRNP M and a scrambled mammalian control for 72h prior to infection. Cells were then infected with ZIKV for 12 to 48h. **(A)** A549 cells were transduced with lentivirus particles containing either scrambled control shRNA or shRNA directed against hnRNP M or NF90/NF110 for 72h. Whole cell lysates were then collected to assess knockdown. Other samples were then infected with ZIKV for 24 to 48h. Whole cell lysates were collected and analyzed by SDS-PAGE and western blot using antibodies directed against host hnRNP M or NF90/NF110, ZIKV NS5, or host GAPDH as a loading control. Blots were detected with ECL and HRP-conjugated secondary antibodies and imaged in an ImageQuant chemiluminescence detection system. **(B and C)** A549 cells transduced with lentivirus containing shRNA constructs were grown for 72h prior to infection with ZIKV for indicated durations. Total RNA was collected using TriZOL reagent and the RNA was reverse transcribed. cDNA was then analyzed by quantitative PCR using probes directed at the ZIKV genome and run in technical duplicate. Data were analyzed using the comparative C_t method. Changes are for the NF90/NF110 and hnRNP M depletions are shown in **(B)** and **(C)** respectively. Error bars represent triplicate biological replicates. One sample t-test was run on results from 3 biological replicates. Adjusted p-values in comparisons of results to null hypothesis are shown as *<0.05 and **<0.001. **(D and E)** Supernatants collected the cells grown for RNA analysis were analyzed by plaque assay in Vero cells for 96h. Assays were fixed, stained, and counted to calculate plaque forming units per mL (PFU/mL). Supernatants from the NF90/NF110 and hnRNP M depleted cells are shown in **(D)** and **(E)** respectively. Error bars represent triplicate biological replicates. Results from 3 biological replicates were submitted to ANOVA followed by Tukey HSD post hoc tests. Adjusted p-values for Tukey HSD in pairwise comparisons between the depletion condition and scambled control are indicated as *<0.01 and **<0.001. **(F)** A549 cells were transduced with lentiviral constructs containing either scrambled shRNA or shRNA targeting NF90/NF110 or hnRNP M. Cell viability was then measured from 72h to 132h post transduction. Viability was measured by examining ATP levels with a luciferase ATP assay. Luminescence was recorded in a plate reader and knockdown viabilities are shown as a percentage of the scrambled control luminescence signal. Error bars represent quadruplicate biological replicates.

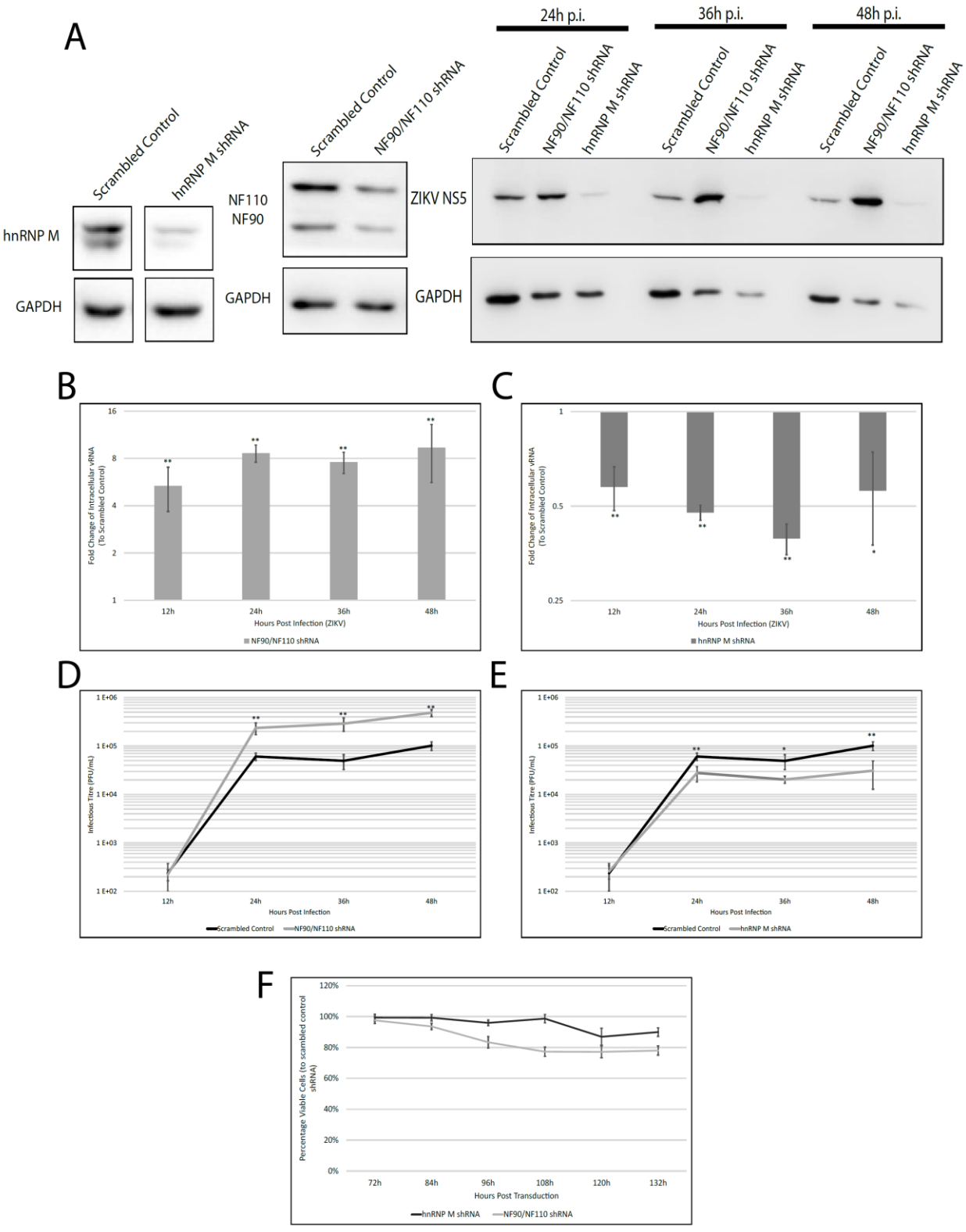
A
24h p.i.
36h p.i.
48h p.i.
Scrambled Control
hnRNP M shRNA
NF90/NF110 shRNA
hnRNP M
GAPDH
NF110
NF90
ZIKV NS5
B
Fold Change of Intracellular vRNA (To Scrambled Control)
Hours Post Infection (ZIKV)
NF90/NF110 shRNA
C
hnRNP M shRNA
D
Infectious Titre (PFU/mL)
Hours Post Infection
E
F
Percentage Viable Cells (to scambled control shRNA)
Hours Post Transduction

To assess the effects of the depletion of NF90/NF110 on the lifecycle of ZIKV infection in A549 cells, we examined three different measures of viral replication. We first assessed the level of ZIKV NS5 protein in whole cell lysates by SDS-PAGE and western blotting. We observed that the depletion of NF90/NF110 resulted in a robust increase in the amount of NS5 protein in observed by western blot (Figure 3.12A). Next, we assessed the steady state levels of intracellular ZIKV +vRNA using quantitative RT-PCR analysis. The depletion of NF90/NF110 resulted in a 5-fold increase in ZIKV +vRNA 12h post infection which increased to an 8-fold increase of ZIKV +vRNA from 24 to 48h post infection (Figure 3.12B) in comparison to the scrambled control samples. Lastly, we assessed the production of infectious virus produced in the supernatant of the depleted cells using a plaque forming assay in Vero cells. We observed an increase in the amount of infectious virus produced in the NF90/NF110 depleted cells in the 24 to 48h post infection time points but did not observe a difference at 12h post infection. These data suggest that the depletion of NF90/NF110 results in increased levels of NS5 and + strand ZIKV RNA in depleted cultures, and an increase of infectious viral titers in supernatants collected from those cultures suggesting an anti-viral role for NF90/NF110 in ZIKV infection.

We repeated the above experiments for samples depleted of hnRNP M and compared the results to the scrambled non-mammalian control knockdowns. We observed a robust decrease in the amounts of NS5 protein in whole cell lysates of cells that had been depleted of hnRNP M (Figure 3.12A). We also observed a decrease in the total amount of protein in the hnRNP M depleted samples collected at 36 and 48h post ZIKV infection. When we assessed the levels of intracellular ZIKV +vRNA by quantitative PCR, we observed a 2-fold reduction in the production of ZIKV vRNA

throughout the time course of ZIKV infection as compared to the scrambled non-mammalian control samples (Figure 3.12C). When we assessed the levels of infectious virus produced by the hnRNP M depleted cells by plaque forming assay, we observed a marginal decrease in the amounts of infectious virus produced with no observed difference at 12h post infection (Figure 3.12E). These data suggest that the depletion of hnRNP M results in lower levels of NS5 and + strand ZIKV RNA in hnRNP M depleted cultures, and a corresponding decrease in the infectious viral titers in supernatants collected from cultures depleted of hnRNP M suggesting a pro-viral role of hnRNP M in ZIKV infection.

3.7 Depletion of NF90/NF110 or hnRNP M alters the distribution of vRNA and viral proteins

The depletion of NF90/NF110 and the depletion of hnRNP M both affect the ZIKV infection in cells by increasing and decreasing viral production, respectively. These data do not address possible changes in the distribution of ZIKV +vRNA or ZIKV proteins in cells depleted of NF90/NF110 or hnRNP M. To assess the effect of NF90/NF110 or hnRNP M depletions on the localization of ZIKV vRNA or proteins, we infected cells depleted of NF90/NF110 or hnRNP M and then subjected samples to FISH (to examine vRNA localization) or immunofluorescence (to examine viral protein localization) analysis.

First, for our FISH experiments (Figure 3.13), we utilized two probe sets, each labeled with a distinct fluorophore, that hybridize to ORF regions positioned either near the 3’ or 5’ end of the viral genome. The FISH protocol also allowed us to examine the host proteins by immunofluorescence at the same time to ensure that we were examining cells depleted of NF90/NF110 or hnRNP M. As shown in Figure 3.13A, we were able to ensure that we were examining cells that were depleted of NF90/NF110 by comparing the NF90/NF110 immunofluorescence signal in the non-mammalian scrambled control shRNA and the NF90/NF110 shRNA conditions. This increases the likelihood that the observed differences between the two conditions are a result of the depletion NF90/NF110. Because of the stringent fixation and permeabilization conditions of the FISH protocol much of the NF90/NF110 signal usually seen in the cytoplasm is not seen in these images. We observed that the depletion of NF90/NF110 resulted in increased + strand vRNA signal in the cytoplasm of infected

cells. The vRNA signal in the cytoplasm of cells depleted of NF90/NF110 is much more robust than is seen in the scrambled control cells infected for the same amount of time. There are also small circular areas of the cytoplasm that do not have vRNA signal. This mimics a phenotype observed by Monel et al.[52]. The authors describe massive cytoplasmic vacuolization and paraptosis-like death. The authors compare the cell death to paraptosis because it is independent of caspases, non-apoptotic, and associated with the formation of large cytoplasmic vacuoles. Monel et al. suggest that the depletion of IFITM3 exacerbates this occurrence. These FISH data in cells depleted of NF90/NF110 suggest that the depletion of NF90/NF110 results in increased levels of ZIKV RNA in the cytoplasm of infected and depleted cells and are consistent with the observed increase in intracellular + strand vRNA as observed by quantitative RT-PCR (Figure 3.12B). These data suggest that the depletion of NF90/NF110 results in a more robust ZIKV infection as well as increased ZIKV E protein observed by IF and increased ZIKV +vRNA observed by FISH.

In Figure 3.13B, we assess the effect of the depletion of hnRNP M on the localization and fluorescent intensity of ZIKV +vRNA by FISH following infection with ZIKV. Importantly, the antibody directed against hnRNP M shows which cells are depleted of hnRNP M in the field and ensures that any changes we observe are more likely to be a result of hnRNP M depletion. The depletion hnRNP M resulted in decreased + strand vRNA FISH signal intensity in the cytoplasm of infected cells. These data suggest that the depletion of hnRNP M results in decreased levels of ZIKV RNA in the cytoplasm of infected hnRNP M depleted cells. These observations are consistent with the observed decrease in intracellular + strand vRNA as observed by quantitative RT-PCR (Figure 3.12C).

Figure 3.13: Depletion of NF90/NF110 or hnRNP M alter the amount and morphology of +vRNA in A549 cells.

A549 cells were transduced with lentiviruses containing either scrambled control shRNA or shRNA constructs directed at NF90/110 or hnRNP M for 72h prior to infection. Cells were then infected for 24h and the distribution of vRNA was examined using fluorescence in situ hybridization (FISH). Knockdown conditions are indicated to the left of the panels. smFISH probes that hybridize to the 3' (nucleotides 1,500-3,500) and 5' (nucleotides 6,500-8,500) ends of the ZIKV ORF were used to determine the distribution of the ZIKV + strand vRNA. The position of the nuclei was determined using the DNA stain DAPI (blue). The localization of host NF9090/NF110 or hnRNP M was determined by indirect immunofluorescence using antibodies targeted against NF90/NF110 or hnRNP M. Merged images show host nuclear factors pseudo coloured green, 3' probes pseudo coloured yellow, and 5' probes pseudo coloured red. Representative images were captured using epiflourescent microscopy and deconvolved. **(A)** The distribution of NF90/NF110 was determined using antibodies directed against NF90/NF110. Because the depletion of NF90/NF110 results in such a strong increase in RNA it is necessary to show a longer exposure to show that the cells are indeed infected without overexposing the signal in the depletion condition. **(B)** The distribution of hnRNP M was determined using antibodies directed against hnRNP M. Scale bars, 10μm.

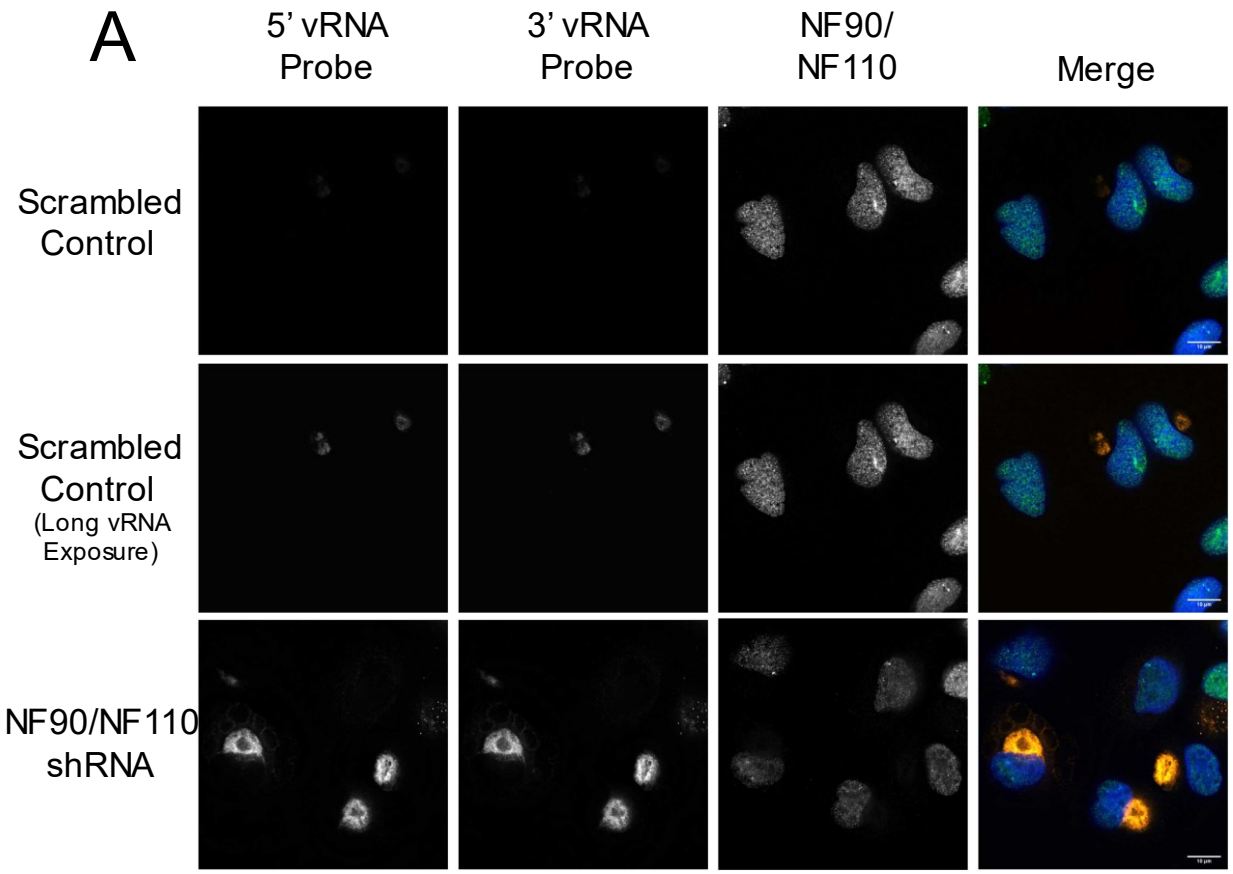
A
5' vRNA Probe
3' vRNA Probe
NF90/ NF110
Merge
Scrambled Control
Scrambled Control (Long vRNA Exposure)
NF90/NF110 shRNA

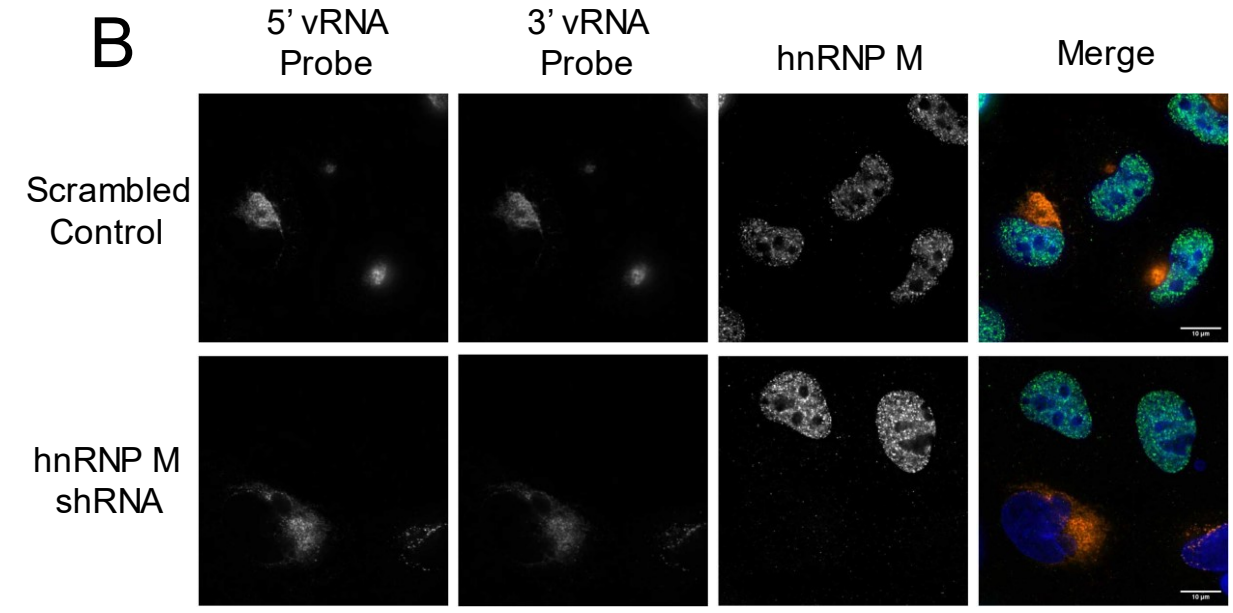
B
5' vRNA Probe
3' vRNA Probe
hnRNP M
Merge
Scrambled Control
hnRNP M shRNA

Second, to assess the effect of the depletion of NF90/NF110 or hnRNP M on the localization of ZIKV E protein in depleted cells, we used indirect immunofluorescence and antibodies directed at ZIKV E protein and either NF90/NF110 or hnRNP M. As shown in Figure 3.14A, we observe that the antibody directed at NF90/NF110 ensures that the cells that we are observing are depleted of NF90/NF110 and increases the likelihood that any changes in viral signal between the NF90/NF110 depleted condition and the non-mammalian scrambled control samples are a result of the depletion of NF90/NF110. We also observe that the depletion of NF90/NF110 results in a robust ZIKV E signal in the cytoplasm of infected and depleted cells when compared to the scrambled control depletion condition (Figure 3.14A). These data suggest that the depletion of NF90/NF110 results in an increase in levels of ZIKV E protein without any significant changes in localization of the ZIKV E protein.

In Figure 3.14B, we assess the effect of the depletion of hnRNP M on the localization and signal intensity of ZIKV E protein. Using antibodies directed against hnRNP M, we can ensure that we are observing a robust depletion of hnRNP M in the depletion condition. We observe that the depletion of hnRNP M results in a decreased ZIKV E protein signal compared to the scrambled control conditions. We needed to increase the exposure time of the depleted cells to see the E protein, thus this exposure leads to an increased signal in the scrambled control. Additionally, the depletion of hnRNP M appears to inhibit the phenotype of a robust concentration of the E protein in areas we suspect are replication factories (Figure 3.2). It is also possible that hnRNP M depleted cells fail to properly form replication factories, however, this was not directly examined. While the mechanism remains to be determined, these data suggest that

the depletion of hnRNP M results in a decreased level of viral protein in infected cells and an altered distribution of ZIKV E protein in hnRNP M depleted cells.

Figure 3.14: Localization and intensity of ZIKV E protein is altered in NF90/NF110 or hnRNP M depleted cells.

A549 cells were transduced with lentiviruses containing either scrambled control shRNA or shRNA constructs directed at NF90/110 or hnRNP M for 72h prior to infection. Cells were then infected for 24h and the distribution of ZIKV E protein was examined using indirect immunofluorescence with antibodies directed against the ZIKV E protein. Knockdown conditions are indicated to the left of the panels. The position of the nucleus was determined using the DNA stain DAPI (blue). The localization of host NF9090/NF110 or hnRNP M was determined by indirect immunofluorescence using antibodies targeted against NF90/NF110 or hnRNP M. Merged images show host nuclear factors pseudo coloured green, and ZIKV E protein pseudo coloured red. Representative images were captured using epiflourescent microscopy and deconvolved. **(A)** The distribution of NF90/NF110 was determined using antibodies directed against NF90/NF110. **(B)** The distribution of hnRNP M was determined using antibodies directed against hnRNP M. Scale bars, 10μm.

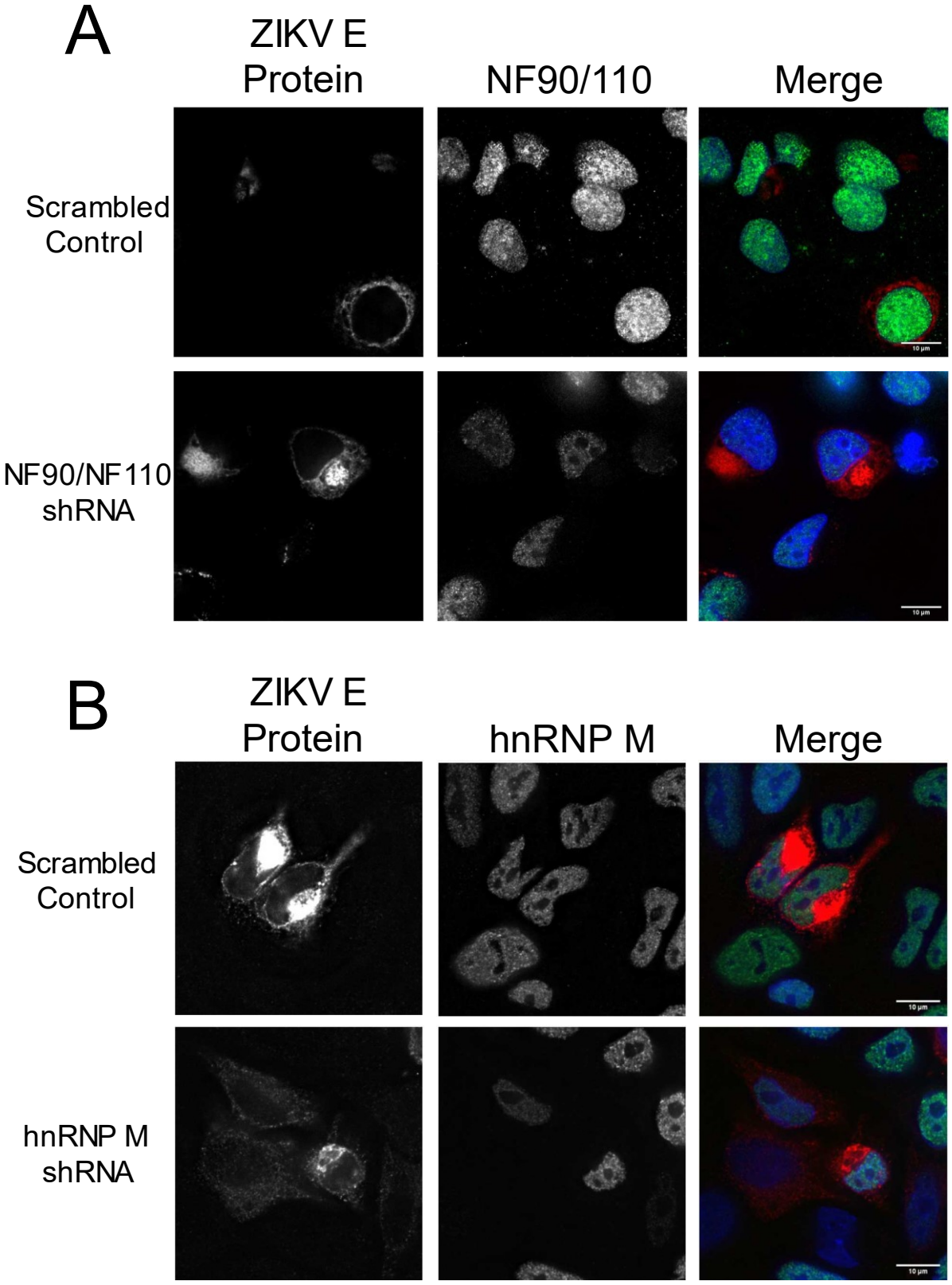
A
ZIKV E Protein
NF90/110
Merge
Scrambled Control
NF90/NF110 shRNA
B
ZIKV E Protein
hnRNP M
Merge
Scrambled Control
hnRNP M shRNA

3.8 Depletion of hnRNP M alters the PKR response to infection

Evidence presented above suggests that the depletion of hnRNP M results in an attenuated ZIKV infection but does not address possible reasons for this. Cao et al. present data that suggest hnRNP M may act as a decoy in SeV infection and interfere with the ability of PRRs to sense viral RNA [92]. To assess if the depletion of hnRNP M attenuates ZIKV infection in A549 cells in a similar manner, we explored the effect of hnRNP M depletion on the phosphorylation of PKR in response to ZIKV infection. To accomplish this, we assayed the response of phosphorylated PKR in whole cells lysates by SDS-PAGE and western blotting through a time course of ZIKV infection in samples transduced with scrambled control shRNAs or shRNAs targeting NF90/NF110 or hnRNP M transcripts. We collected whole cell lysates from A549 cells that were depleted of NF90/NF110 or hnRNP M and then infected with ZIKV for the indicated lengths of time (Figure 3.15A). We then used antibodies directed at PKR, phosphorylated PKR, tubulin or ZIKV NS5 protein in a western blot analysis to assess the steady state levels of these proteins. The protein levels of PKR remained constant relative to tubulin controls, which suggests that neither infection nor depletion of NF90/NF110 or hnRNP M influence the overall PKR levels. However, we did observe differences in the induction of phospho-PKR in the hnRNP M depletion conditions. To compare the mock and early infection time points, we examined two exposures of phospho-PKR (short and long) as indicated. In mock infected cells (0h post infection) there is little phosphorylation of PKR in any of the three depletion conditions. However, by 12h post infection phosphorylation of PKR was increased in cells depleted of hnRNP M as compared to the NF90/NF110 depleted cells and the

scrambled control condition. The phosphorylation profiles of the depletion conditions and the control become more equivalent 24-36h post infection. At 48h post infection, the p-PKR levels in the scrambled control condition began to decrease compared to the NF90/NF110 and hnRNP M depletion conditions. In support of the observed effects of the depletion of NF90/NF110 and hnRNP M on the levels of NS5 in infected and depleted cells (Figure 3.12A), we observe similar differences in the NS5 protein levels in this experiment as well. It does not appear that the depletion of NF90/NF110 has any effect on the phosphorylation profile of PKR compared to the scrambled control condition. These data suggest that cells that are depleted of hnRNP M have an increased PKR responsiveness to infection, which supports our observation that the depletion of hnRNP M attenuates the viral lifecycle.

The data presented above suggest that the depletion of hnRNP M results in a more robust phosphorylation of PKR following infection with ZIKV. These data do not provide any information regarding the localization of PKR in hnRNP M depleted cells. To assess the effect of NF90/NF110 or hnRNP M depletion on the localization of PKR, we used indirect immunofluorescence to examine the distribution of PKR. We transduced A549 cells with lentiviral particles to deplete cells of either NF90/NF110 or hnRNP M, and then we infected them with ZIKV. Following ZIKV infection of cells transduced with scrambled control shRNA or shRNA targeting hnRNP M, we observed a punctate PKR signal distribution in areas overlapped by the ZIKV E protein (Figure 3.15B). In cells depleted of NF90/NF110, we observed that there was a buildup of PKR signal in the same area as the ZIKV E protein signal that may represent a sequestration of PKR in the replication factories of infected cells. A limitation of this experiment is that we unable to directly demonstrate NF90/NF110 depletion in cells

exhibiting increased PKR signal in regions containing E protein. However, this phenotype of sequestered PKR was only observed in the NF90/NF110 depleted condition. These data suggest that the depletion of NF90/NF110 may result in the sequestration of PKR in replication factories following ZIKV infection and supports our observation of increased viral production in cells depleted of NF90/NF110.

Figure 3.15: hnRNP M depletion affects the profile of PKR phosphorylation while NF90/NF110 depletion affects the localization of PKR.

A549 cells were transduced with lentiviruses containing either scrambled control shRNA or shRNA targeting hnRNP M or NF90/NF110 for 72h prior to infection with ZIKV. Cells were infected with ZIKV for the indicated durations, from 12h to 48h of ZIKV infection. **(A)** Whole cell lysates were collected, and an SDS-PAGE and western blot was done using antibodies directed at PKR, phosphorylated PKR (T446), tubulin, and ZIKV NS5, as indicated. The phosphorylated-PKR blot was given a longer exposure to observe the responses of the phosphorylation of PKR in uninfected and cells at 12h post infection. At 12h of ZIKV infection NS5 is not detectable by western blot. **(B)** A549 cells were transduced with lentivirus particles as indicated above and either mock infected or infected with ZIKV for 24h. Samples were analyzed using indirect immunofluorescence using antibodies directed against host cell PKR or ZIKV E protein. The position of nuclei was determined using the DNA stain DAPI. Merged images show the host PKR pseudo coloured green, and ZIKV E protein pseudo coloured red. Representative images were acquired using epifluorescence microscopy and deconvolved. Scale bars, 10 μm.

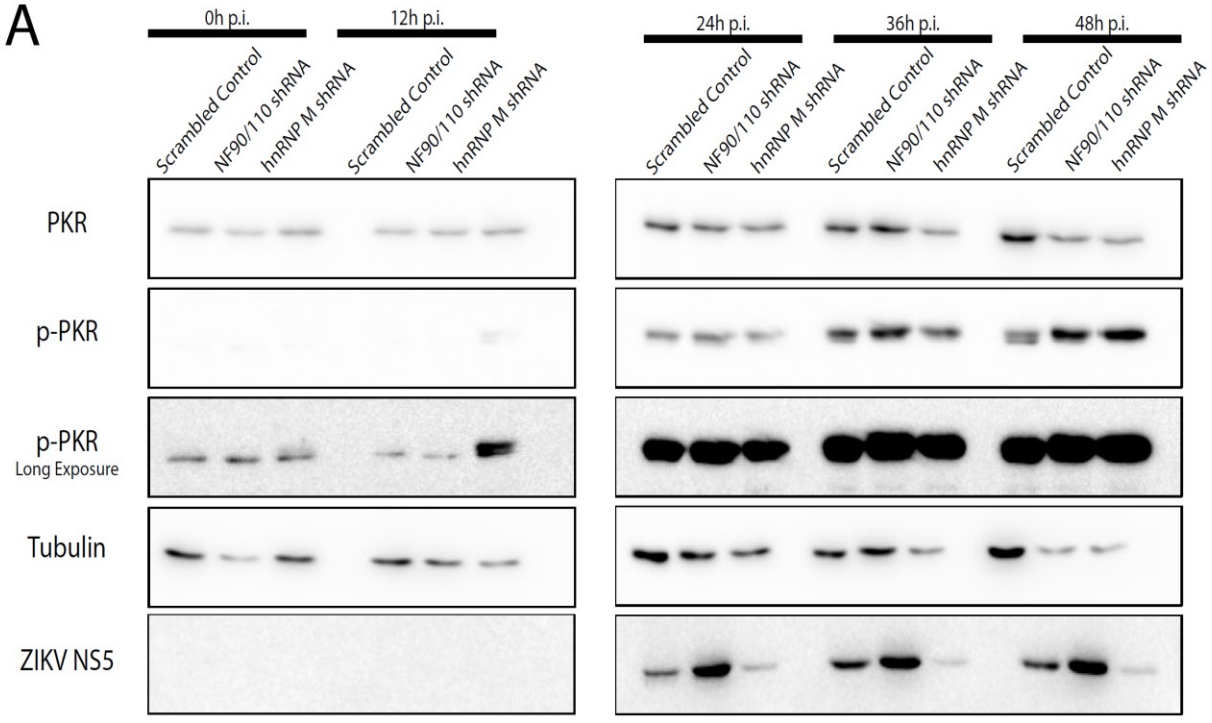
A
0h p.i.
12h p.i.
24h p.i.
36h p.i.
48h p.i.
Scrambled Control
NF90/110 shRNA
hnRNP M shRNA
PKR
p-PKR
p-PKR
Long Exposure
Tubulin
ZIKV NS5

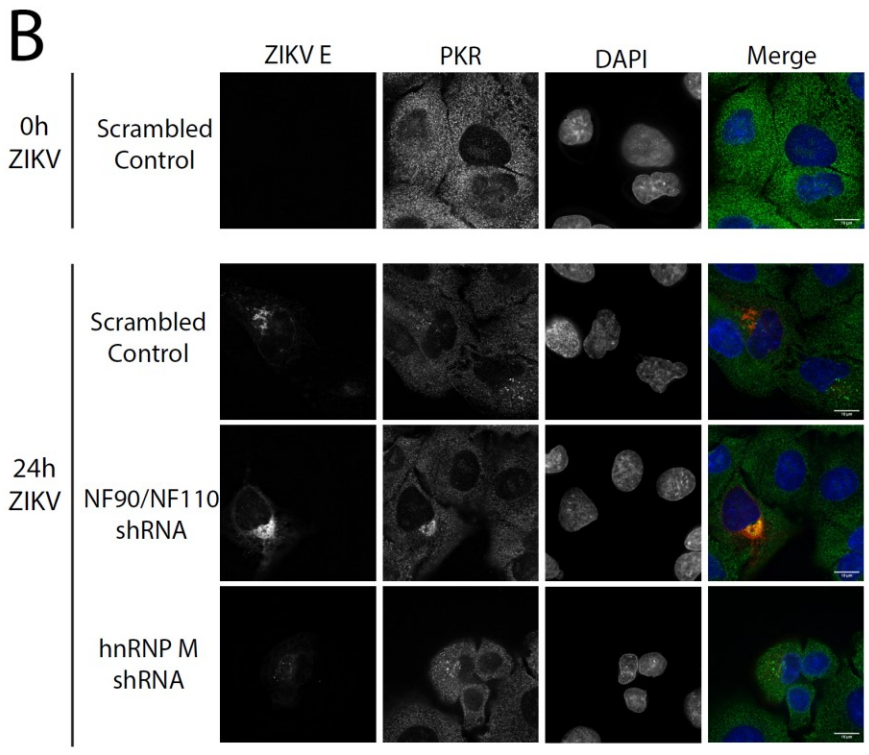
B
ZIKV E
PKR
DAPI
Merge
0h
ZIKV
Scrambled
Control
24h
ZIKV
Scrambled
Control
NF90/NF110
shRNA
hnRNP M
shRNA

3.9 Depletion of hnRNP M or NF90/NF110 alters the induction of interferon-stimulated genes upon ZIKV infection

A robust infection with ZIKV results in a strong induction of the host immune response that is blunted by numerous ZIKV strategies (as discussed in Section 1.3). To assess for the induction of interferon-stimulated genes (ISGs) following ZIKV infection, we used quantitative RT-PCR to measure mRNA transcript levels for 7 ISGs: interferon alpha 1 (IFNA1), interferon beta 1 (IFNB1), interferon-induced GTP-binding protein Mx1 (MX1), 2'-5'-oligoadenylate synthetase 1 (OAS1), protein kinase R (PKR), nuclear factor kappa B subunit 1 (NFKB1), and tumor necrosis factor alpha (TNF). We infected A549 cells for 12-48h with ZIKV as indicated (Figure 3.16), and then isolated total RNA from these samples. This RNA was reverse transcribed, and the resulting cDNA was then analyzed by quantitative PCR using primer sets targeted to specific ISGs. As shown in Figure 3.16, following infection of A549 cells with ZIKV, we observed a robust increase in the mRNA transcripts levels of several ISGs, including IFNB1, MX1, OAS1, PKR, NFKB, and TNF. IFNB1 and MX1 mRNA levels were increased more than 100- and 1000-fold, respectively, at 36h and 48h post infection. Similarly, Hertzog and colleagues observed a similar robust induction of the ISGs IFNB1, MX1, and IFIT1 following infection with a Brazilian isolate of ZIKV [144]. These data suggest that, following infection with ZIKV, A549 cells are capable of mounting a robust induction of ISGs.

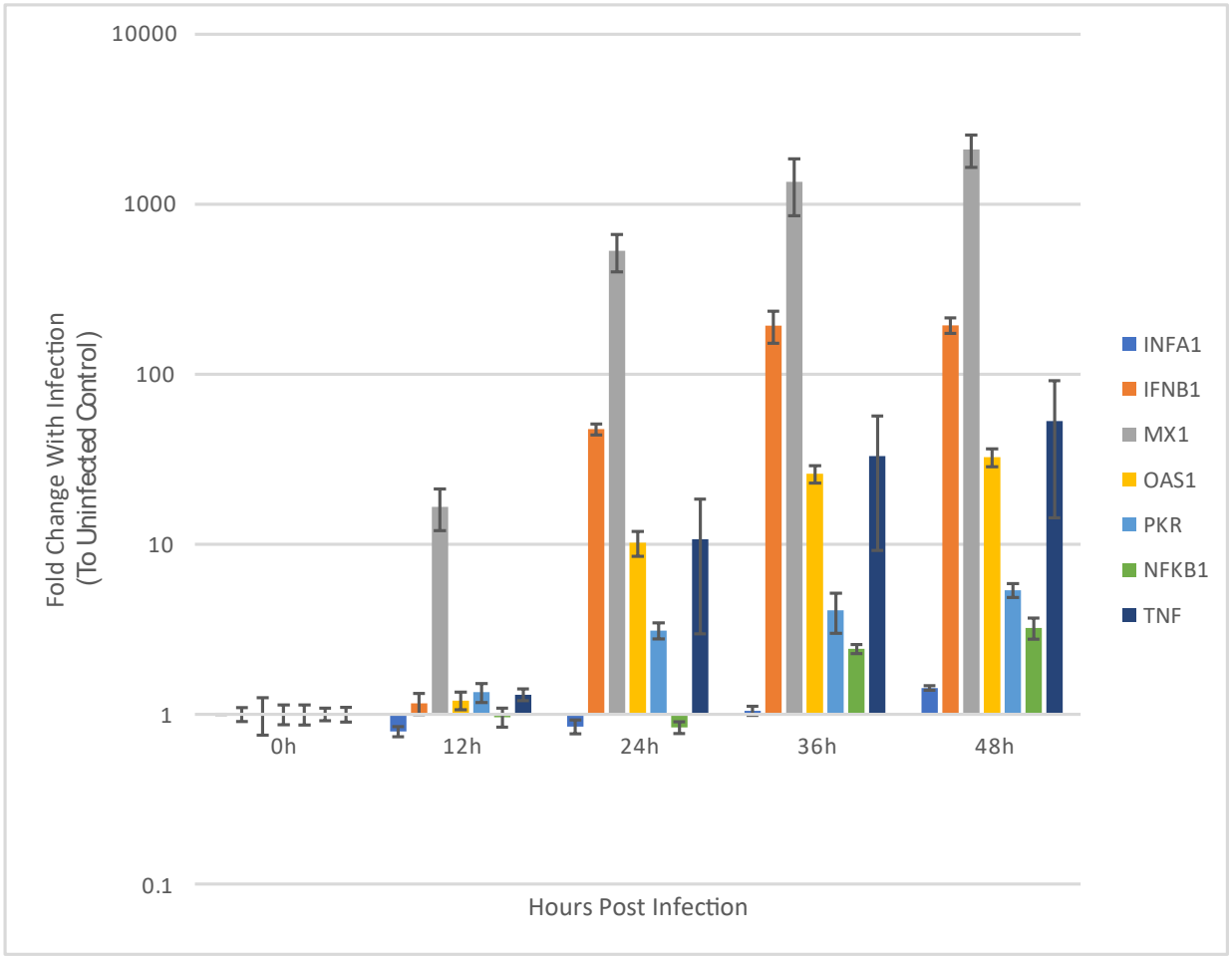

Figure 3.16: ZIKV infection induces robust increase of interferon stimulated gene (ISG) transcripts.

A549 cells were infected with ZIKV. Following either mock infection, or ZIKV infection of 12, 24, 36, or 48h. Cells were collected in TriZOL and total cellular RNA was isolated. Collected RNA was reverse transcribed using random primers. cDNA was then analyzed using quantitative PCR using primer sets directed at the indicated ISGs in technical duplicates. Data were analyzed by the comparative C_t method. Error bars represent triplicate biological replicates.

Given the roles that NF90/NF110 play in the host immune response, one possibility was that the depletion of NF90/NF110 interferes with the proper initiation of the host immune response. By contrast, since we observed that the depletion of hnRNP M resulted in an attenuated ZIKV infection, it is possible that there was a more robust immune response in hnRNP M depleted cells. In order to assess if the depletion of NF90/NF110 or hnRNP M altered ISG transcript levels in response to ZIKV infection, we examined if either of the depletion conditions altered levels of ISG transcripts outside of the context of ZIKV infection. To accomplish this, we analyzed ISG transcript levels in depleted cells. We collected total RNA samples from A549 cells that had been transduced with lentiviral particles containing either a scrambled control shRNA, or an shRNA targeting NF90/NF110 or hnRNP M 72h post transduction. These RNA samples were analyzed as above. As shown in Figure 3.17A, we observed that the depletion of NF90/NF110 did not result in any significant alterations in ISG transcript levels in depleted cells. Conversely, we observed that the depletion of hnRNP M resulted in a 2-fold increase in NFKB, TNF, and OAS1 transcript levels. These data suggest that while the depletion of NF90/NF110 does not affect basal ISG induction, the depletion of hnRNP M results in a modest induction of some ISGs in uninfected A549 cells.

To assess how the depletion of either NF90/NF110 or hnRNP M affected the induction of ISGs in A549 cells infected with ZIKV, we analyzed total RNA from infected and depleted cells in the same manner as the uninfected cells above. The depletion of NF90/NF110 resulted in marginally increased the mRNA transcript levels of TNF but not of other ISGs that we examined. The depletion of hnRNP M resulted in decreased induction of ISGs following infection with ZIKV compared to the scrambled control

condition. These data suggest that the depletion of NF90/NF110 does not antagonize the immune response with respect to the ISG transcript levels following infection with ZIKV. Conversely, these data suggest that the depletion of hnRNP M results in lower ISG transcript levels in infected cultures following infection with ZIKV. This is contrary to the expected results as the depletion of hnRNP M results in an attenuated ZIKV infection and an early increase in p-PKR (Figure 3.12 and Figure 3.15). Taken together, these data suggest that the mechanism by which the depletion of either NF90/NF110 and hnRNP M are affecting the ZIKV lifecycle is not a result of altered ISG transcript levels in infected cells.

Figure 3.17: Depletion of hnRNP M or NF90/NF110 alters the induction of interferon stimulated genes.

A549 cells were transduced with lentiviruses encoding either scrambled control shRNA or shRNA directed against hnRNP M or NF90/NF110 for 72h. **(A)** Transduced cells were collected with TriZOL and total RNA was purified and reverse transcribed using random primers. cDNA was analyzed using quantitative PCR using primers directed at the indicated ISGs and run in technical duplicate. Data were analyzed using the comparative C_t method. Error bars represent triplicate biological replicates. Results from three biological replicates were subjected to one sample t-test and p-values are indicated as *<0.05. **(B)** Following transduction for 72h, A549 cells were then infected for the indicated durations with ZIKV. Samples were collected and analyzed as above. Error bars represent triplicate biological replicates. Results from triplicate biological replicates were subjected to ANOVA and post hoc Tukey HSD tests. Adjusted p-values for pairwise comparisons between the NF90/NF110, hnRNP M and scrambled control conditions are indicated as *<0.05, **<0.01, and ***<0.001.

A

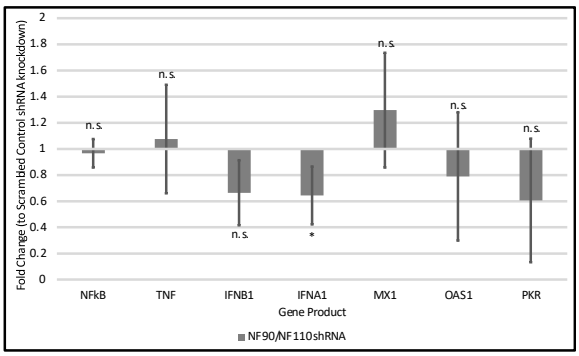
Fold Change (to Scrambled Control shRNA knockdown)
n.s.
NFkB
TNF
IFNB1
IFNA1
MX1
OAS1
PKR
Gene Product
NF90/NF110 shRNA

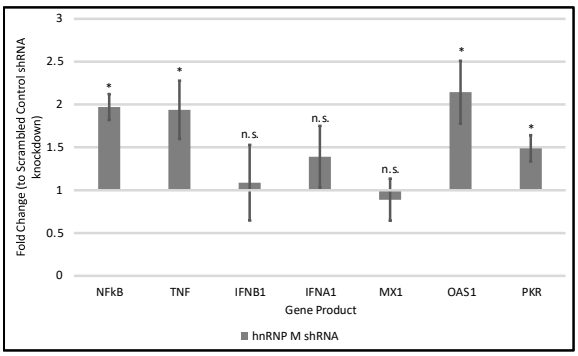
Fold Change (to Scrambled Control shRNA knockdown)
n.s.
NFkB
TNF
IFNB1
IFNA1
MX1
OAS1
PKR
Gene Product
hnRNP M shRNA

B

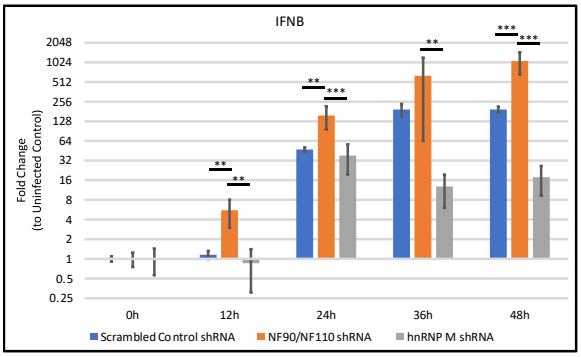
IFNB
Fold Change (to Uninfected Control)
0h
12h
24h
36h
48h
Scrambled Control shRNA
NF90/NF110 shRNA
hnRNP M shRNA

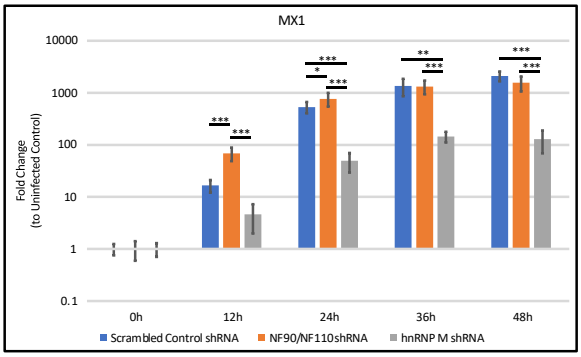
MX1
Fold Change (to Uninfected Control)
0h
12h
24h
36h
48h
Scrambled Control shRNA
NF90/NF110 shRNA
hnRNP M shRNA

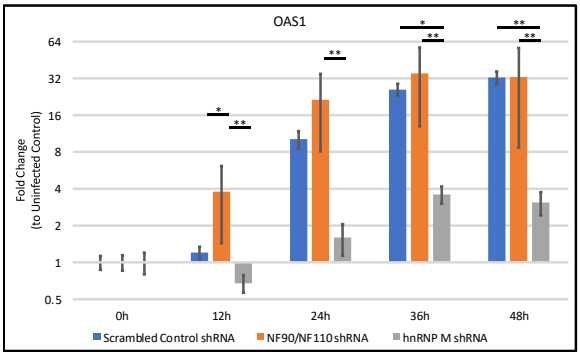
OAS1
Fold Change (to Uninfected Control)
0h
12h
24h
36h
48h
Scrambled Control shRNA
NF90/NF110 shRNA
hnRNP M shRNA

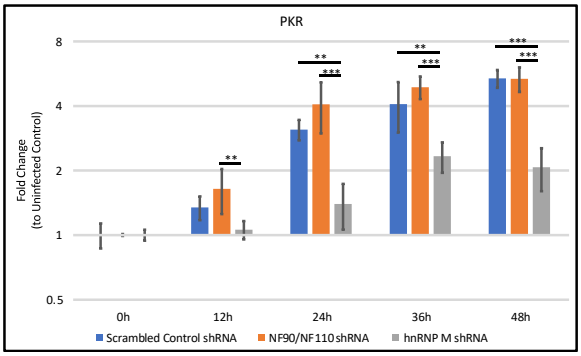
PKR
Fold Change (to Uninfected Control)
0h
12h
24h
36h
48h
Scrambled Control shRNA
NF90/NF110 shRNA
hnRNP M shRNA

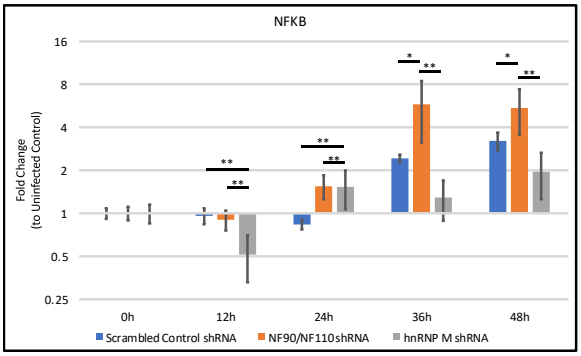
NFKB
Fold Change (to Uninfected Control)
0h
12h
24h
36h
48h
Scrambled Control shRNA
NF90/NF110 shRNA
hnRNP M shRNA

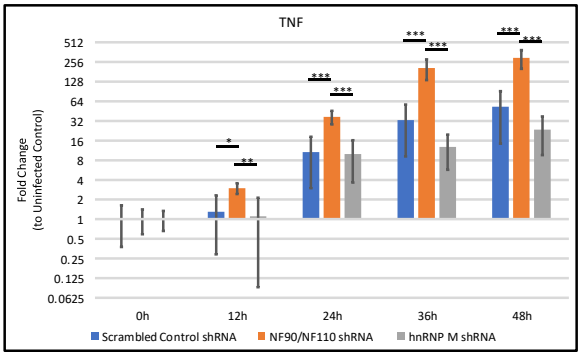
TNF
Fold Change (to Uninfected Control)
0h
12h
24h
36h
48h
Scrambled Control shRNA
NF90/NF110 shRNA
hnRNP M shRNA

4 DISCUSSION

4.1 Introduction

ZIKV is a single-stranded positive sense RNA virus belonging to the *Flavivirus* genus and the *Flaviviridae* family of viruses. The central dogma surrounding plus-strand RNA viruses is that they enter cells, decapsulate, and enter directly into the host translation machinery to begin replicating in the host cell. Recent evidence suggests that there are many nuclear factors involved in ZIKV infection, that are either being redistributed to the cytoplasm or found to be binding to either the viral genome or viral proteins. Some of the roles that these proteins play have been elucidated but there are countless proteins associated with viral proteins or RNAs in infected cells that have not been studied. To provide some insight on the possible roles of nuclear factors in viral infection our starting point was with an analysis of a comprehensive identification of RNA-binding proteins by mass spectrometry (ChIRP-MS) experiment [145] run by our collaborators. These data provided a long list of host proteins that interact with the ZIKV genome, many of which are nuclear factors. Out of this list we selected two different types of proteins, dsRNA binding proteins and heterogeneous nuclear ribonucleoproteins (hnRNPs). Of the top hits of dsRNA binding proteins were peptides encoded by the *ILF3* gene, which, being implicated in so many diverse cellular processes, and such a diverse range of viral lifecycles, was a good candidate to study. With respect to the hnRNPs, seven were enriched more than two-fold compared to control RNAs. These were hnRNP M, H, L, A, K, U, and F, with hnRNP M being the most enriched in this ChIRP-MS study. The hnRNP family of proteins have multiple different functional domains but are all related in that they contact RNA through RNA recognition motifs (RRMs). hnRNP M specifically contains three RRMS. With very little information available on hnRNP M in relation to viruses and being the

top hnRNP hit on the ChIRP-MS study, it was a good candidate for further study in ZIKV infection.

Our project focused on the possible role of nuclear factors during a ZIKV infection, and using our collaborators ChIRP-MS data, we narrowed our focus down to the isoforms encoded by the *ILF3* gene and the protein hnRNP M. Through our experiments we observed that NF90/NF110 is redistributed to areas of viral replication and colocalize with viral dsRNA in the cytoplasm of infected cells, while hnRNP M remains in the nucleus of infected cells. The depletion of these proteins also results in contrasting effects on viral replication. For example, depletion of NF90 and NF110 results in increased viral replication following ZIKV infection while the depletion of hnRNP M results in the attenuation of the viral lifecycle. These data suggest that NF90/NF110 and hnRNP M are playing anti-viral and pro-viral roles in ZIKV infection, respectively.

4.2 *ILF3* gene encoded proteins as antiviral proteins in ZIKV infection

The literature involving NF110 and its role in viral infections is wide ranging and diverse. NF110 not only participates in the shutdown of global host translation in response to viral infection [124], [129], but it is also involved in the successful translation of the host immune proteins IFNB1 and a subgroup of other ISGs through the host translation blockade [131]. This evidence would suggest that NF110 acts as an antiviral player in viral infections, however for other *Flaviviridae* family viruses NF110 plays a pro-viral role in infection. For example, NF110 aids in the replication

of DENV, HCV and BVDV [100], [101], [149]. We present evidence that NF110 plays an antiviral role in ZIKV infection, a diversion from the role of NF110 in other viruses belonging to the *Flaviviridae* family.

Initial characterization of the role of NF110 in ZIKV infection relied on data from collaborators ChIRP-MS analysis that identified peptides encoded by the *ILF3* gene bound to ZIKV RNA [145]. Utilizing immunofluorescence imaging, we were able to show that NF110 signal co-localizes with dsRNA in the cytoplasm of infected cells (Figure 3.7). These data suggest that NF110 is interacting with ZIKV RNA, however the purpose of this interaction is unclear. In other viruses, this interaction functions to aid in the replication of viruses. For example, NF110 aids in the circularization of the HCV genomic material which aids in replication [101]. In DENV, which is more closely related to ZIKV, NF90 interacts with the 3' UTRs of DENV genomic RNA and aids in its replication [100]. Given that the depletion of NF110 results in an increase in viral replication in host cells, it is unlikely that the interaction of NF110 with the ZIKV genome is aiding in its replication, however, our data cannot rule out this possibility. It may be that NF110 is being sequestered away from its downstream targets within the replication factories by the viral RNA. This would, for example, result in the loss of the host cell ability to successfully translate host immune proteins through the host cell translational blockade as shown by Watson et al. [131]. Having the viral genome sequester NF110 inside replication factories may also disrupt the establishment of the global host translation shutdown as NF90/NF110 play significant roles in the shutdown of host translation following viral infection [124], [129]. While it is currently unclear what precise role the binding of NF110 to vRNA plays in ZIKV

infection, we hypothesize that NF90/NF110 is binding to the viral dsRNA intermediates and preventing their replication and/or translation.

Previous work in DENV and HCV provided evidence that infection with *Flaviviridae* viruses result in the redistribution of NF110 to areas of viral replication in infected cells [100], [132]. Given this data, we hypothesized that NF110 would also be redistributed in infection with ZIKV. As shown in Figure 3.6, ZIKV infection results in the redistribution of NF110 in the cytoplasm of infected cells. Moreover, this redistribution appears to be in the same area of the cytoplasm as the viral replication factories. However, the redistribution observed in HCV is suggested by the authors to sequester NF110 in the membranous web of the HCV viral replication factories to prevent it from playing a role in the immune response and assist in the circularization of the HCV genome [101]. A similar role of NF110 has also been shown in BVDV infection as NF110 also aids in the circularization of the BVDV genome [134]. While there is evidence that there is an ultrastructure created with ZIKV infection [29] that parallels the HCV membranous web, so the argument suggested by Isken et al. that the redistribution of NF110 to the replication complexes following infection with HCV as a way to prevent NF110 from playing a role in the host immune response could also be applicable in ZIKV infections. To confirm this, we could examine ZIKV infected cells for tubulin exclusion and test whether the redistributed NF90/NF110 was within the areas of tubulin exclusion. Given evidence we observed on the effect of the depletion of NF110 on the lifecycle of the virus, it is likely that this redistribution of NF110 to the cytoplasm of infected cells is a host response to the viral infection and our data suggest it is likely antiviral in nature.

To test the hypothesis that NF110 was playing an anti-viral role in ZIKV infection, it was necessary that we undertake depletion experiments. To accomplish this, we used shRNA constructs in a PLKO.1 backbone delivered through a lentiviral vector. As shown by western blot in Figure 3.12A, we achieved a successful depletion of both NF110 and NF90. We also ensured to assess the viability of the NF90/NF110 depleted cells as shown in Figure 3.12F and saw that there was a minimal loss of viability with depletion. To assay the virus in the context of the NF110 depletion, we examined: whole cell lysates for ZIKV NS5, intracellular RNA extracts for ZIKV vRNA, and supernatants for infectious ZIKV titers. With an increase in all three of the measures of viral replication, these data suggest that NF110 acts as a robust negative mediator of ZIKV infection (Figure 3.12A, B, and D). This is contrary to the effect of NF110 depletion on HCV and DENV [100], [132], as both of these *Flaviviridae* viruses require NF110 for efficient replication. Interestingly however, NF110 depletion in both VSV and IAV resulted in enhanced susceptibility of those cells to infection [109]. While these data suggest that NF110 is an antiviral player in ZIKV infection as it is in VSV and IAV, the mechanism by which NF110 is inhibiting replication in ZIKV remains to be elucidated. While HCV and DENV both result in the redistribution of NF110 in infected cells [100], [132], and require NF110 for efficient replication, it is interesting that infection with VSV or IAV, which do not result in the redistribution of NF110 [109], flourish in the absence of NF110. This raises the question of why the absence of NF110 in the context of a ZIKV infection results in increased viral susceptibility similar to that seen in the negative sense RNA viruses VSV and IAV, opposite that of other plus-strand RNA viruses like HCV and DENV. Pfiefer et al. suggest that NF90 and NF110 are involved with mRNA trafficking and they cite the role of NF110 in

negatively influencing translation rates in cells [108]. They suggest that the loss of this negative force on translation with the depletion of NF90 and NF110 could be why there is a greatly increased replication of VSV. Isken et al. suggest that in BVDV infection (also a +ssRNA virus), NF110 is involved not only in the circularization of the genome, but that its association with the UTRs of the BVDV genome facilitate a switch from genome translation to replication [133]. Our data cannot rule out that NF110 is playing an assistive role in some aspect of the ZIKV infection lifecycle as in HCV or DENV. However, our data demonstrate that the depletion of NF90/NF110 results in an increase in the replication of the virus suggesting that NF90/NF110 do not likely assist ZIKV replication.

When we examined the localization of ZIKV E protein in cells depleted of NF90/NF110 following ZIKV infection, we see that there are round areas absent of viral signal in the cytoplasm of the depleted cells. We do not see this phenotype until late stage infection and cell death (>48h). This has been described by Monel et al. as 'massive cytoplasmic vacuolization' which they classify as a type of paraptosis [52]. This was a condition that the authors found was exacerbated by the depletion of interferon-induced transmembrane proteins (IFITMs). Given the observation that similar vascularization of the NF110 depleted and ZIKV infected cells was observed, it may be that the depletion of NF110 is resulting in the down regulation of important immune response proteins like the IFITM proteins [150]. If the depletion of NF90/NF110 is affecting expression of the IFITM proteins then it could explain the increased levels of infectivity seen in NF90/NF110 depleted cells. Watson et al. observed that upon depleting NF110, the expression and translation of IFIT2 and translation of IFIT3 were inhibited compared to wild type induction following the

addition of Poly I:C [131]. This inhibition of the IFIT proteins in response to Poly I:C could explain how we observe a similar vacuolization phenotype as was observed my Monel et al. Recent research by Lennemann and Coyne suggests that ZIKV NS2B/3 complex cleaves the ER-autophagy specific receptor FAM134B [51]. They suggest that this cleavage results in ER expansion providing increased membrane surfaces for ZIKV viral replication. This ER expansion is very similar to the expansion observed with the depletion of IFITM3 by Monel et al., as well as our observation with the NF90/NF110 depletion. It would be interesting to examine the production of these proteins or their distribution in the context of an NF110 depletion and ZIKV infection or examine the effect of the depletion of NF90/NF110 on selective autophagy. Conversely, it may be that the depletion of NF90/NF110 results in a much stronger infection and initiates the formation of these paroptotic vacuoles much sooner than it would otherwise be observed solely because of a more robust ZIKV infection.

Another reason for the increased susceptibility to infection that is seen in the NF90/NF110 depleted cells is that the PKR response is altered. There is ample evidence that NF110 is both a cofactor to, and a target of phosphorylation for, PKR. PKR targets all of the isoforms by phosphorylating NF110 at T188 and T315 which then results in the global shutdown of host translation [129]. It has also been shown that NF110 interacts with PKR and plays a role in the formation of stress granules [124]. This response has been established as a part of the immune response role played by both PKR and NF110. There does not appear to be any change in the phosphorylation profile of PKR following depletion of NF90/NF110 (Figure 3.15A). However, when we deplete NF90/NF110 and examine the localization of PKR, we observed the apparent sequestration of PKR to the replication factories within the

cytoplasm of NF90/NF110 depleted cells (Figure 3.15B). To properly assess if this is in fact occurring, we would need to do multi-channel immunofluorescence to ensure that cells that we are observing the sequestration of PKR in are in fact depleted of NF90/NF110. In support of our hypothesis is that we only observe the redistribution phenotype of PKR in the same localization as ZIKV E protein in cultures that have been depleted of NF90/NF110. If PKR is being sequestered in this location and prevented from translocating to the nucleus and/or initiating the stress granule response, then this could provide a possible mechanism by which NF110 depletion increases cellular susceptibility to ZIKV infection. Courtney et al. demonstrated that the depletion of PKR results in increased titers and a complete loss of stress granule formation in WNV infected mouse embryonic fibroblasts [151]. This observation supports the hypothesis that the depletion of NF110 may result in the sequestration of PKR within the replication complex and the prevention of the action of PKR producing an increase in titers similar to those seen with a PKR knockout in MEFs.

Given that NF110 plays a role in the induction of IL-2 and other immune responses including the PKR response, we wanted to see if the reason that the depletion of NF110 resulted in increased susceptibility to ZIKV infection was due to an attenuated induction of ISGs. The depletion of NF110 in uninfected cells did not alter the expression of NFKB, TNF, IFNB1, IFNA1, MX1, OAS1, or PKR (Figure 3.17A). Moreover, upon infection with ZIKV, there was an increased expression of all the ISGs (compared to the scrambled control) that we examined, except for MX1. This suggests that the depletion of NF110 resulting in increased susceptibility to ZIKV is not immune mediated as the ISG response is activated without issue. One possible explanation for the increased expression of ISGs is an increase in overall infection as

previously shown. As well, that genes are expressed does not ensure that they are translated. Indeed, recent research by Watson et al. suggests that NF110 is required for the efficient translation of the important antiviral cytokine IFNB1 as well as a number of other ISGs [131]. They propose that NF110 provides a bypass mechanism of the global host translation shutoff that allows for the translation of required ISGs and an efficient antiviral host response. It may be that in ZIKV infection, the depletion of NF90/NF110 results in the loss of translation of important host immune cytokines and that results in an increased susceptibility to ZIKV infection. Moreover, this may provide a possible explanation of why both HCV and DENV rely on the binding of NF110 to their genome for efficient replication in the context of antiviral host translation shutdowns. In order to elucidate this possible role of NF110 we would need to examine the levels of the ISGs at the protein level to see if indeed the depletion of NF90/NF110 is resulting in the loss of the translation of these important antiviral proteins. This would need to be done in the context of Poly I:C treatment in parallel with ZIKV infection to validate that we would be observing similar effects as Watson et al. did. Additionally, the use of Poly I:C in a parallel experiment removes the multiple confounding effects of wild type ZIKV infection on the host cells.

In summary, there is evidence that isoforms encoded by the *ILF3* gene are associated with ZIKV +vRNA [145]. As well, we have observed that NF110 colocalizes strongly with dsRNA in ZIKV infected cells, and that following infection with ZIKV NF90/NF110 are redistributed to the cytoplasm and to areas that we suspect are viral replication factories. When we deplete NF90/NF110 from cells and infect them with ZIKV we observe a robust increase in the replication of ZIKV. There also appears to be a possible sequestration of PKR in areas that are likely replication factories in cells

depleted of NF90/NF110. Taken together, these data suggest that NF90/NF110 acts as an antiviral protein in ZIKV infections and that the depletion of NF90/NF110 results in increased susceptibility to ZIKV infection.

4.3 hnRNP M as a pro-viral factor in ZIKV infection

Following the identification of hnRNP M as a nuclear protein associated with ZIKV RNA in infected Huh7.5.1 cells [145], we started to attempt to elucidate the role that hnRNP M may be playing in ZIKV infection in human A549 cells. Unlike NF90/NF110, hnRNP M did not redistribute following ZIKV infection. Moreover, the depletion of hnRNP M resulted in an attenuated ZIKV infection. Herein, we discuss and contextualize a possible pro-viral role for hnRNP M in a ZIKV infection in A549 cells.

Data from our collaborators ChIRP-MS experiments suggest that hnRNP M is associated with ZIKV vRNA following ZIKV infection in Huh7.5.1 cells [145]. While this observation is like that of NF90/NF110, the remainder of our data support a pro-viral role of hnRNP M in ZIKV infection. We were not able to observe any colocalization of hnRNP M with dsRNA intermediates by IF nor with ZIKV +vRNA by FISH. LaPointe et al. had previously shown using cross-link-assisted mRNP purification (CLAMP) that hnRNP M will bind to SINV RNA, and the mutation of the hnRNP M interaction site resulted in decreased production of SINV [94]. The authors suggest that this binding to the viral RNA is pro-viral in nature. This is currently the only data in literature of hnRNP M interacting with viral RNA.

Contrary to observations with NF90/NF110, when we examined the distribution of hnRNP M following infection with ZIKV, we did not observe any changes in cellular distribution of hnRNP M. Jagdeo et al. showed that following infection with either poliovirus or coxsackievirus B3 (CVB3), that hnRNP M was cleaved by a viral protease and fragments were then shown to relocalize to the cytoplasm of infected cells [91]. This is arguably not true relocalization of a functional full hnRNP M protein. Another group that studied the possible role of hnRNP M in Sendai virus (SeV) infection (recently renamed murine respirovirus) claimed that infection with SeV or treatment with Poly I:C was sufficient to facilitate the cytoplasmic redistribution of hnRNP M in HeLa cells [92]. Several of the cells the group claims redistribution is occurring in appear to be exiting mitosis and perhaps not a true redistribution of hnRNP M. While we did not try an infection with SeV, we were unable to show cytoplasmic redistribution following Poly I:C treatment in our A549 cells (Figure 3.8). Varjak et al. showed that hnRNP M was redistributed to the cytoplasm of cells infected with SFV [95]. However, even with the perturbation of host nucleocytoplasmic transport, we were unable to show any redistribution of hnRNP M in A549 cells.

In order to determine what role hnRNP M may have in the life cycle of a ZIKV infection, we utilized depletion experiments and found that the depletion of hnRNP M resulted in a decreased production of ZIKV intracellular vRNA, NS5 in whole cell lysates, infectious titers in the supernatants, and both protein and vRNA observed with immunofluorescence and FISH respectively (Figure 3.12-14). This supports the pro-viral role of hnRNP M in ZIKV infection. Following DENV infection, Viktorovskaya et al. showed that the depletion of hnRNP M from cells resulted in an attenuation of the viral infection [90]. The depletion of hnRNP M resulted in decreased infectious

titers and DENV vRNA levels in infected and depleted cells, however they did not provide a possible explanation for this observation. This observation does support a possible pan-*Flaviviral* pro-viral role for hnRNP M. It would be interesting to observe how the depletion of hnRNP M affects other *Flaviviruses* such as WNV, JEV or the *Flaviviridae* virus HCV. The depletion of hnRNP M results in a delay and inhibition of poliovirus and CVB3 infection, and a stronger immune response and lowered viral replication in SeV [91], [92]. Conversely, the depletion of hnRNP M resulted in enhanced replication of the alphaviruses SFV, CHIKV, and SINV [95]. These observations in other viruses suggest that hnRNP M may be either pro- or anti-viral depending upon the virus being studied.

One possible mechanism by which the depletion of hnRNP M results in an attenuated ZIKV infection is by 'priming' the host cell immune response. Upon depletion of hnRNP M, we observed a 2-fold increase of the mRNA transcript levels of the ISGs NFKB, TNF, and OAS1 in uninfected A549 cells (Figure 3.17). While a 2-fold increase in transcript levels is not a robust induction the small increase may be enough to prime the cells immune response to infection with ZIKV. Cao et al. observed that the depletion of hnRNP M resulted in an increase in the responsiveness of ISGs following SeV infection in HEK293 cells and a corresponding decrease in the replication of SeV [92]. Following ZIKV infection in A549 cells however, we observed a decreased level of ISG mRNA transcripts (Figure 3.17). We attributed this observation to a less robust ZIKV infection resulting in less robust activation of ISGs in A549 cells. To better understand what effect the depletion of hnRNP M may have on the induction of ISGs, an interesting experiment to undertake is treating hnRNP M depleted cells with infection mimetics (like Poly I:C, LPS or IFN) and observe the ISG response in the

depleted cells. The use of infection mimetics in this context would help to control for the differing levels of infection that we observed in the hnRNP M depleted cells. Following ZIKV infection, we also observed an early increased phosphorylation of PKR (Figure 3.15A) that would result in a decreased ability of ZIKV to replicate in depleted cells. This observation suggests that the inhibition of the ZIKV infection in the hnRNP M depleted cells is possibly being inhibited before the ISGs have an opportunity to respond. Treatment with Poly I:C results in the phosphorylation of PKR and induction of stress granules [68], while pre-infection treatment with Poly I:C results in a decrease in the levels of ZIKV mRNA compared to mock treated cells [152]. These two observations support the hypothesis that an early and more robust phosphorylation of PKR following ZIKV infection could result in a decreased production of ZIKV as we observed. To confirm this, it would be interesting to examine the phosphorylation profile of eIF2α and other downstream elements of the p-PKR signalling cascade in the context of an hnRNP M depletion.

The observation that treatment with type I interferon (IFNα) results in a decrease in the levels of hnRNP M observed by immunofluorescence imaging (Figure 3.9) also provides support for a pro-viral role of hnRNP M. Kumar et al. observed that an IFN pre-treatment in A549 cells (alpha (α), lambda (λ), and gamma (γ)), results in a robust inhibition of viral replication measured by ZIKV mRNA level [152]. The observation that treatment with IFN results in a decreased hnRNP M level in A549 cells, pre-treatment with IFN results in a decreased ZIKV infection [152], and that a depletion of hnRNP M prior to infection with ZIKV results in decreased ZIKV replication (Figure 3.12-14), all support a pro-viral role for hnRNP M in ZIKV infection in A549 cells. It would be interesting to validate the possible depletion of hnRNP M protein

levels by all three types of IFN in A549 cells and also important to validate those observations using SDS-PAGE western blot analysis of the hnRNP M protein levels in whole cell lysates. Moreover, testing the effect of hnRNP M depletion against other *Flaviviridae* family viruses (such as HCV, DENV, WNV etc.) may show that hnRNP M plays a pro-viral role across the genus or family of viruses.

4.4 Conclusions

We have explored the possible roles of two different nuclear factors that were found to bind to ZIKV vRNA by our collaborators. NF90/NF110 were found to be redistributed following ZIKV infection. This cytoplasmic redistribution to the cytoplasm was localized to the same area as ZIKV E and was found to colocalize with viral dsRNA intermediates. The depletion of NF90/NF110 results in a more robust viral infection and may result in the sequestration of PKR to replication factories in infected cells. Together, these data suggest an anti-viral role for the NF90/NF110 proteins in ZIKV infection. Conversely, the other nuclear factor we studied, hnRNP M was not redistributed following ZIKV infection. The depletion of hnRNP M resulted in a less robust ZIKV infection, possibly mediated by an early phosphorylation event of the dsRNA surveillance protein PKR. Together these data suggest a pro-viral role for hnRNP M in ZIKV infection. Overall, these data provide a rationale to continue to explore the roles of nuclear factors in viruses that are traditionally cytoplasmic replicative viruses.

5 BIBLIOGRAPHY

[1] E. V. Koonin, V. V. Dolja, and M. Krupovic, "Origins and evolution of viruses of eukaryotes: The ultimate modularity," *Virology*, vol. 479–480. Academic Press Inc., pp. 2–25, May-2015.

[2] J. Durzyńska and A. Goździcka-Józefiak, "Viruses and cells intertwined since the dawn of evolution Emerging viruses," *Virology Journal*, vol. 12, no. 1. BioMed Central Ltd., pp. e1–e10, Oct-2015.

[3] T. Phan, "Genetic diversity and evolution of SARS-CoV-2," *Infect. Genet. Evol.*, vol. 81, no. 104260, Jul. 2020.

[4] E. V. Koonin, Y. I. Wolf, K. Nagasaki, and V. V. Dolja, "The Big Bang of picorna-like virus evolution antedates the radiation of eukaryotic supergroups," *Nat. Rev. Microbiol.*, vol. 6, no. 12, pp. 925–939, Nov. 2008.

[5] E. V. Koonin, V. V. Dolja, and T. J. Morris, "Evolution and taxonomy of positive-Strand RNA viruses: Implications of comparative analysis of amino acid sequences," *Crit. Rev. Biochem. Mol. Biol.*, vol. 28, no. 5, pp. 375–430, 1993.

[6] Z. Zhang, L. Rong, and Y. P. Li, "Flaviviridae Viruses and Oxidative Stress: Implications for Viral Pathogenesis," *Oxidative medicine and cellular longevity*, vol. 2019. NLM (Medline), p. 1409582, 2019.

[7] D. Musso and D. J. Gubler, "Zika virus," *Clin. Microbiol. Rev.*, vol. 29, no. 3, pp. 487–524, Jul. 2016.

[8] E. B. Hayes, "Zika virus outside Africa," *Emerging Infectious Diseases*, vol. 15, no. 9. Centers for Disease Control and Prevention, pp. 1347–1350, Sep-2009.

[9] D. Musso, E. J. Nilles, and V.-M. Cao-Lormeau, "Rapid spread of emerging Zika virus in the Pacific area," vol. 20, no. 10, pp. O595–O596, 2014.

[10] B. H. Song, S. I. Yun, M. Woolley, and Y. M. Lee, "Zika virus: History, epidemiology, transmission, and clinical presentation," *Journal of Neuroimmunology*, vol. 308. Elsevier B.V., pp. 50–64, Jul-2017.

[11] J. M. Mansuy *et al.*, "Zika virus: High infectious viral load in semen, a new sexually transmitted pathogen?," *The Lancet Infectious Diseases*, vol. 16, no. 4. Lancet Publishing Group, p. 405, Apr-2016.

[12] L. Barzon *et al.*, "Isolation of infectious Zika virus from saliva and prolonged viral RNA shedding in a traveller returning from the Dominican Republic to Italy, January 2016," *Eurosurveillance*, vol. 21, no. 10, p. 30159, Mar. 2016.

[13] A. C. Gourinat, O. O'Connor, E. Calvez, C. Goarant, and M. Dupont-Rouzeyrol, "Detection of zika virus in urine," *Emerg. Infect. Dis.*, vol. 21, no. 1, pp. 84–86, 2015.

[14] S. Schrauf, R. Tschismarov, E. Tauber, and K. Ramsauer, "Current Efforts in the Development of Vaccines for the Prevention of Zika and Chikungunya Virus

Infections," *Frontiers in Immunology*, vol. 11. Frontiers Media S.A., p. 592, Apr-2020.

[15] N. S. Gokhale *et al.*, "N6-Methyladenosine in Flaviviridae Viral RNA Genomes Regulates Infection," *Cell Host Microbe*, vol. 20, no. 5, pp. 654–665, Nov. 2016.

[16] D. Sirohi and R. J. Kuhn, "Zika Virus Structure, Maturation, and Receptors," *Journal of Infectious Diseases*, vol. 216, no. Suppl 10. Oxford University Press, pp. S935–S944, 2017.

[17] B. Zhao *et al.*, "Structure and function of the Zika virus full-length NS5 protein," *Nat. Commun.*, vol. 8, no. 1, pp. 1–9, Mar. 2017.

[18] S. M. Best, "The Many Faces of the Flavivirus NS5 Protein in Antagonism of Type I Interferon Signaling," *J. Virol.*, vol. 91, no. 3, Feb. 2017.

[19] V. A. Kostyuchenko *et al.*, "Structure of the thermally stable Zika virus," *Nature*, vol. 533, no. 7603, pp. 425–428, Apr. 2016.

[20] Y. Kuwano *et al.*, "MKP-1 mRNA Stabilization and Translational Control by RNA-Binding Proteins HuR and NF90 ," *Mol. Cell. Biol.*, vol. 28, no. 14, pp. 4562–4575, 2008.

[21] S. Kim, B. Li, and R. Linhardt, "Pathogenesis and Inhibition of Flaviviruses from a Carbohydrate Perspective," *Pharmaceuticals*, vol. 10, no. 4, p. 44, May 2017.

[22] A. K. Hastings *et al.*, "TAM Receptors Are Not Required for Zika Virus Infection in Mice," *Cell Rep.*, vol. 19, no. 3, pp. 558–568, Apr. 2017.

[23] S. Liu, L. J. Delalio, B. E. Isakson, and T. T. Wang, "AXL-Mediated Productive Infection of Human Endothelial Cells by Zika Virus," *Circ. Res.*, vol. 119, no. 11, pp. 1183–1189, Nov. 2016.

[24] L. Meertens *et al.*, "Axl Mediates ZIKA Virus Entry in Human Glial Cells and Modulates Innate Immune Responses," *Cell Rep.*, vol. 18, no. 2, pp. 324–333, Jan. 2017.

[25] A. Elong Ngono and S. Shresta, "Immune Response to Dengue and Zika," *Annu. Rev. Immunol.*, vol. 36, no. 1, pp. 279–308, Apr. 2018.

[26] J. Bhatnagar *et al.*, "Zika virus RNA replication and persistence in brain and placental tissue," *Emerg. Infect. Dis.*, vol. 23, no. 3, pp. 405–414, Mar. 2017.

[27] H. Tang *et al.*, "Zika virus infects human cortical neural progenitors and attenuates their growth," *Cell Stem Cell*, vol. 18, no. 5, pp. 587–590, May 2016.

[28] M. Persaud, A. Martinez-Lopez, C. Buffone, S. A. Porcelli, and F. Diaz-Griffero, "Infection by Zika viruses requires the transmembrane protein AXL, endocytosis and low pH," *Virology*, vol. 518, pp. 301–312, May 2018.

[29] M. Cortese *et al.*, "Ultrastructural Characterization of Zika Virus Replication Factories," *Cell Rep.*, vol. 18, no. 9, pp. 2113–2123, Feb. 2017.

[30] L. K. Gillespie, A. Hoenen, G. Morgan, and J. M. Mackenzie, "The Endoplasmic Reticulum Provides the Membrane Platform for Biogenesis of the Flavivirus Replication Complex," *J. Virol.*, vol. 84, no. 20, pp. 10438–10447, 2010.

[31] C. J. Neufeldt *et al.*, "Hepatitis C Virus-Induced Cytoplasmic Organelles Use the Nuclear Transport Machinery to Establish an Environment Conducive to Virus Replication," *PLoS Pathog.*, vol. 9, no. 10, Oct. 2013.

[32] D. Paul, "Architecture and biogenesis of plus-strand RNA virus replication factories," *World J. Virol.*, vol. 2, no. 2, p. 32, 2013.

[33] I. C. Lorenz, S. L. Allison, F. X. Heinz, and A. Helenius, "Folding and Dimerization of Tick-Borne Encephalitis Virus Envelope Proteins prM and E in the Endoplasmic Reticulum," *J. Virol.*, vol. 76, no. 11, pp. 5480–5491, Jun. 2002.

[34] G. Sager, S. Gabaglio, E. Sztul, and G. Belov, "Role of Host Cell Secretory Machinery in Zika Virus Life Cycle," *Viruses*, vol. 10, no. 10, p. 559, Oct. 2018.

[35] I. M. Yu *et al.*, "Structure of the immature dengue virus at low pH primes proteolytic maturation," *Science (80-.).*, vol. 319, no. 5871, pp. 1834–1837, Mar. 2008.

[36] T. C. Pierson and M. S. Diamond, "Degrees of maturity: The complex structure and biology of flaviviruses," *Current Opinion in Virology*, vol. 2, no. 2. Elsevier B.V., pp. 168–175, 01-Apr-2012.

[37] H. Dong, K. Fink, R. Züst, S. P. Lim, C. F. Qin, and P. Y. Shi, "Flavivirus RNA methylation," *Journal of General Virology*, vol. 95, no. 4. Society for General Microbiology, pp. 763–778, 01-Apr-2014.

[38] G. Lichinchi *et al.*, "Dynamics of Human and Viral RNA Methylation during Zika Virus Infection," *Cell Host Microbe*, vol. 20, no. 5, pp. 666–673, Nov. 2016.

[39] G. P. Göertz, S. R. Abbo, J. J. Fros, and G. P. Pijlman, "Functional RNA during Zika virus infection," *Virus Research*, vol. 254. Elsevier B.V., pp. 41–53, 02-Aug-2018.

[40] B. D. Clarke, J. A. Roby, A. Slonchak, and A. A. Khromykh, "Functional non-coding RNAs derived from the flavivirus 3' untranslated region," *Virus Res.*, vol. 206, pp. 53–61, Aug. 2015.

[41] C. L. Donald *et al.*, "Full Genome Sequence and sfRNA Interferon Antagonist Activity of Zika Virus from Recife, Brazil," *PLoS Negl. Trop. Dis.*, vol. 10, no. 10, p. e0005048, Oct. 2016.

[42] M. Garcia, M. Wehbe, N. Lévêque, and C. Bodet, "Skin innate immune response to flaviviral infection," *Cytokine Netw*, vol. 28, no. 2, pp. 41–51, 2017.

[43] R. Hamel *et al.*, "Biology of Zika Virus Infection in Human Skin Cells," *J. Virol.*, vol. 89, no. 17, pp. 8880–8896, Sep. 2015.

[44] M. I. Faizan, M. Abdullah, S. Ali, I. H. Naqvi, A. Ahmed, and S. Parveen, "Zika Virus-Induced Microcephaly and Its Possible Molecular Mechanism," *Intervirology*, vol. 59, no. 3, pp. 152–158, Feb. 2016.

[45] I. G. Olmo *et al.*, "Zika virus promotes neuronal cell death in a non-cell autonomous manner by triggering the release of neurotoxic factors," *Front. Immunol.*, vol. 8, no. 1016, pp. 1–14, 2017.

[46] V. El Ghouzzi *et al.*, "ZIKA virus elicits P53 activation and genotoxic stress in human neural progenitors similar to mutations involved in severe forms of genetic microcephaly and p53," *Cell Death Dis.*, vol. 7, no. 10, pp. e2440–e2440, Oct. 2016.

[47] D. Limonta *et al.*, "Human fetal astrocytes infected with zika virus exhibit delayed apoptosis and resistance to interferon: Implications for persistence," *Viruses*, vol. 10, no. 11, Nov. 2018.

[48] A. I. Chiramel and S. M. Best, "Role of autophagy in Zika virus infection and pathogenesis," *Virus Research*, vol. 254. Elsevier B.V., pp. 34–40, 02-Aug-2018.

[49] G. li Ming, H. Tang, and H. Song, "Advances in Zika Virus Research: Stem Cell Models, Challenges, and Opportunities," *Cell Stem Cell*, vol. 19, no. 6. Cell Press, pp. 690–702, 01-Dec-2016.

[50] B. Cao, L. A. Parnell, M. S. Diamond, and I. U. Mysorekar, "Inhibition of autophagy limits vertical transmission of Zika virus in pregnant mice," *J. Exp. Med.*, vol. 214, no. 8, pp. 2303–2313, Aug. 2017.

[51] N. J. Lennemann and C. B. Coyne, "Dengue and Zika viruses subvert reticulophagy by NS2B3-mediated cleavage of FAM134B," *Autophagy*, vol. 13, no. 2, pp. 322–332, Feb. 2017.

[52] B. Monel *et al.*, "Zika virus induces massive cytoplasmic vacuolization and paraptosis-like death in infected cells," *EMBO J.*, vol. 36, no. 12, pp. 1653–1668, Jun. 2017.

[53] A. Chakrabarti, A. W. Chen, and J. D. Varner, "A review of the mammalian unfolded protein response," *Biotechnology and Bioengineering*, vol. 108, no. 12. John Wiley & Sons, Ltd, pp. 2777–2793, 01-Dec-2011.

[54] A. Oyarzún-Arrau, L. Alonso-Palomares, F. Valiente-Echeverría, F. Osorio, and R. Soto-Rifo, "Crosstalk between RNA metabolism and cellular stress responses during zika virus replication," *Pathogens*, vol. 9, no. 3, p. 158, Feb. 2020.

[55] I. Gladwyn-Ng *et al.*, "Stress-induced unfolded protein response contributes to Zika virus-associated microcephaly," *Nature Neuroscience*, vol. 21, no. 1. Nature Publishing Group, pp. 63–73, 01-Jan-2018.

[56] Z. Tan *et al.*, "ZIKV infection activates the IRE1-XBP1 and ATF6 pathways of unfolded protein response in neural cells," *J. Neuroinflammation*, vol. 15, no.

1, Sep. 2018.

[57] C. Alfano, I. Gladwyn-Ng, T. Couderc, M. Lecuit, and L. Nguyen, "The unfolded protein response: A key player in zika virus-associated congenital microcephaly," *Front. Cell. Neurosci.*, vol. 13, p. 94, Jan. 2019.

[58] O. Takeuchi and S. Akira, "Pattern Recognition Receptors and Inflammation," *Cell*, vol. 140, no. 6. Cell Press, pp. 805–820, 19-Mar-2010.

[59] D. Goubau, S. Deddouche, and C. Reis e Sousa, "Cytosolic Sensing of Viruses," *Immunity*, vol. 38, no. 5. Cell Press, pp. 855–869, May-2013.

[60] J. Ma *et al.*, "Zika virus non-structural protein 4A blocks the RLR-MAVS signaling," *Front. Microbiol.*, vol. 9, Jun. 2018.

[61] Y. Zheng *et al.*, " Zika virus elicits inflammation to evade antiviral response by cleaving cGAS via NS 1-caspase-1 axis ," *EMBO J.*, vol. 37, no. 18, Sep. 2018.

[62] Q. Ding *et al.*, "Species-specific disruption of STING-dependent antiviral cellular defenses by the Zika virus NS2B3 protease," *Proc. Natl. Acad. Sci. U. S. A.*, vol. 115, no. 27, pp. E6310–E6318, Jul. 2018.

[63] H. Xia *et al.*, "An evolutionary NS1 mutation enhances Zika virus evasion of host interferon induction," *Nat. Commun.*, vol. 9, no. 1, Dec. 2018.

[64] Y. Wu *et al.*, "Zika virus evades interferon-mediated antiviral response through the co-operation of multiple nonstructural proteins in vitro," *Cell Discov.*, vol. 3, Mar. 2017.

[65] T. M. Serman and M. U. Gack, "Evasion of innate and intrinsic antiviral pathways by the Zika Virus," *Viruses*, vol. 11, no. 10. MDPI AG, Oct-2019.

[66] W. M. Schneider, M. D. Chevillotte, and C. M. Rice, "Interferon-stimulated genes: A complex web of host defenses," *Annual Review of Immunology*, vol. 32. Annual Reviews Inc., pp. 513–545, 2014.

[67] M. A. Joyce *et al.*, "HCV and flaviviruses hijack cellular mechanisms for nuclear STAT2 degradation: Up-regulation of PDLIM2 suppresses the innate immune response," *PLoS Pathog.*, vol. 15, no. 8, 2019.

[68] S. Hou *et al.*, "Zika Virus Hijacks Stress Granule Proteins and Modulates the Host Stress Response," *J. Virol.*, vol. 91, no. 16, Aug. 2017.

[69] G. Dreyfuss, M. J. Matunis, S. Piiiol-Roma, and C. G. Burd, "hnRNP PROTEINS AND THE BIOGENESIS OF mRNA," 1993.

[70] E. Birney, S. Kumar, and A. R. Krainer, "Analysis of the RNA-recognition motif and RS and RGG domains: conservation in metazoan pre-mRNA splicing factors," 1993.

[71] C. Maris, C. Dominguez, and F. H. T. Allain, "The RNA recognition motif, a plastic RNA-binding platform to regulate post-transcriptional gene expression," *FEBS*

Journal, vol. 272, no. 9. John Wiley & Sons, Ltd, pp. 2118–2131, 01-May-2005.

[72] T. Geuens, D. Bouhy, and V. Timmerman, "The hnRNP family: insights into their role in health and disease," *Human Genetics*, vol. 135, no. 8. Springer Verlag, pp. 851–867, Aug-2016.

[73] M. Marko, M. Leichter, M. Patrinou-Georgoula, and A. Guialis, "hnRNP M interacts with PSF and p54nrb and co-localizes within defined nuclear structures," *Exp. Cell Res.*, vol. 316, no. 3, pp. 390–400, Feb. 2010.

[74] M. T. Vassileva and M. J. Matunis, "SUMO Modification of Heterogeneous Nuclear Ribonucleoproteins," *Mol. Cell. Biol.*, vol. 24, no. 9, pp. 3623–3632, May 2004.

[75] A. C. O. Vertegaal *et al.*, "A proteomic study of SUMO-2 target proteins," *J. Biol. Chem.*, vol. 279, no. 32, pp. 33791–33798, Aug. 2004.

[76] E. Kiesler, M. E. Hase, D. Brodin, and N. Visa, "Hrp59, an hnRNP M protein in Chironomus and Drosophila, binds to exonic splicing enhancers and is required for expression of a subset of mRNAs," *J. Cell Biol.*, vol. 168, no. 7, pp. 1013–1025, Mar. 2005.

[77] P. Thomas, R. A. Forse, and O. Bajenova, "Carcinoembryonic antigen (CEA) and its receptor hnRNP M are mediators of metastasis and the inflammatory response in the liver," *Clinical and Experimental Metastasis*, vol. 28, no. 8. Springer, pp. 923–932, Dec-2011.

[78] O. Bajenova, E. Stolper, S. Gapon, N. Sundina, R. Zimmer, and P. Thomas, "Surface expression of heterogeneous nuclear RNA binding protein M4 on Kupffer cell relates to its function as a carcinoembryonic antigen receptor," *Exp. Cell Res.*, vol. 291, no. 1, pp. 228–241, Nov. 2003.

[79] D. Llères, M. Denegri, M. Biggiogera, P. Ajuh, and A. I. Lamond, "Direct interaction between hnRNP-M and CDC5L/PLRG1 proteins affects alternative splice site choice," *EMBO Rep.*, vol. 11, no. 6, pp. 445–451, Jun. 2010.

[80] J. P. Venables *et al.*, "Multiple and Specific mRNA Processing Targets for the Major Human hnRNP Proteins," *Mol. Cell. Biol.*, vol. 28, no. 19, pp. 6033–6043, Oct. 2008.

[81] R. H. Hovhannisyan and R. P. Carstens, "Heterogeneous ribonucleoprotein M is a splicing regulatory protein that can enhance or silence splicing of alternatively spliced exons," *J. Biol. Chem.*, vol. 282, no. 50, pp. 36265–36274, Dec. 2007.

[82] A. E. Cansizoglu, B. J. Lee, Z. C. Zhang, B. M. A. Fontoura, and Y. M. Chook, "Structure-based design of a pathway-specific nuclear import inhibitor," *Nat. Struct. Mol. Biol.*, vol. 14, no. 5, pp. 452–454, May 2007.

[83] W. Y. Chen *et al.*, "Heterogeneous nuclear ribonucleoprotein M associates with mTORC2 and regulates muscle differentiation," *Sci. Rep.*, vol. 7, Jan. 2017.

[84] N. Ainaoui *et al.*, "Promoter-dependent translation controlled by p54nrb and hnRNPM during myoblast differentiation," *PLoS One*, vol. 10, no. 9, Sep. 2015.

[85] S. Chen *et al.*, "Identification of HnRNP M as a novel biomarker for colorectal carcinoma by quantitative proteomics," *Am. J. Physiol. Liver Physiol.*, vol. 306, no. 5, pp. G394–G403, Mar. 2014.

[86] Y. Xu *et al.*, "Cell type-restricted activity of hnRNPM promotes breast cancer metastasis via regulating alternative splicing," *Genes Dev.*, vol. 28, no. 11, pp. 1191–1203, Jun. 2014.

[87] S. Cho *et al.*, "HnRNP M facilitates exon 7 inclusion of SMN2 pre-mRNA in spinal muscular atrophy by targeting an enhancer on exon 7," *Biochim. Biophys. Acta - Gene Regul. Mech.*, vol. 1839, no. 4, pp. 306–315, Apr. 2014.

[88] K. J. Dery, S. Gaur, M. Gencheva, Y. Yen, J. E. Shively, and R. K. Gaur, "Mechanistic control of carcinoembryonic antigen-related cell adhesion molecule-1 (CEACAM1) splice isoforms by the heterogeneous nuclear ribonuclear proteins hnRNP L, hnRNP A1, and hnRNP M," *J. Biol. Chem.*, vol. 286, no. 18, pp. 16039–16051, May 2011.

[89] K. O. West, H. M. Scott, S. Torres-Odio, A. P. West, K. L. Patrick, and R. O. Watson, "The Splicing Factor hnRNP M Is a Critical Regulator of Innate Immune Gene Expression in Macrophages," *Cell Rep.*, vol. 29, no. 6, pp. 1594-1609.e5, Nov. 2019.

[90] O. V. Viktorovskaya, T. M. Greco, I. M. Cristea, and S. R. Thompson, "Identification of RNA Binding Proteins Associated with Dengue Virus RNA in Infected Cells Reveals Temporally Distinct Host Factor Requirements," *PLoS Negl. Trop. Dis.*, vol. 10, no. 8, Aug. 2016.

[91] J. M. Jagdeo *et al.*, "Heterogeneous Nuclear Ribonucleoprotein M Facilitates Enterovirus Infection," *J. Virol.*, vol. 89, no. 14, pp. 7064–7078, Jul. 2015.

[92] P. Cao *et al.*, "The heterogeneous nuclear ribonucleoprotein hnRNPM inhibits RNA virus-triggered innate immunity by antagonizing RNA sensing of RIG-I-like receptors," *PLoS Pathog.*, vol. 15, no. 8, 2019.

[93] Z. Luo *et al.*, "Engagement of heterogeneous nuclear ribonucleoprotein M with listeriolysin O induces type I interferon expression and restricts Listeria monocytogenes growth in host cells," *Immunobiology*, vol. 217, no. 10, pp. 972–981, Oct. 2012.

[94] A. T. LaPointe, N. N. Gebhart, M. E. Meller, R. W. Hardy, and K. J. Sokoloski, "Identification and Characterization of Sindbis Virus RNA-Host Protein Interactions," *J. Virol.*, vol. 92, no. 7, pp. 2171–2188, Jan. 2018.

[95] M. Varjak, S. Saul, L. Arike, A. Lulla, L. Peil, and A. Merits, "Magnetic Fractionation and Proteomic Dissection of Cellular Organelles Occupied by the Late Replication Complexes of Semliki Forest Virus," *J. Virol.*, vol. 87, no. 18, pp. 10295–10312, Sep. 2013.

[96] N. Duchange, J. Pidoux, E. Camus, and D. Sauvaget, "Alternative splicing in the human interleukin enhancer binding factor 3 (ILF3) gene," *Gene*, vol. 261, no. 2, pp. 345–353, Dec. 2000.

[97] D. Guan *et al.*, "Nuclear Factor 45 (NF45) Is a Regulatory Subunit of Complexes with NF90/110 Involved in Mitotic Control," *Mol. Cell. Biol.*, vol. 28, no. 14, pp. 4629–4641, Jul. 2008.

[98] J. O. Langland, P. N. Kao, and B. L. Jacobs, "Nuclear factor-90 of activated T-cells: A double-stranded RNA-binding protein and substrate for the double-stranded RNA-dependent protein kinase, PKR," *Biochemistry*, vol. 38, no. 19, pp. 6361–6368, May 1999.

[99] T. W. Reichman, L. C. Muñiz, and M. B. Mathews, "The RNA Binding Protein Nuclear Factor 90 Functions as Both a Positive and Negative Regulator of Gene Expression in Mammalian Cells," *Mol. Cell. Biol.*, vol. 22, no. 1, pp. 343–356, 2002.

[100] R. C. Gomila, G. W. Martin, and L. Gehrke, "NF90 Binds the Dengue Virus RNA 3' Terminus and Is a Positive Regulator of Dengue Virus Replication," *PLoS One*, vol. 6, no. 2, p. e16687, Feb. 2011.

[101] O. Isken *et al.*, "Nuclear factors are involved in hepatitis C virus RNA replication," *RNA*, vol. 13, no. 10, pp. 1675–1692, Oct. 2007.

[102] M. Uhlén *et al.*, "Tissue-based map of the human proteome," *Science (80-.).*, vol. 347, no. 6220, pp. 394–402, Jan. 2015.

[103] "Tissue expression of ILF3 - Summary - The Human Protein Atlas." [Online]. Available: https://www.proteinatlas.org/ENSG00000129351-ILF3/tissue. [Accessed: 20-Jul-2020].

[104] B. C. and P. N. Kao, "Purification by DNA Affinity Chromatography of Two Polypeptides That Contact the NF-AT DNA Binding Site in the Interleukin 2 Promoter," *J. Biol. Chem.*, vol. 269, no. 32, pp. 20682–20690, 1994.

[105] L. R. Saunders *et al.*, "Characterization of Two Evolutionarily Conserved, Alternatively Spliced Nuclear Phosphoproteins, NFAR-1 and-2, That Function in mRNA Processing and Interact with the Double-stranded RNA-dependent Protein Kinase, PKR*," 2001.

[106] Y. Kuwano *et al.*, "NF90 selectively represses the translation of target mRNAs bearing an AU-rich signature motif."

[107] L. Shi *et al.*, "NF90 Regulates Cell Cycle Exit and Terminal Myogenic Differentiation by Direct Binding to the 3-Untranslated Region of MyoD and p21 WAF1/CIP1 mRNAs," *J. Biol. Chem.*, vol. 280, no. 19, pp. 15851–15859, 2005.

[108] K. Masuda, Y. Kuwano, K. Nishida, K. Rokutan, and I. Imoto, "NF90 in Posttranscriptional Gene Regulation and MicroRNA Biogenesis," *Int. J. Mol. Sci.*, vol. 14, no. 8, pp. 17111–17121, Aug. 2013.

[109] I. Pfeifer *et al.*, "NFAR-1 and -2 modulate translation and are required for efficient host defense," *PNAS*, vol. 105, no. 11, pp. 4173–4178, 2008.

[110] J. Shim, H. Lim, J. R. Yates, and M. Karin, "Nuclear export of NF90 is required for interleukin-2 mRNA stabilization," *Mol. Cell*, vol. 10, no. 6, pp. 1331–1344, Dec. 2002.

[111] F. Vumbaca, K. N. Phoenix, D. Rodriguez-Pinto, D. K. Han, and K. P. Claffey, "Double-Stranded RNA-Binding Protein Regulates Vascular Endothelial Growth Factor mRNA Stability, Translation, and Breast Cancer Angiogenesis," *Mol. Cell. Biol.*, vol. 28, no. 2, pp. 772–783, 2008.

[112] T. X. Lu and M. E. Rothenberg, "MicroRNA," *J. Allergy Clin. Immunol.*, vol. 141, no. 4, pp. 1202–1207, Apr. 2018.

[113] R. Rupaimoole and F. J. Slack, "MicroRNA therapeutics: Towards a new era for the management of cancer and other diseases," *Nature Reviews Drug Discovery*, vol. 16, no. 3. Nature Publishing Group, pp. 203–221, 01-Mar-2017.

[114] D. P. Bartel, "MicroRNAs: Genomics, Biogenesis, Mechanism, and Function," *Cell*, vol. 116, no. 2. Cell Press, pp. 281–297, 23-Jan-2004.

[115] R. I. Gregory *et al.*, "The Microprocessor complex mediates the genesis of microRNAs," *Nature*, vol. 432, no. 7014, pp. 235–240, Nov. 2004.

[116] S. Sakamoto *et al.*, "The NF90-NF45 Complex Functions as a Negative Regulator in the MicroRNA Processing Pathway," *Mol. Cell. Biol.*, vol. 29, no. 13, pp. 3754–3769, Jul. 2009.

[117] J. K. Nussbacher and G. W. Yeo, "Systematic Discovery of RNA Binding Proteins that Regulate MicroRNA Levels," *Mol. Cell*, vol. 69, no. 6, pp. 1005–1016, Mar. 2018.

[118] N. Volk and N. Shomron, "Versatility of MicroRNA Biogenesis," *PLoS One*, vol. 6, no. 5, p. e19391, May 2011.

[119] Q. Hu *et al.*, "Interleukin enhancer-binding factor 3 promotes breast tumor progression by regulating sustained urokinase-type plasminogen activator expression," *Oncogene*, vol. 32, no. 34, pp. 3933–3943, Aug. 2013.

[120] Y. Guo *et al.*, "Correlations among ERCC1, XPB, UBE2I, EGF, TAL2 and ILF3 revealed by gene signatures of histological subtypes of patients with epithelial ovarian cancer," *Oncol. Rep.*, vol. 27, no. 1, pp. 286–292, Jan. 2012.

[121] N. L. Guo *et al.*, "Confirmation of gene expression - based prediction of survival in non-small cell lung cancer," *Clin. Cancer Res.*, vol. 14, no. 24, pp. 8213–8220, Dec. 2008.

[122] L. F. Fung, A. K. F. Lo, P. W. Yuen, Y. Liu, X. H. Wang, and S. W. Tsao, "Differential gene expression in nasopharyngeal carcinoma cells," *Life Sci.*, vol. 67, no. 8, pp. 923–936, Jul. 2000.

[123] Y. Liu *et al.*, "ILF3 promotes gastric cancer proliferation and may be used as a prognostic marker," *Mol. Med. Rep.*, vol. 20, no. 1, pp. 125–134, 2019.

[124] W. Zhang *et al.*, "Nuclear factor 90 promotes angiogenesis by regulating HIF-1α/VEGF-A expression through the PI3K/Akt signaling pathway in human cervical cancer article," *Cell Death Dis.*, vol. 9, no. 3, Mar. 2018.

[125] Q. Zhou *et al.*, "MiR-590-5p inhibits colorectal cancer angiogenesis and metastasis by regulating nuclear factor 90/vascular endothelial growth factor A axis," *Cell Death Dis.*, vol. 7, no. 10, 2016.

[126] J. Zhuang *et al.*, "TGFβ1 promotes gemcitabine resistance through regulating the LncRNA-LET/NF90/miR-145 signaling axis in bladder cancer," *Theranostics*, vol. 7, no. 12, pp. 3053–3067, 2017.

[127] J. Barbier *et al.*, "An NF90/NF110-mediated feedback amplification loop regulates dicer expression and controls ovarian carcinoma progression," *Cell Res.*, vol. 28, no. 5, pp. 556–571, May 2018.

[128] D. Levin and I. M. London, "Regulation of protein synthesis: activation by double-stranded RNA of a protein kinase that phosphorylates eukaryotic initiation factor 2," *Proc. Natl. Acad. Sci. U. S. A.*, vol. 75, no. 3, pp. 1121–1125, 1978.

[129] A. Harashima, T. Guettouche, and G. N. Barber, "Phosphorylation of the NFAR proteins by the dsRNA-dependent protein kinase PKR constitutes a novel mechanism of translational regulation and cellular defense," *Genes Dev.*, vol. 24, no. 23, pp. 2640–2653, Dec. 2010.

[130] X. Li *et al.*, "Coordinated circRNA Biogenesis and Function with NF90/NF110 in Viral Infection," *Mol. Cell*, vol. 67, no. 2, pp. 214–227, Jul. 2017.

[131] S. F. Watson, N. Bellora, and S. Macias, "ILF3 contributes to the establishment of the antiviral type I interferon program," *Nucleic Acids Res.*, vol. 48, no. 1, pp. 116–129, 2020.

[132] Y. Li, T. Masaki, T. Shimakami, and S. M. Lemon, "hnRNP L and NF90 Interact with Hepatitis C Virus 5′-Terminal Untranslated RNA and Promote Efficient Replication," *J. Virol.*, vol. 88, no. 13, pp. 7199–7209, Jul. 2014.

[133] O. Isken, C. W. Grassmann, H. Yu, and S. E. Behrens, "Complex signals in the genomic 3′ nontranslated region of bovine viral diarrhea virus coordinate translation and replication of the viral RNA," *RNA*, vol. 10, no. 10, pp. 1637–1652, Oct. 2004.

[134] M. Muto *et al.*, "Identification and analysis of host proteins that interact with the 3′-untranslated region of tick-borne encephalitis virus genomic RNA," *Virus Res.*, vol. 249, pp. 52–56, Apr. 2018.

[135] P. Wang *et al.*, "Nuclear Factor 90 Negatively Regulates Influenza Virus Replication by Interacting with Viral Nucleoprotein," *J. Virol.*, vol. 83, no. 16,

pp. 7850–7861, 2009.

[136] S. Urcuqui-Inchima, M. E. Castaño, D. Hernandez-Verdun, G. St-Laurent, and A. Kumar, "Nuclear factor 90, a cellular dsRNA binding protein inhibits the HIV Rev-export function," *Retrovirology*, vol. 3, no. 1, pp. 1–13, Nov. 2006.

[137] R. A. Shamanna, M. Hoque, T. Pe'ery, and M. B. Mathews, "Induction of p53, p21 and apoptosis by silencing the NF90/NF45 complex in human papilloma virus-transformed cervical carcinoma cells," *Oncogene*, vol. 32, no. 43, pp. 5176–5185, Dec. 2013.

[138] M. K. Merrill and M. Gromeier, "The Double-Stranded RNA Binding Protein 76:NF45 Heterodimer Inhibits Translation Initiation at the Rhinovirus Type 2 Internal Ribosome Entry Site," *J. Virol.*, vol. 80, no. 14, pp. 6936–6942, Jul. 2006.

[139] R. S. Shabman *et al.*, "DRBP76 Associates With Ebola Virus VP35 and Suppresses Viral Polymerase Function DRBP76 Suppresses Ebola Virus Polymerase," *J. Infect. Dis.*, vol. 204, no. 3, pp. 911–918, 2011.

[140] J. W. Schoggins *et al.*, "A diverse range of gene products are effectors of the type i interferon antiviral response," *Nature*, vol. 472, no. 7344, pp. 481–485, Apr. 2011.

[141] C. A. Schneider, W. S. Rasband, and K. W. Eliceiri, "NIH Image to ImageJ: 25 years of image analysis," *Nature Methods*, vol. 9, no. 7. Nature Publishing Group, pp. 671–675, 28-Jul-2012.

[142] J. Ye, G. Coulouris, I. Zaretskaya, I. Cutcutache, S. Rozen, and T. Madden, "Primer-BLAST: A tool to design target-specific primers for polymerase chain reaction." BMC Bioinformatics, p. 13:134, 2012.

[143] W. Hou *et al.*, "Molecular cloning and characterization of the genes encoding the proteins of Zika virus," *Gene*, vol. 628, pp. 117–128, Sep. 2017.

[144] J. Hertzog *et al.*, "Infection with a Brazilian isolate of Zika virus generates RIG-I stimulatory RNA and the viral NS5 protein blocks type I IFN induction and signaling," *Eur. J. Immunol.*, vol. 48, no. 7, pp. 1120–1136, Jul. 2018.

[145] Y. S. Ooi *et al.*, "An RNA-centric dissection of host complexes controlling flavivirus infection," *Nat. Microbiol.*, vol. 4, no. 12, pp. 2369–2382, Dec. 2019.

[146] M. L. Goulet *et al.*, "Systems Analysis of a RIG-I Agonist Inducing Broad Spectrum Inhibition of Virus Infectivity," *PLoS Pathog.*, vol. 9, no. 4, p. 1003298, Apr. 2013.

[147] L. Giovannini-Chami *et al.*, "Distinct epithelial gene expression phenotypes in childhood respiratory allergy," *Eur. Respir. J.*, vol. 39, no. 5, pp. 1197–1205, May 2012.

[148] N. J. Barrows *et al.*, "A Screen of FDA-Approved Drugs for Inhibitors of Zika

Virus Infection," *Cell Host Microbe*, vol. 20, no. 2, pp. 259–270, Aug. 2016.

[149] O. Isken, C. W. Grassmann, R. Sarisky, and M. Kann, "Members of the NF90/NFAR protein group are involved in the life cycle of a positive-strand RNA virus," *EMBO J*, vol. 22, no. 21, pp. 5655–5665, 2003.

[150] M. S. Diamond and M. Farzan, "The broad-spectrum antiviral functions of IFIT and IFITM proteins," *Nature Reviews Immunology*, vol. 13, no. 1. Nature Publishing Group, pp. 46–57, 14-Jan-2013.

[151] S. C. Courtney, S. V. Scherbik, B. M. Stockman, and M. A. Brinton, "West Nile Virus Infections Suppress Early Viral RNA Synthesis and Avoid Inducing the Cell Stress Granule Response," *J. Virol.*, vol. 86, no. 7, pp. 3647–3657, Apr. 2012.

[152] A. Kumar *et al.*, "Zika virus inhibits type-I interferon production and downstream signaling," *EMBO Rep.*, vol. 17, no. 12, pp. 1766–1775, Dec. 2016.

A APPENDIX

A.1 ImageJ macro for immunofluorescence analysis

```
/*
 Macro template to process multiple images in a folder and quantify the
 fluorescence in the nucleus and the cytoplasm of each cell in the image.

 This macro is separate into different steps so the results can be checked
 during the process of creating the 2D images for quantification, creating the
 separate cell masks, masking the nuclei and the cytoplasm and finaly quantifying
 the fluorescence in these compartments.

 You need the EDF (developer distribution), the Find Focused Slices, the
 Bio-Formats Importer and the Morphology plugins installed.

 Info: https://sites.google.com/site/qingzongtseng/find-focus - Download: http://goo.gl/ZVQn1
 Info: bigwww.epfl.ch/demo/edf/ - Download: http://bigwww.epfl.ch/demo/edf/EDF.zip
 Info: https://www.openmicroscopy.org/site/support/bio-formats5.1/users/imagej/ - Download:
http://downloads.openmicroscopy.org/latest/bio-formats5.1/artifacts/bioformats_package.jar
 Info: http://www.mecourse.com/landinig/software/software.html - ImageJ subscription site:
 http://sites.imagej.net/Landini/

 This is part 1, it'll create the 2D projection of each channel in your stack.
 These images will be used later to quantify fluorescence.
*/

//OPEN THE FILES

input = getDirectory("Input directory - your original microscope files");
output = getDirectory("Output directory - a folder to save all your analysis");

Dialog.create("File type");
Dialog.addString("File suffix: ", ".dv", 5);
Dialog.show();
suffix = Dialog.getString();

// Create directories in output folder
EDFdir = output+"EDF"+File.separator;
File.makeDirectory(EDFdir);
if (!File.exists(EDFdir))
    exit("Unable to create directory");
print("");
print("creating " + EDFdir);

CMdir = output+"CellMasks"+File.separator;
File.makeDirectory(CMdir);
if (!File.exists(CMdir))
    exit("Unable to create directory");
print("");
print("creating " + CMdir);

dapiC = getNumber("Number of the channel that contains your nuclear stain (DAPI), (i.e. 0,1,2...)", 2);

suffixDAPI = "C="+ dapiC + ".tif";

// Create directories in output folder
Segdir = output+"SegMasks"+File.separator;
File.makeDirectory(Segdir);
if (!File.exists(Segdir))
    exit("Unable to create directory");
print("");
```

```
58.  print("creating " + Segdir);
59.
60.  Nucdir = output+"NucleiMasks"+File.separator;
61.  File.makeDirectory(Nucdir);
62.  if (!File.exists(Nucdir))
63.      exit("Unable to create directory");
64.  print("");
65.  print("creating " + Nucdir);
66.
67.  Cytodir = output+"CytoMasks"+File.separator;
68.  File.makeDirectory(Cytodir);
69.  if (!File.exists(Cytodir))
70.      exit("Unable to create directory");
71.  print("");
72.  print("creating " + Cytodir);
73.
74.  Subsetdir = output+"Subset Infected"+File.separator;
75.  File.makeDirectory(Subsetdir);
76.  if (!File.exists(Subsetdir))
77.      exit("Unable to create directory");
78.  print("");
79.  print("creating " + Subsetdir);
80.
81.  NucdirI = Subsetdir+"NucleiMasks"+File.separator;
82.  File.makeDirectory(NucdirI);
83.  if (!File.exists(NucdirI))
84.      exit("Unable to create directory");
85.  print("");
86.  print("creating " + NucdirI);
87.
88.  CytodirI = Subsetdir+"CytoMasks"+File.separator;
89.  File.makeDirectory(CytodirI);
90.  if (!File.exists(CytodirI))
91.      exit("Unable to create directory");
92.  print("");
93.  print("creating " + CytodirI);
94.
95.  Cquant = getNumber("Number of the channel to quantify fluorescence, (i.e. 0,1,2...)", 1);
96.
97.  suffixCquant = "C="+ Cquant + ".tif";
98.
99.  Resdir = output+"ResultsDir"+File.separator;
100. File.makeDirectory(Resdir);
101. if (!File.exists(Resdir))
102.     exit("Unable to create directory");
103. print("");
104. print("creating " + Resdir);
105.
106. viralC = getNumber("Number of the channel that contains your viral protein, (i.e. 0,1,2...)", 0);
107.
108. suffixViral = "C="+ viralC + ".tif";
109.
110. Viraldir = Subsetdir+"ViralMasks"+File.separator;
111. File.makeDirectory(Viraldir);
112. if (!File.exists(Viraldir))
113.     exit("Unable to create directory");
114. print("");
115. print("creating " + Viraldir);
116.
117. ResdirI = Subsetdir+"ResultsDir"+File.separator;
118. File.makeDirectory(ResdirI);
119. if (!File.exists(ResdirI))
```

```
    exit("Unable to create directory");
print("");
print("creating " + ResdirI);

// Set batchmode to true to hide the windows away so you can still do things with the
// program running in the background

setBatchMode(true);


processFolder(input);
processFolderN(EDFdir);
processFolderC(input);
processFolderQ(EDFdir);
processFolderV(EDFdir);
processFolderI(input);
processFolderQI(EDFdir);

print("Analysis finished.");

function processFolder(input) {
    list = getFileList(input);
    for (i = 0; i < list.length; i++) {
             if(File.isDirectory(input + list[i]))
                      processFolder("" + input + list[i]);
             if(endsWith(list[i], suffix))
                      processFile(input, output, list[i]);
    }
}

function processFile(input, output, file) {

    print("Processing: " + input + file);

    newfile = input + file;
    options = "open=newfile autoscale color_mode=Default split_channels view=[Standard ImageJ] stack_order=XYZCT";
    run("Bio-Formats Importer",options);

    imageslist = getList("image.titles");
    selectWindow(imageslist[0]);
    run("Properties...", "global");

    run("Brightness/Contrast...");
    for (i = 0; i < imageslist.length; i++) {
             selectWindow(imageslist[i]);
             resetMinAndMax();
    }

    for (i = 0; i < imageslist.length; i++) {

             selectWindow(imageslist[i]);
             run("EDF Easy ", "quality='4' topology='0' show-topology='off' show-view='off'");

                      // The following code is required in order to wait for the the EDF plugin to finish, and
open the expected image.
                      // We must wait for a window called "Output" . Batch mode cannot be true, because if so the
window will not open.
             initTime = getTime();
             oldTime = initTime;
             while (!isOpen("Output")) {
                      elapsedTime = getTime() - initTime;
                      newTime = getTime() - oldTime;
```

```
180.             // print something every 10 seconds so that we will know it is still runnning
181.                     if (newTime > 10000) {
182.                             oldTime = getTime();
183.                                     newTime = 0;
184.                             print(elapsedTime/1000, " seconds elapsed");
185.                     }
186.             }
187.             wait(1000); // let's really make sure that window is open -- give it another second
188.             selectImage("Output");
189.             rename(imageslist[i] + "EDF");
190.             saveAs("Tiff", EDFdir + imageslist[i] + ".tif");
191.             //close(); remove if adding below
192.             selectWindow(imageslist[i]);
193.             close();
194.     }
195.
196.     run("Images to Stack", "name=Stack title=[]");
197.     run("Gaussian Blur...", "sigma=10 stack");
198.     setOption("BlackBackground", true);
199.     run("Convert to Mask", "method=Huang background=Dark calculate black");
200.
201.     run("Z Project...", "projection=[Max Intensity]");
202.     selectWindow("Stack");
203.     close();
204.     selectWindow("MAX_Stack");
205.     run("Fill Holes");
206.     saveAs("Tiff", CMdir + file + "cellMask.tif");
207.     close();
208. }
209.
210.
211. function processFolderN(EDFdir) {
212.     list = getFileList(EDFdir);
213.     for (i = 0; i < list.length; i++) {
214.             if(File.isDirectory(EDFdir + list[i]))
215.                     processFolderN("" + EDFdir + list[i]);
216.             if(endsWith(list[i], suffixDAPI))
217.                     processNuclei(EDFdir, Nucdir, NucdirI, Segdir, list[i]);
218.     }
219. }
220.
221. function processFolderC(input) {
222.     list = getFileList(input);
223.     for (i = 0; i < list.length; i++) {
224.             if(File.isDirectory(input + list[i]))
225.                     processFolderC("" + input + list[i]);
226.             if(endsWith(list[i], suffix))
227.                     processCyto(CMdir, Nucdir, Segdir, Cytodir, CytodirI, list[i]);
228.     }
229. }
230.
231. function processNuclei(EDFdir, Nucdir, NucdirI, Segdir, file) {
232.
233.     print("Processing: " + EDFdir + file);
234.     newfile = EDFdir + file;
235.     open(newfile);
236.     run("Gaussian Blur...", "sigma=10");
237.     rename("DAPIblur");
238.     setOption("BlackBackground", true);
239.     run("Convert to Mask", "method=Huang background=Dark black");
240.     run("Fill Holes");
241.     run("Watershed");
```

```
    rename("NucMask");

    file=replace(file," - " + suffixDAPI,"");

    saveAs("Tiff", Nucdir + file + "NucMask.tif");
    saveAs("Tiff", NucdirI + file + "NucMask.tif");
    //
    // This is where the code segments based on the viral channel.
    // May need to alter the noise level to weed out the uninfected cells
    // Also need to alter the method depending on the viral antigen dirstribution ie: NS5 vs E vs dsRNA
    //
    run("Find Maxima...", "noise=10 output=[Segmented Particles]");
    saveAs("Tiff", Segdir + file + "SegMask.tif");
    close();
    selectWindow(file + "NucMask.tif");
    close();
}

function processCyto(CMdir, Nucdir, Segdir, Cytodir, CytodirI, file) {

    newfile = Nucdir + file + "NucMask.tif";
    open(newfile);
    rename("NucMask");
    newfile2 = CMdir + file + "cellMask.tif";
    open(newfile2);
    rename("CellMask");
    newfile3 = Segdir + file + "SegMask.tif";
    open(newfile3);
    rename("SegMask");
    imageCalculator("AND create", "CellMask","SegMask");
    selectWindow("CellMask");
    close();
    selectWindow("Result of CellMask");
    rename("CellMask");
    run("BinaryReconstruct ", "mask=CellMask seed=NucMask create white");
    rename("CellMask2");
    run("Options...", "iterations=20 count=1 black do=Dilate");
    run("Fill Holes");
    selectWindow("CellMask");
    close();
    imageCalculator("AND create", "CellMask2","SegMask");
    selectWindow("CellMask2");
    close();
    selectWindow("SegMask");
    close();
    selectWindow("Result of CellMask2");
    rename("CellMask2");
    run("BinaryReconstruct ", "mask=CellMask2 seed=NucMask create white");
    selectWindow("CellMask2");
    close();
    selectWindow("Reconstructed");
    rename("CellMask2");
    run("BinaryReconstruct ", "mask=NucMask seed=CellMask2 create white");
    rename("NucMask2");
    selectWindow("NucMask");
    close();
    imageCalculator("Subtract create", "CellMask2","NucMask2");
    selectWindow("Result of CellMask2");
    saveAs("Tiff", Cytodir + file + "CytoMask.tif");
    saveAs("Tiff", CytodirI + file + "CytoMask.tif");
    close();
    selectWindow("NucMask2");
```

```
    saveAs("Tiff", Nucdir + file + "NucMask.tif");
    saveAs("Tiff", NucdirI + file + "NucMask.tif");
    close();
    selectWindow("CellMask2");
    close();
}

function processFolderQ(EDFdir) {
    listI = getFileList(EDFdir);
    for (i = 0; i < listI.length; i++) {
             if(File.isDirectory(EDFdir + listI[i]))
                      processFolderQ("" + EDFdir + listI[i]);
             if(endsWith(listI[i], suffixCquant))
                      processFileQ(EDFdir, Nucdir, Cytodir, Resdir, listI[i]);
    }
}

function processFileQ(EDFdir, Nucdir, Cytodir, Resdir, fileI) {

    print("Processing: " + EDFdir + fileI);
    newfile = EDFdir + fileI;
    open(newfile);
    run("8-bit");
    rename("Nuclear");

    file=replace(fileI," - " + suffixCquant,"");

    newfile2 = Nucdir + file + "NucMask.tif";
    open(newfile2);
    rename("NucMask");

    run("Set Measurements...", "area mean standard min centroid center bounding median display redirect=Nuclear
decimal=3");
    selectWindow("NucMask");
    run("Analyze Particles...", "size=0-Infinity show=Outlines display clear");
    selectWindow("NucMask");
    close();
    selectWindow("Drawing of NucMask");
    saveAs("Tiff", Resdir + file + "Nuc.tif");
    selectWindow(file + "Nuc.tif");
    close();
    selectWindow("Results");
    saveAs("Results", Resdir + file + "_NucResults.csv");
    selectWindow("Results");
    close();

    open(newfile);
    run("8-bit");
    rename("Cytoplasmic");

    newfile3 = Cytodir + file + "CytoMask.tif";
    open(newfile3);
    rename("CytoMask");
    run("Set Measurements...", "area mean standard min centroid center bounding median display
redirect=Cytoplasmic decimal=3");
    selectWindow("CytoMask");
    run("Analyze Particles...", "size=0-Infinity show=Outlines display clear");
    selectWindow("CytoMask");
    close();
    selectWindow("Drawing of CytoMask");
    saveAs("Tiff", Resdir + file + "Cyto.tif");
    selectWindow(file + "Cyto.tif");
```

```
364.     close();
365.     selectWindow("Results");
366.     saveAs("Results", Resdir + file + "_CytoResults.csv");
367.     selectWindow("Results");
368.     close();
369. }
370. 
371. function processFolderV(EDFdir) {
372.     list = getFileList(EDFdir);
373.     for (i = 0; i < list.length; i++) {
374.              if(File.isDirectory(EDFdir + list[i]))
375.                       processFolderV("" + EDFdir + list[i]);
376.              if(endsWith(list[i], suffixViral))
377.                       processViral(EDFdir, Viraldir, list[i]);
378.     }
379. }
380. 
381. function processFolderI(input) {
382.     list = getFileList(input);
383.     for (i = 0; i < list.length; i++) {
384.              if(File.isDirectory(input + list[i]))
385.                       processFolderI("" + input + list[i]);
386.              if(endsWith(list[i], suffix))
387.                       processInfected(NucdirI, CytodirI, Viraldir, list[i]);
388.     }
389. }
390. 
391. function processViral(EDFdir, Viraldir, file) {
392. 
393.     print("Processing: " + EDFdir + file);
394.     newfile = EDFdir + file;
395.     open(newfile);
396.     run("Gaussian Blur...", "sigma=10");
397.     rename("Virusblur");
398. 
399.     //run("Threshold...");
400.     setAutoThreshold("Default dark");
401.     setOption("BlackBackground", true);
402.     run("Convert to Mask","method=Default background=Dark black"); // This part can be changed if masks are too
    large.
403.     //run("Options...", "iterations=20 count=1 black do=Dilate");
404.     run("Fill Holes");
405.     rename("ViralMask");
406. 
407.     file=replace(file," - " + suffixViral,"");
408.     saveAs("Tiff", Viraldir + file + "ViralMask.tif");
409.     close();
410. }
411. 
412. function processInfected(NucdirI, CytodirI, Viraldir, file) {
413. 
414.     newfile = NucdirI + file + "NucMask.tif";
415.     open(newfile);
416.     rename("NucMask");
417.     newfile2 = CytodirI + file + "CytoMask.tif";
418.     open(newfile2);
419.     rename("CytoMask");
420.     newfile3 = Viraldir + file + "ViralMask.tif";
421.     open(newfile3);
422.     rename("ViralMask");
423. 
424.     run("BinaryReconstruct ", "mask=CytoMask seed=ViralMask create white");
```

```
    //saveAs("Tiff", CytodirI + fileC);
    //close();
    selectWindow("CytoMask");
    close();
    selectWindow("Reconstructed");
    rename("CytoMask");
    selectWindow("ViralMask");
    //run("Options...", "iterations=25 count=1 black do=Dilate");
    run("Fill Holes");
    run("BinaryReconstruct ", "mask=NucMask seed=ViralMask create white");
    //saveAs("Tiff", NucdirI + fileN);
    //close();
    selectWindow("NucMask");
    close();
    selectWindow("Reconstructed");
    rename("NucMask");
    selectWindow("ViralMask");
    close();

    run("Images to Stack", "name=Stack title=[] keep");
    selectWindow("Stack");
    run("Z Project...", "projection=[Max Intensity]");
    selectWindow("Stack");
    close();
    selectWindow("CytoMask");
    close();
    selectWindow("MAX_Stack");
    rename("CytoMask");
    run("BinaryReconstruct ", "mask=CytoMask seed=NucMask create white");
    selectWindow("CytoMask");
    close();
    selectWindow("Reconstructed");
    rename("CytoMask");
    run("BinaryReconstruct ", "mask=NucMask seed=CytoMask create white");
    selectWindow("NucMask");
    close();
    selectWindow("Reconstructed");
    rename("NucMask");

    imageCalculator("Subtract create", "CytoMask","NucMask");
    selectWindow("Result of CytoMask");
    saveAs("Tiff", CytodirI + file + "CytoMask.tif");
    close();
    selectWindow("NucMask");
    saveAs("Tiff",  NucdirI + file + "NucMask.tif");
    close();
    selectWindow("CytoMask");
    close();

}

function processFolderQI(EDFdir) {
    listI = getFileList(EDFdir);
    for (i = 0; i < listI.length; i++) {
            if(File.isDirectory(EDFdir + listI[i]))
                    processFolderQI("" + EDFdir + listI[i]);
            if(endsWith(listI[i], suffixCquant))
                    processFileQI(EDFdir, NucdirI, CytodirI, ResdirI, listI[i]);
    }
}

function processFileQI(EDFdir, NucdirI, CytodirI, ResdirI, fileI) {
```

```
487.
488.     print("Processing: " + EDFdir + fileI);
489.     newfile = EDFdir + fileI;
490.     open(newfile);
491.     run("8-bit");
492.     rename("Nuclear");
493.
494.     file=replace(fileI," - " + suffixCquant,"");
495.
496.     newfile2 = NucdirI + file + "NucMask.tif";
497.     open(newfile2);
498.     rename("NucMask");
499.
500.     run("Set Measurements...", "area mean standard min centroid center bounding median display redirect=Nuclear
    decimal=3");
501.     selectWindow("NucMask");
502.     run("Analyze Particles...", "size=0-Infinity show=Outlines display clear");
503.     selectWindow("NucMask");
504.     close();
505.     selectWindow("Drawing of NucMask");
506.     saveAs("Tiff", ResdirI + file + "Nuc.tif");
507.     selectWindow(file + "Nuc.tif");
508.     close();
509.     selectWindow("Results");
510.     saveAs("Results", ResdirI + file + "_NucResults.csv");
511.     selectWindow("Results");
512.     close();
513.
514.     open(newfile);
515.     run("8-bit");
516.     rename("Cytoplasmic");
517.
518.     newfile3 = CytodirI + file + "CytoMask.tif";
519.     open(newfile3);
520.     rename("CytoMask");
521.     run("Set Measurements...", "area mean standard min centroid center bounding median display
    redirect=Cytoplasmic decimal=3");
522.     selectWindow("CytoMask");
523.     run("Analyze Particles...", "size=0-Infinity show=Outlines display clear");
524.     selectWindow("CytoMask");
525.     close();
526.     selectWindow("Drawing of CytoMask");
527.     saveAs("Tiff", ResdirI + file + "Cyto.tif");
528.     selectWindow(file + "Cyto.tif");
529.     close();
530.     selectWindow("Results");
531.     saveAs("Results", ResdirI + file + "_CytoResults.csv");
532.     selectWindow("Results");
533.     close();
534. }
```

A.2 R script for cytoplasmic/nuclear ratio analysis

````
---
title: "R Notebook"
output: html_notebook
---

# Nuclear and cytoplasmic fluorescence analysis

## Importing quantification files from ImageJ

This will import all files into a single data frame and simultaneously add columns to indicate the original file used for quantification. Make sure to change the path to your files before running the chunk below.

```{r}
install.packages("readr")
 install.packages("plyr")
 install.packages("tidyr")
 install.packages("fields")
 install.packages("clue")
 install.packages("ggplot2")

library(readr)
library(plyr)
library(tidyr)
library(fields)
library(clue)
library(ggplot2)

# import all files into a single data frame and simultaneously add column for filename.

readFun <- function( filename ) {

    data <- read.csv( filename,
                      header = FALSE, skip=1,
                      col.names   =   c(   "ID",    "Label","Area",    "Mean",    "Stdev",    "Min","Max",    "X","Y","XM","YM","BX","BY","Width","Height","Median" ) )

    # add a file column containing the file name
    data$file <- filename

    return( data )
}

# Now execute that function across all files, outputting a data frame.
# You need to indicate the folder where your result spreadsheets are. Make sure you change that path below.
# Note to use / and not \ in the file path for windows too.

setwd("C:/Users/")

fluor <- ldply(.data = list.files(pattern = "*.csv"),.fun = readFun)
```

We need to extract the Ab used, the time after infection and the cell compartment quantified. So we'll do that below:

```{r}
# create a function to add columns indicating the IFs performed, the infection timepoint and the cell region quantified.
newColsname <- function (filename) {
    elems <- unlist(strsplit( filename , "_" )) # THIS INDICATES THE NAME IS SPLIT AT CHARACTER _, SO CHANGE IF YOU HAVE A DIFFERENT CHARACTER.
````
````

```
    Time.pi <- elems[1] # THIS INDICATES THAT THE 1ST THING IN THE NAME IS THE TIME POST INFECTION VARIABLE
    IF1 <- elems[2] # THIS INDICATES THAT THE SECOND THING IN THE NAME IS THE ANTIBODY USED.
    Cellreg <- elems[length(elems)] # THIS INDICATES THAT THE LAST THING IN THE NAME IS THE  CELL REGION QUANTIFIED. THIS SHOULD NOT CHANGED AS IT IS ADDED BY THE IMAGEJ SCRIPT.
    #YOU CAN ADD MORE VARIABLES HERE IF NECESSARY.
    All <- cbind(IF1,Time.pi, Cellreg) # THIS PUTS ALL VARIABLES TOGETHER TO RETURN
    return(All)
}


test <- sapply(fluor$file,newColsname)
test <- t(test)
fluor$IF1 <- test[1:dim(test)[1],1]
fluor$Time.pi <- test[1:dim(test)[1],2]
fluor$celReg <- test[1:dim(test)[1],3]
rm(test)
```

```{r}
# add a column with the original file name, so we can match nuclei and cytoplasm quantifications.

fluor$file <- gsub("_NucResults.csv", "-NucResults.csv", fluor$file)
fluor$file <- gsub("_CytoResults.csv", "-CytoResults.csv", fluor$file)

newColsnameFile <- function (filename) {
    elems <- unlist(strsplit( filename , "-" ))
    fileOrig <- elems[1]
    return(fileOrig)
}

test <- sapply(fluor$file,newColsnameFile)

fluor$fileOrig <- test
rm(test)
```

Clean up the useless columns:
```{r}
colnames(fluor)
# Keep ID, Area, Mean, X, Y, Median, IF1, Time.pi, celReg, fileOrig
```

```{r}

fluorSimp <- fluor[,c(1,3,4,8,9,16,18,19,20,21)]
```

Match nuclei and cytoplasm, then remove more useless columns:
```{r}
# Function to match nuclei and cytoplam quantification per cell.

CellAssign <- function( image_data ) {

    testC <- image_data[image_data$celReg == "CytoResults.csv" & image_data$Area > 1,]
    testN <- image_data[image_data$celReg == "NucResults.csv" & image_data$Area >1,]

    distancesXY <- rdist(cbind(testC$X,testC$Y),cbind(testN$X,testN$Y))
    if (nrow(t(distancesXY)) > ncol(t(distancesXY))) {
        distancesXY <- rdist(cbind(testN$X,testN$Y),cbind(testC$X,testC$Y))
        solXY <- solve_LSAP(t(distancesXY))
        testNC <- cbind(testN[solXY,],testC)
        return(testNC)
```

```
    } else {
        solXY <- solve_LSAP(t(distancesXY))
        testNC <- cbind(testN,testC[solXY,])
        return(testNC)
    }
}

quicktry <- by(fluorSimp, fluorSimp$fileOrig, CellAssign)

FluorMatch <- do.call("rbind", quicktry)

colnames(FluorMatch)
# Remove repeated columns and change column names to indicate N for nuclei and C for cytoplasmic measurement.
```

```{r}

FluorMatchSimp <- FluorMatch[,c(20,18,17,1,2,3,6,11,12,13,16)]
colnames(FluorMatchSimp) <- c("fileOrig","Time.pi","IF1","IDn","AreaN","MeanN","MedianN","IDc","AreaC","MeanC","MedianC")
```

Calculate the cytoplasmic/nuclear fluorescence ratios per cell and clean up data

```{r}
FluorMatchSimp$CNratio <- FluorMatchSimp$MeanC / FluorMatchSimp$MeanN
```

Let's see what the size of the nuclei and cytoplasm look like first:

```{r}
par(mfrow=c(2,1))
hist(FluorMatchSimp$AreaN, breaks = 50)
hist(FluorMatchSimp$AreaC, breaks = 50)
```
Quick hist of C/N per IF:

```{r, message=FALSE, warning=FALSE}

ggplot(FluorMatchSimp, aes(CNratio, fill = IF1)) +
  geom_histogram(show.legend = T) +
  facet_grid(IF1 ~ Time.pi)
  theme_minimal()
```
```{r}
boxplot(FluorMatchSimp$CNratio ~ FluorMatchSimp$Time.pi*FluorMatchSimp$IF1, las = 2)
stripchart(FluorMatchSimp$CNratio~FluorMatchSimp$Time.pi*FluorMatchSimp$IF1, vertical = TRUE, data = FluorMatchSimp, method = "jitter", add = TRUE, pch = 20, col = 'blue')
```

We can have some outliers for the cell sizes and for the cyto/nuc fluorescence ratio. Let's compare stuff:

```{r}
#This will plot the cytoplasm area vs the mean fluorescence in the cytoplasm
par(mfrow=c(1,3))
plot(FluorMatchSimp$MeanC,FluorMatchSimp$AreaC, col=as.factor(FluorMatchSimp$IF1),pch=19)

#This will plot the nuclear area vs the mean fluorescence in the nucleus
plot(FluorMatchSimp$MeanN,FluorMatchSimp$AreaN, col=as.factor(FluorMatchSimp$IF1),pch=19)
legend('topright',unique(FluorMatchSimp$IF1),col=1:length(FluorMatchSimp$IF1),pch=19)

#This will plot the cytoplasm/nucleus mean fluorescence vs the nucleus/cytoplasm area
```

````
plot(FluorMatchSimp$CNratio,FluorMatchSimp$AreaN/FluorMatchSimp$AreaC,
col=as.factor(FluorMatchSimp$IF1),pch=19)




## ADJUST THE NUMBERS BELOW TO FIND THE BEST FILTER FOR YOUR DATASET.
abline(v=2, col="orange")
abline(h=60, col="red")
```

Let's clean up the outliers a bit according to the plot above, by C/N ratio eliminating those above 60 and by N/C area eliminating those above 2. This filter can be made more stringent if necessary, for example by making the N/C area < 2 we require that the cytoplasm has at least half the area of the nucleus.

```{r}
# C/N ratio < 2 and N/C area < 60
FluorMatchSimp$NCarea <- FluorMatchSimp$AreaN/FluorMatchSimp$AreaC

FluorFilter <- FluorMatchSimp[FluorMatchSimp$CNratio < 2 & FluorMatchSimp$NCarea < 60,]

boxplot(FluorFilter$CNratio ~ FluorFilter$Time.pi*FluorFilter$IF1,las=2)
stripchart(FluorFilter$CNratio~FluorFilter$Time.pi*FluorFilter$IF1, vertical = TRUE, data = FluorFilter, method = "jitter", add = TRUE, pch = 20, col = 'blue')
```
Let's see if the distributions look better:

```{r, message=FALSE, warning=FALSE}
ggplot(FluorFilter, aes(CNratio, fill = IF1)) +
  geom_histogram(show.legend = T) +
  facet_grid(IF1 ~ Time.pi) +
  theme_minimal()
```

# Repeat all steps above for the uninfected dataset

```{r}
fluorinf <- fluor
fluorfiltinf <- FluorFilter
```

```{r}
setwd("C:/Users/abc ")

fluor <- ldply(.data = list.files(pattern = "*.csv"),.fun = readFun)
```

Now we'll create other variables to indicate the IF we are analyzing, the time post infection and cell region that was quantified. For this to work well it's very important to keep the file names consistent in the entire experiment.
We need to extract the Ab used, the time after infection and the cell compartment quantified. So we'll do that below:

```{r}
# create a function to add columns indicating the IFs performed, the infection timepoint and the cell region quantified.

newColsname <- function (filename) {
    elems <- unlist(strsplit( filename , "_" )) # THIS INDICATES THE NAME IS SPLIT AT CHARACTER _, SO CHANGE IF YOU HAVE A DIFFERENT CHARACTER.
    Time.pi <- elems[1] # THIS INDICATES THAT THE 1ST THING IN THE NAME IS THE TIME POST INFECTION VARIABLE
    IF1 <- elems[2] # THIS INDICATES THAT THE SECOND THING IN THE NAME IS THE ANTIBODY USED.
````

```
    Cellreg <- elems[length(elems)] # THIS INDICATES THAT THE LAST THING IN THE NAME IS THE  CELL REGION QUANTIFIED. THIS SHOULD NOT CHANGED AS IT IS ADDED BY THE IMAGEJ SCRIPT.
    #YOU CAN ADD MORE VARIABLES HERE IF NECESSARY.
    All <- cbind(IF1,Time.pi, Cellreg) # THIS PUTS ALL VARIABLES TOGETHER TO RETURN
    return(All)
}

test <- sapply(fluor$file,newColsname)
test <- t(test)
# THE NUMBERS 1, 2, 3 BELOW REFER TO THE ORDER OF VARIABLE CREATED ABOVE IN THE RETURNED TABLE.
fluor$IF1 <- test[1:dim(test)[1],1]
fluor$Time.pi <- test[1:dim(test)[1],2]
fluor$celReg <- test[1:dim(test)[1],3]
## MAKE SURE YOU CHECK YOU GOT THE EXPECTED RESULTS IN THE fluor TABLE ON THE RIGHT.
```

```{r}
# add a column with the original file name, so we can match nuclei and cytoplasm quantifications.

fluor$file <- gsub("_NucResults.csv", "-NucResults.csv", fluor$file)
fluor$file <- gsub("_CytoResults.csv", "-CytoResults.csv", fluor$file)

newColsnameFile <- function (filename) {
    elems <- unlist(strsplit( filename , "-" ))
    fileOrig <- elems[1]
    return(fileOrig)
}

test <- sapply(fluor$file,newColsnameFile)

fluor$fileOrig <- test
```

Clean up the useless columns:
```{r}
colnames(fluor)
# Keep ID, Area, Mean, X, Y, Median, IF1, Time.pi, celReg, fileOrig
```

```{r}
fluorSimp <- fluor[,c(1,3,4,8,9,16,18,19,20,21)]
```

Match nuclei and cytoplasm, then remove more useless columns:
```{r}
# Function to match nuclei and cytoplam quantification per cell.

CellAssign <- function( image_data ) {

    testC <- image_data[image_data$celReg == "CytoResults.csv" & image_data$Area > 1,]
    testN <- image_data[image_data$celReg == "NucResults.csv" & image_data$Area >1,]

    distancesXY <- rdist(cbind(testC$X,testC$Y),cbind(testN$X,testN$Y))
    if (nrow(t(distancesXY)) > ncol(t(distancesXY))) {
        distancesXY <- rdist(cbind(testN$X,testN$Y),cbind(testC$X,testC$Y))
        solXY <- solve_LSAP(t(distancesXY))
        testNC <- cbind(testN[solXY,],testC)
        return(testNC)
    } else {
        solXY <- solve_LSAP(t(distancesXY))
        testNC <- cbind(testN,testC[solXY,])
        return(testNC)
```

```
    }
}

quicktry <- by(fluorSimp, fluorSimp$fileOrig, CellAssign)

FluorMatch <- do.call("rbind", quicktry)

colnames(FluorMatch)
# Remove repeated columns and change column names to indicate N for nuclei and C for cytoplasmic measurement.
```

```{r}

FluorMatchSimp <- FluorMatch[,c(20,18,17,1,2,3,6,11,12,13,16)]
colnames(FluorMatchSimp) <- c("fileOrig","Time.pi","IF1","IDn","AreaN","MeanN","MedianN","IDc","AreaC","MeanC","MedianC")
```

Calculate the cytoplasmic/nuclear fluorescence ratios per cell and clean up data

```{r}
FluorMatchSimp$CNratio <- FluorMatchSimp$MeanC / FluorMatchSimp$MeanN
```

Let's see what the size of the nuclei and cytoplasm look like first:

```{r}
par(mfrow=c(2,1))
hist(FluorMatchSimp$AreaN, breaks = 50)
hist(FluorMatchSimp$AreaC, breaks = 50)
```
Quick hist of C/N per IF:

```{r, message=FALSE, warning=FALSE}

ggplot(FluorMatchSimp, aes(CNratio, fill = IF1)) +
  geom_histogram(show.legend = T) +
  facet_grid(IF1 ~ Time.pi)
  theme_minimal()
```
```{r}
boxplot(FluorMatchSimp$CNratio ~ FluorMatchSimp$IF1)
stripchart(FluorMatchSimp$CNratio~FluorMatchSimp$IF1, vertical = TRUE, data = FluorMatchSimp, method = "jitter", add = TRUE, pch = 20, col = 'blue')
```

We can have some outliers for the cell sizes and for the cyto/nuc fluorescence ratio. Let's compare stuff:

```{r}
#This will plot the cytoplasm area vs the mean fluorescence in the cytoplasm
par(mfrow=c(1,3))
plot(FluorMatchSimp$MeanC,FluorMatchSimp$AreaC, col=as.factor(FluorMatchSimp$IF1),pch=19)

#This will plot the nuclear area vs the mean fluorescence in the nucleus
plot(FluorMatchSimp$MeanN,FluorMatchSimp$AreaN, col=as.factor(FluorMatchSimp$IF1),pch=19)
legend('topright',unique(FluorMatchSimp$IF1),col=1:length(FluorMatchSimp$IF1),pch=19)

#This will plot the cytoplasm/nucleus mean fluorescence vs the nucleus/cytoplasm area
plot(FluorMatchSimp$CNratio,FluorMatchSimp$AreaN/FluorMatchSimp$AreaC,
col=as.factor(FluorMatchSimp$IF1),pch=19)
abline(v=2, col="orange")
abline(h=60, col="red")
```

```
```{r}
# C/N ratio < 2 and N/C area < 60
FluorMatchSimp$NCarea <- FluorMatchSimp$AreaN/FluorMatchSimp$AreaC

FluorFilter <- FluorMatchSimp[FluorMatchSimp$CNratio < 2 & FluorMatchSimp$NCarea < 60,]

boxplot(FluorFilter$CNratio ~ FluorFilter$IF1)
stripchart(FluorFilter$CNratio~FluorFilter$IF1, vertical = TRUE, data = FluorFilter, method = "jitter", add = TRUE, pch = 20, col = 'blue')
```
Let's see if the distributions look better:

```{r, message=FALSE, warning=FALSE}
ggplot(FluorFilter, aes(CNratio, fill = IF1)) +
  geom_histogram(show.legend = T) +
  facet_grid(IF1 ~ .)
  theme_minimal()
```

```{r}
fluorfiltuninf <- FluorFilter
fluoruninf <- fluor
```

Comparing infected and uninfected cells

Let's start by creating a single spreadsheet with all the data from infected and uninfected cells.

```{r}
fluorfiltinf$Type <- rep("Infected", length(fluorfiltinf$fileOrig))

fluorfiltuninf$Type <- rep("Uninfected",length(fluorfiltuninf$fileOrig))

fluorfilt <- rbind(fluorfiltinf,fluorfiltuninf)
```

Let's save just the data of interest in a file and clear everything else to speed up calculations.

```{r}
#load("/Users/ ")
```

Let's plot the uninfected and the infected side by side for each IF.

```{r}
ggplot(fluorfilt, aes(x=Time.pi, y=CNratio, fill=IF1))+
  geom_boxplot()+
  facet_grid(facets=.~as.factor(IF1))+
  scale_y_continuous()+
  labs(x="ZIKV infection", y= "Cytoplasmic/Nuclear fluorescence")+ theme_minimal()+
  theme(axis.text.x=element_text(angle=-90))
```

Are differences statistically significant?

Let's test if the change in C/N fluorescence ratio is statistically significant in ZIKV infected cells.

We'll use ANOVA followed by TukeyHSD first.

Anova test Uninfected vs. Infected cells.
```

```{r}
fit <- aov(fluorfilt$CNratio ~ fluorfilt$IF1*fluorfilt$Time.pi, fluorfilt)
summary(fit)
```

Post-test for all pairwise comparisons:

```{r}
posttest <- TukeyHSD(fit)
Ptinterest <- data.frame(posttest$`fluorfilt$IF1:fluorfilt$Time.pi`)
```

Clean up the result above only for the comparisons of interest. Such as, the last table comparing for each nup infected vs uninfected:

```{r}
Ptinterest$Comps <- rownames(Ptinterest)
newColsname <- function (filename) {
    elems <- unlist(strsplit( filename , "-" ))
    Comp1 <- elems[1]
    Comp2 <- elems[2]
    All <- cbind(Comp1,Comp2)
    return(All)
}

test <- sapply(Ptinterest$Comps,newColsname)
test <- t(test)
Ptinterest$Comp1 <- test[1:dim(test)[1],1]
Ptinterest$Comp2 <- test[1:dim(test)[1],2]
```

```{r}
newColsname <- function (filename) {
    elems <- unlist(strsplit( filename , ":" ))
    IF <- elems[1]
    Time.pi <- elems[2]
    All <- cbind(IF,Time.pi)
    return(All)
}

test <- sapply(Ptinterest$Comp1,newColsname)
test <- t(test)
Ptinterest$IF1 <- test[1:dim(test)[1],1]
Ptinterest$Time.pi1 <- test[1:dim(test)[1],2]

test <- sapply(Ptinterest$Comp2,newColsname)
test <- t(test)
Ptinterest$IF2 <- test[1:dim(test)[1],1]
Ptinterest$Time.pi2 <- test[1:dim(test)[1],2]
```

```{r}
Ptint <- Ptinterest[Ptinterest$IF1 == Ptinterest$IF2,c(4, 8:11)]
Ptint
```

We'll use ANOVA followed by TukeyHSD first.

Anova test Uninfected vs. Infected cells.

```{r}
fit <- aov(fluorfilt$CNratio ~ fluorfilt$IF1*fluorfilt$Time.pi, fluorfilt)
```

````
summary(fit)
```

Post-test for all pairwise comparisons:

```{r}
posttest <- TukeyHSD(fit)
Ptinterest <- data.frame(posttest$`fluorfilt$IF1:fluorfilt$Time.pi`)
```

```{r}
Ptinterest$Comps <- rownames(Ptinterest)
newColsname <- function (filename) {
    elems <- unlist(strsplit( filename , "-" ))
    Comp1 <- elems[1]
    Comp2 <- elems[2]
    All <- cbind(Comp1,Comp2)
    return(All)
}

test <- sapply(Ptinterest$Comps,newColsname)
test <- t(test)
Ptinterest$Comp1 <- test[1:dim(test)[1],1]
Ptinterest$Comp2 <- test[1:dim(test)[1],2]
```

```{r}
newColsname <- function (filename) {
    elems <- unlist(strsplit( filename , ":" ))
    IF <- elems[1]
    Type <- elems[2]
    All <- cbind(IF,Type)
    return(All)
}

test <- sapply(Ptinterest$Comp1,newColsname)
test <- t(test)
Ptinterest$IF1 <- test[1:dim(test)[1],1]
Ptinterest$Type1 <- test[1:dim(test)[1],2]

test <- sapply(Ptinterest$Comp2,newColsname)
test <- t(test)
Ptinterest$IF2 <- test[1:dim(test)[1],1]
Ptinterest$Type2 <- test[1:dim(test)[1],2]
```

```{r}
Ptint <- Ptinterest[Ptinterest$IF1 == Ptinterest$IF2,4:5]
Ptint
```
````
````